John William Bandler
B Sc (Eng), ACGI

STABLE BROADBAND TUNNEL-DIODE AMPLIFIERS IN RECTANGULAR WAVEGUIDES

a thesis
submitted for the degree of

doctor of philosophy

in the Faculty of Engineering
University of London

Electrical Engineering Department
Imperial College of Science and Technology
London, SW 7

January 1967

to Judy

ABSTRACT

This project has concerned itself with the theoretical and experimental investigation into the electrical behaviour of tunnel-diodes mounted in rectangular waveguides. Attention is focussed mainly on the methods of achieving stable, broadband amplification of microwave signals from one tunnel-diode.

Two theoretical chapters deriving and discussing the stability of a negative resistance device such as the tunnel-diode are presented. One deals with stability analysis in the immittance planes, discussing, in particular, the effects of treating the tunnel-diode's package capacitance as part of its equivalent circuit. The other deals with stability analysis in the reflection coefficient plane or Smith chart. The graphical Nyquist approach to stability is used throughout. It is shown that for reflection amplifiers, the gain and stability can be simultaneously predicted from a Smith chart plot of the amplifier's immittance.

Two experimental amplifiers utilizing S-band rectangular waveguide were designed. A full account of their theoretical and experimental behaviour is presented. In both cases the tunnel-diode is centrally mounted in a reduced height waveguide section. The computer optimization technique used in the design of the coaxial-line band-rejection filter for stabilizing in the second amplifier is described in some detail. The first amplifier worked substantially in accordance with theory. The second failed to operate satisfactorily, which is attributed to the critical dependence of the series inductance of the tunnel-diode on its mounting configuration - an effect which was not appreciated during the design stage.

ACKNOWLEDGEMENTS

The author must thank Mr. J. Roberts of the Electrical Engineering Department, Imperial College, who proposed the project and guided the research. The untiring interest and encouragement throughout of Dr. A. Wexler, now at the University of Manitoba, Canada, is greatly appreciated.

Associated Semiconductor Manufacturers Ltd. kindly provided the tunnel-diodes. Mr. J. Kenny constructed the two amplifiers. Discussions with Mr. J.D. Penney of University College, London, are acknowledged; the author is also grateful for his cooperation during some of the latter measurements reported in chapter 7. In this context, Mr. M.K. McPhun, then of Mullard Research Laboratories, Surrey, is also thanked. Stimulating discussions with colleages are acknowledged, in particular with Mr. G.E. Crossley. Some of the final measurements of chapter 7 were carried out while the author was with Mullard Research Laboratories. The author is indebted to the organisation for this and also for its drawing, photographing, and printing services. Miss J. Clift is thanked for plotting graphs and checking the manuscript. Miss M. Hudgell is thanked for her able typing.

Financial support for the three years in the form of a Research Studentship from the Science Research Council is appreciated. During his first year, the author also held a John and Frances Jones Scholarship.

CONTENTS

Abstract 3
Acknowledgements 4
Principal Symbols 11
Subscripts 13
Abbreviations 14

1 INTRODUCTION 15

1.1 BACKGROUND 15
1.2 TD SMALL SIGNAL EQUIVALENT CIRCUIT 16
1.3 EQUATIONS CHARACTERIZING THE TD 18
1.4 STABILITY 20
1.5 THE TDs USED IN THIS PROJECT 21
1.6 SCOPE OF THIS THESIS 22
1.7 ORIGINALITY 22
1.8 References 23

2 DESIGN OF TDA 1 24

2.1 Introduction 24
2.2 THE STABILIZING AND BIASING NETWORK 25
The radial-line 25
The biasing circuit 26
The frequency response of the network 27
2.3 WAVEGUIDE IMPEDANCES SEEN BY TD 28
Experimental investigations to determine Z_0 28
Impedance levels and gain considerations 31
The exponential taper 32
The s.c. stub 33
2.4 CONSTRUCTIONAL DETAILS 35
2.5 Conclusion 37
2.6 References 39

3 STABILITY ANALYSIS IN THE H-PLANES 40

3.1 Introduction 40
3.2 THEORY OF NYQUIST-TYPE STABILITY CRITERION 41
A theorem 41
Application to TDA stability 43
3.3 TD EQUIVALENT CIRCUIT 45
Some simplified equivalent circuits 45
The complete equivalent circuit 47
3.4 THE IDEAL STABILIZING NETWORK 49
3.5 TYPES OF AMPLIFIER 50
3.6 THE CONSEQUENCES OF ADDING THE PACKAGE CAPACITANCE 52
3.7 ADDITION OF STABILIZING NETWORK 57
3.8 THE CONNECTED AMPLIFIER 61
3.9 Conclusion 62
3.10 References 63

4 STABILITY ANALYSIS IN THE ρ-PLANE 66

4.1 Introduction 66
4.2 TRANSMISSION-LINE WITH NEGATIVE CONDUCTANCE LOAD 67
4.3 REPRESENTATION OF IMMITTANCES WITH NEGATIVE REAL PARTS ON THE SMITH CHART 69
The complete ρ-plane 69
The ρ'-plane: a transformed ρ-plane 69
4.4 ADAPTING H-PLANE STABILITY ANALYSIS TO THE ρ-PLANE 72
4.5 DIRECT INTERPRETATION OF STABILITY IN THE ρ-PLANE 73
The stability criterion 73
Limiting cases for $\rho'(p)$ as $p \rightarrow \infty$ 74
The arbitrary closing loop 75
Concluding comments 76
4.6 ANOTHER TYPE OF NEGATIVE SMITH CHART 77
4.7 REFLECTION AMPLIFIER CONNECTED TO MISMATCHED LINE 78
Stability criterion in terms of amplifier and source reflection coefficients 78
Stability criterion in terms of gain equation 79
4.8 McPHUN'S STABILITY CRITERION 80
The criterion 80
Its application to a particular case 80
4.9 Conclusion 85
4.10 References 86

5 PREDICTED AND EXPERIMENTAL PERFORMANCE OF TDA 1 88

5.1 Introduction 88
5.2 TD SMITH CHART NOMOGRAM 89

5.3 THEORETICAL CALCULATIONS 92
Addition of package capacitance 92
Addition of stabilizing network 95
The connected amplifier 97
5.4 EXPERIMENTAL RESULTS 100
Circulator response 100
Experimental set-up 101
Amplifier performance 104
5.5 COMPARISON OF PREDICTED WITH EXPERIMENTAL RESULTS 106
Amplifier as designed 106
Broadbanded amplifier 106
5.6 Conclusion 107
5.7 References 108

6 DESIGN AND THEORETICAL PERFORMANCE OF TDA 2 109

6.1 Introduction 109
6.2 CHOICE OF AMPLIFIER CONFIGURATION 110
6.3 FREQUENCY RESPONSES IN THE ρ-PLANE PLOTTED BY DIGITAL COMPUTER 112
6.4 ONE-PORT PROGRAM AND CIRCULATOR RESPONSE 112
6.5 THE OPTIMIZED STABILIZING NETWORK 116
6.5.1 Preliminary considerations 116
6.5.2 Its configuration 118
6.5.3 The computer program 121
6.5.4 The present requirements 122
6.5.5 Computer results and discussion 123
6.5.6 Addition of $Z_i(j\omega)$ to $Z_{TD}(j\omega)$ 126
6.6 INDUCTIVE TUNING 128
6.7 POTENTIAL STABILITY OF THE TDA 130
6.8 THE QUARTER WAVE TRANSFORMERS 130
6.9 THEORETICAL GAIN RESPONSE OF TDA2 134
Transformation of admittances to plane of TD 134

Gain equations 134
Stability 136
TDA program 137
Gain response 137
6.10 REALIZATION AND CONSTRUCTIONAL DETAILS 143
The stabilizing network 143
The waveguide transformers 145
The inductive iris 145
6.11 Conclusion 148
6.12 References 148

7 EXPERIMENTAL PERFORMANCE OF TDA 2 151

7.1 Introduction 151
7.2 BRIDGE BIASING CIRCUIT 151
7.3 FAILURE OF TDA 2 TO AMPLIFY 153
7.4 TESTING OF COMPONENT NETWORKS 154
The waveguide transformers 154
Comparison of iris with s.c. line 156
Determination of Z_0 at TD position 157
Test of the stabilizing network 160
7.5 LUMPED EQUIVALENT CIRCUIT FOR LOSSY TRANSMISSION-LINES 164
7.6 EXPLANATION OF THE PERFORMANCE OF TDA 2 165
Calculation of inductance of TD mount 166
Stability of TDA 2 167
Experimental observations 169
Narrow band stabilizing network 170
7.7 Conclusion 171
7.8 References 173

8 GENERAL CONCLUSIONS 174

References 176

APPENDIX

A1	SMITH CHART SUBROUTINE	177
A2	PROGRAM FOR ONE-PORT MEASUREMENTS	182
A3	STABILIZING NETWORK PROGRAM	184
A4	IMMITTANCE TRANSFORMATION THROUGH TRANSMISSION-LINES	189
A5	REPRESENTATION OF TRANSMISSION-LINE LOAD WHEN THE LINE HAS A SMALL BUT FINITE LOSS	190

Author Index 193

PRINCIPAL SYMBOLS

N.B. Lower case symbols shown together with capitals represent normalized quantities.

a	broad dimension of rectangular waveguide
b	height of rectangular waveguide
b,B	susceptance
b'	height of section containing inductive iris
B	bandwidth
B	susceptance due to junction capacitance of TD
B_{re}	see fig. 6.13 (a)
B_p	equivalent parallel susceptance of series circuit
c	velocity of light
C	capacitance
C	junction capacitance of TD
C_1	package capacitance of TD
$C_{1\to9}$	specifications for stabilizing network of TDA 2 in ohms
C_1'	right hand side of (3.26)
d	distance
d	height of radial-line
d	aperture of inductive iris
D	denominator
f	frequency
f_c	cut-off frequency of rectangular waveguide
f_o	resonant or centre frequency
$f_{R,X}$	resistive, reactive cut-off frequency of TD
$f_{1\to6}$	test frequencies for stabilizing network of TDA 2
g,G	conductance
G	magnitude of negative conductance of TD
G	power gain
G_p	equivalent parallel conductance of series circuit
H	immittance
H_0	characteristic immittance of transmission-line
j	$\sqrt{-1}$

ℓ	length of transmission-line
L	inductance
L	series inductance of TD
n	normalized scale of Smith chart
N	numerator
p	$= \sigma + j\omega$, complex frequency
$p_{1,2}$	location of poles in RH p-plane
P	number of RH p-plane poles
P	$= j\Omega$, complex frequency variable for transmission-line
r,R	resistance
r	series resistance of TD
r_c	outer radius of radial-line
$r_{i,o}$	inner, outer radius of coaxial-line
R	magnitude of negative resistance of TD
R_b	bias resistance
R_{min}	minimum magnitude of negative resistance of TD
R_S	equivalent series resistance of parallel circuit
R_{dc}	d.c. resistance
s	value of VSWR
t	transmission coefficient
U	defined by (6.2)
x,X	reactance
X_S	equivalent series reactance of parallel circuit
y,Y	admittance
y_0, Y_0	characteristic admittance of transmission-line
Y_A'	defined by (6.8)
Y_D	$= 1/Z_D$
Y_{rt}	$= G_{rt} + jB_{rt}$; see fig. 6.13 (a)
Y_{tr}	$= G_{tr} + jB_{tr}$; see fig. 6.13 (a)
$Y_{1,3}$	see fig. 3.5 (d)
z	distance along transmission-line
z,Z	impedance
z_0, Z_0	characteristic impedance of transmission-line
$z_{1,2,3}$	location of zeros in RH p-plane

Z	number of RH p-plane zeros
$Z_{a,p}$	active, passive impedance
Z_D	TD impedance (C_1 not included)
Z_{fs}	wave impedance of free space
$Z_{r\ell}$	input impedance to radial-line
Z_2	see fig. 3.5 (d)
Z_2'	$= Z_2 + 1/Y_1'$

β	$= 2\pi/\lambda$
θ	$= \beta\ell$
θ	angle
λ	wavelength, free space wavelength
λ_g	wavelength in rectangular waveguide
λ_{go}	λ_g at f_o
λ_o	λ at f_o
ρ	active or passive voltage reflection coefficient
ρ'	transformed voltage reflection coefficient for active ρ
ρ''	another transformed voltage reflection coefficient for active ρ
ρ_{re}	reflection coefficient of reflection amplifier (TDA 2)
ω	$= 2\pi f$, real frequency
ω_o	$= 2\pi f_o$
$\omega_a, \omega_b, \omega_R'$	see fig. 3.9
$\omega_{R,X}$	$= 2\pi f_{R,X}$
Ω	ohms
Ω	$= \tan\theta$, real frequency variable for transmission-line

SUBSCRIPTS

A	of amplifier

C	of circulator
i	input
i	input quantity of stabilizing network of TDA 2
L	load
o	output
s	source
sc	at the input to the s.c. transmission-line
t	tuning
t	of inductive iris
tr	of transmission amplifier (TDA 2)
T	total
TD	of the TD (C_1 included), e.g. $Z_{TD} = 1/Y_1'$
1,2,3,...n	of transmission-lines 1,2,3 ...n for transmission-line quantities

ABBREVIATIONS

CW	clockwise
CCW	counterclockwise
d.c.	direct current
LH	left half
o.c.	open-circuit
RH	right half
s.c.	short-circuit
SWD	standing wave detector
TD	tunnel-diode
TDA	tunnel-diode amplifier
TE	transverse electric
VSWR	voltage standing wave ratio

If we make up an ad hoc hypothesis for every new case ... then we shall never go beyond the present position where we can explain everything and predict nothing.

Prof. H.J. Eysenck

1 introduction

1.1 BACKGROUND

The discovery of the incremental negative resistance property of the tunnel-diode (TD) is attributed to Esaki,[1] who reported the phenomenon in 1958. He was experimenting on very narrow, highly doped, germanium p-n junctions when he observed an anomalous V-I characteristic in the forward direction. The phenomenon can be explained in terms of quantum mechanical tunnelling.*,[2-5]

Well over 1000 publications have dealt with the TD and its applications, which include low noise amplifiers, oscillators, frequency converters, memory circuits and logic circuits. The TD's distinguishing circuit features are its d.c. voltage controlled negative resistance, its high frequency and large bandwidth capabilities, and its high switching speed.

The availability of low loss broadband circulators has made the TD reflection amplifier an attractive commercial

---

*References 3 and 4 are recommended. Chow[3] has an extensive bibliography; Scanlan[4] is particularly good on amplifiers. Additional reading and an exhaustive bibliography is found in reference 5.

proposition. Typically, it would be a preamplifier mounted on a receiving aerial. A 1965 product survey[6] reveals that the tunnel-diode amplifier (TDA) dominates the TD microwave application market.

Some practical advantages of the microwave TDA are: light weight and small size, simplicity of the associated circuitry, low power consumption, the fact that the TD is relatively unaffected by radiation or temperature changes, and its general reliability of performance over long periods. Resistive cut-off frequencies for microwave TDs above 30 Gc/s are common. Narrow band gains up to 20 dB, and octave bandwidths at 10 dB have been achieved. Amplifier noise figures between 3.5 and 6 dB have been reported.

Presently foreseen disadvantages by comparison with other microwave devices include: low power handling capacity (typically a few microwatts), the problem of instability due to the two terminal negative resistance, the decreasing noise figures of mixers, and the increasing frequency range of transistors (which have superior noise figures at UHF).

1.2 TD SMALL SIGNAL EQUIVALENT CIRCUIT

The circuit behaviour of the TD will be considered solely for the case when it is biased at a unique point in the negative resistance region of the d.c. V-I characteristic. See fig. 1.1. (a). To achieve this, an equivalent d.c. source resistance less than the minimum negative resistance R_{min} is required. Its behaviour for small signals is then completely expressed in terms of its commonly accepted equivalent circuit (fig. 1.1 (b)). R is the magnitude of the junction negative resistance (= 1/G) - it is the gradient of the V-I characteristic at the operating point. C is the junction capacitance.*

---

*C is a function of bias voltage given by $C = k/\sqrt{(V'-V)}$, where k is a constant, and V' is a built-in potential of the junction. C is generally quoted by the manufacturers at the valley voltage - its value near R_{min} is some 20% less.

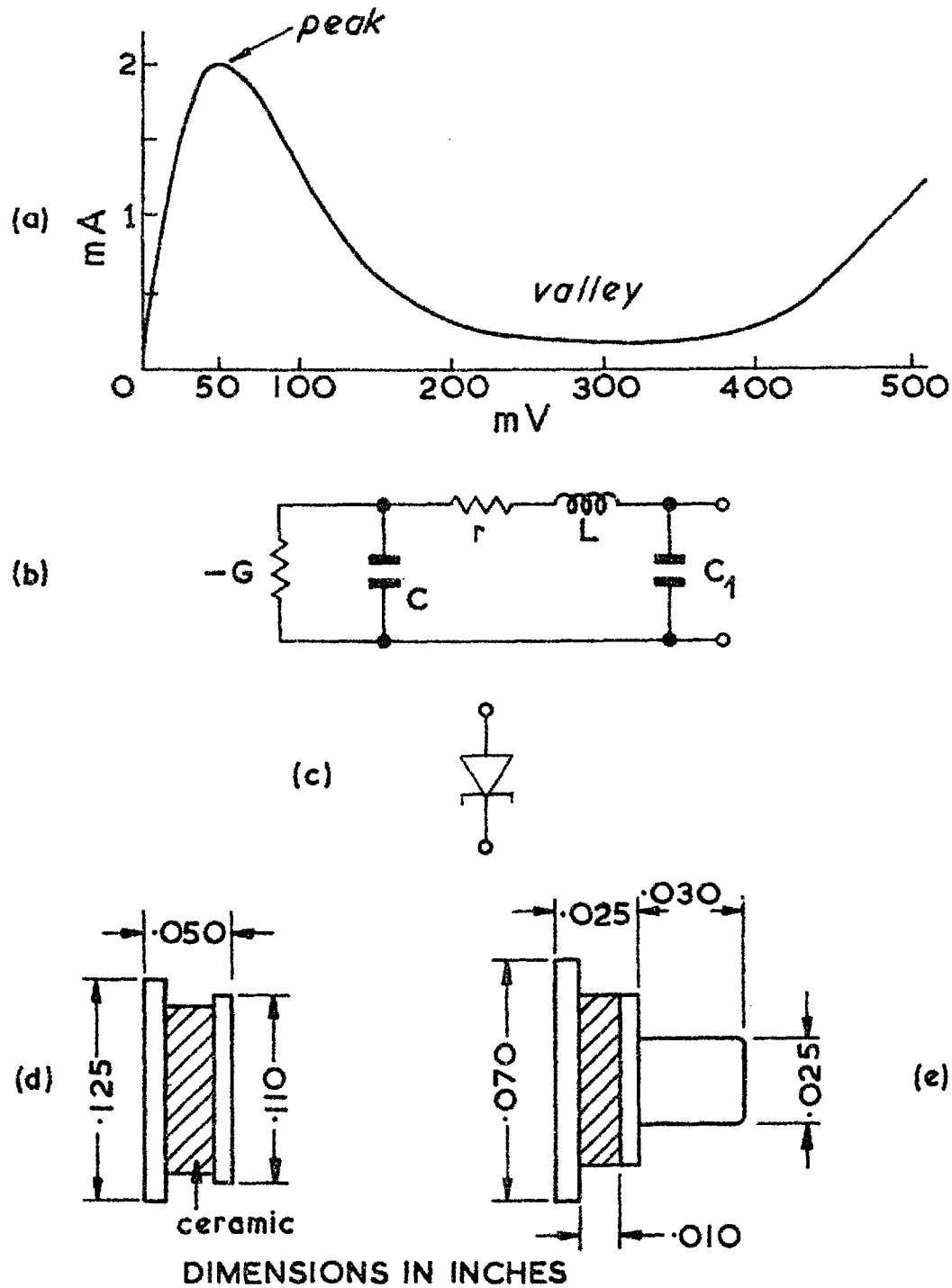

Fig. 1.1: The tunnel-diode, (a) V-I characteristic, (b) equivalent circuit for small signals, (c) symbol, (d) Mullard type 49 AAY, (e) Mullard type AEY 16.

r is the total series resistance, L the series inductance due to lead and package, and C_1 is the external parasitic package capacitance. In the theory presented in this thesis, the parameters are assumed frequency independent.* This is partly justified by the TD's minute p-n junction, and its small housing compared with the wavelengths of interest. The terminals shown are, for practical purposes the only accessible points of the equivalent circuit. (Getsinger[7] has recently considered the influence of coupling the packaged TD with its microwave environment.)

1.3 EQUATIONS CHARACTERIZING THE TD**

A number of readily derivable equations describe the TD and its circuit performance. The resistive cut-off frequency f_R is given by

$$f_R = \frac{1}{2\pi RC}\sqrt{\frac{R}{r} - 1} \quad . \tag{1.1}$$

This is the maximum frequency at which a net negative resistance is observable at the accessible terminals.

$$f_X = \frac{1}{2\pi RC}\sqrt{\frac{R^2C}{L} - 1} \tag{1.2}$$

and is called the reactive cut-off or self-resonant frequency - at which the imaginary part of the TD impedance (neglecting C_1) disappears. A microwave TD has $R >> r$ and $L << R^2C$.

Taking account of both shot noise in the junction and thermal noise due to r, the following is the noise figure for reflection amplifiers:

$$F = \frac{1 + 20IR}{(1 - \frac{r}{R})(1 - (\frac{f}{f_R})^2)} \tag{1.3}$$

---

*Some consequences of frequency dependence are discussed in sections 5.3 and 7.6.

**Ideal, lumped, frequency independent elements are assumed throughout.

where I is the d.c. current. For low noise figures and wide-band performance, TDAs are operated at $f_R/3$ or lower. Minimum F is obtained also for a somewhat higher bias voltage than for $R = R_{min}$.[8]

The gain-bandwidth performance* for the single tuned reflection amplifier (fig. 1.2 (a)) is (neglecting L and C_1)[4]

$$(\sqrt{G} - 1)\sqrt{(1 - \frac{2}{G})}.B = \frac{1}{\pi RC}\,(1 - \frac{r}{R})(1 - (\frac{f}{f_R})^2) \qquad (1.4)$$

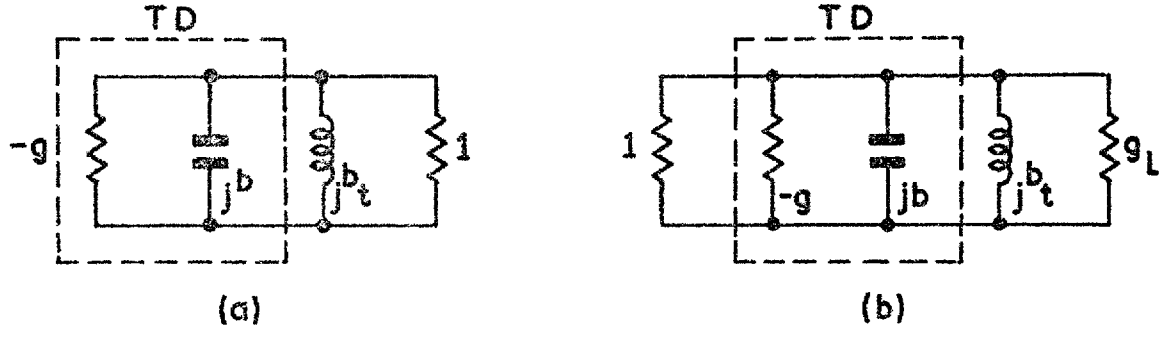

Fig. 1.2: (a) reflection TDA, parameters normalized to source conductance; (b) transmission TDA, parameters normalized to $1/R_s$, the source conductance: $g_L = R_s/R_L$, $g = R_s/R$.

where $\sqrt{G} = |\rho|$, the magnitude of the reflection coefficient. Neglecting L, but including C_1, and for $G \gg 2$ with $r/R \ll 1$,

$$(\sqrt{G} - 1).B = \frac{1}{\pi R(C + C_1)}\,. \qquad (1.5)$$

r, L and C_1 are neglected in the ensuing equations in this section. The ultimate limit for reflection amplifiers is given by[4]

$$B.\log_e\sqrt{G} \leqslant \frac{\pi}{RC}\,. \qquad (1.6)$$

---

*Except in (1.6), B is the 3 dB bandwidth for a peak power gain G.

The single tuned transmission amplifier performance (fig. 1.2 (b)) can be described by

$$\sqrt{G}.B = \frac{1}{\pi C\sqrt{R_s R_L}} \qquad (1.7)$$

where R_s and R_L are the source and load resistances, respectively. Here, $\sqrt{G} = |t|$, the magnitude of the transmission coefficient. Maximum G for a given B occurs when $R_s = R_L$; then

$$(\sqrt{G} - 1).B = \frac{1}{2\pi RC} . \qquad (1.8)$$

For a transmission TDA with a matched input (see fig. 1.2. (b)) $g_L - g = 1$, and

$$(G - 1).B = \frac{1}{\pi RC} . \qquad (1.9)$$

Here, $t = t_m$, say.

For a gain of 20 dB the bandwidth ratio given by (1.4), (1.6), (1.8), and (1.9) is 10 : 43 : 5 : 1. For high G the reflection amplifier is 6 dB better than the best transmission amplifier having the same bandwidth. It is easily verified that the return gain at the output of the matched transmission amplifier is, for high G, very nearly equal to the gain of the corresponding reflection amplifier. The implications of this fact on stability are evident.

1.4 STABILITY

Consider the three circuits shown in fig. 1.3. Circuit (a) is described as short-circuit stable : $R_L < R$ for stability. Circuit (b) is described as open-circuit stable : $R_L > R$ for stability. Circuit (c) (a TD minus C_1) must satisfy $LG/C - r < R_L < 1/G - r$ for stability. At resonance, for example, it is impossible to distinguish between (a) and (b), and yet R_L needs to be of a different value in each case.

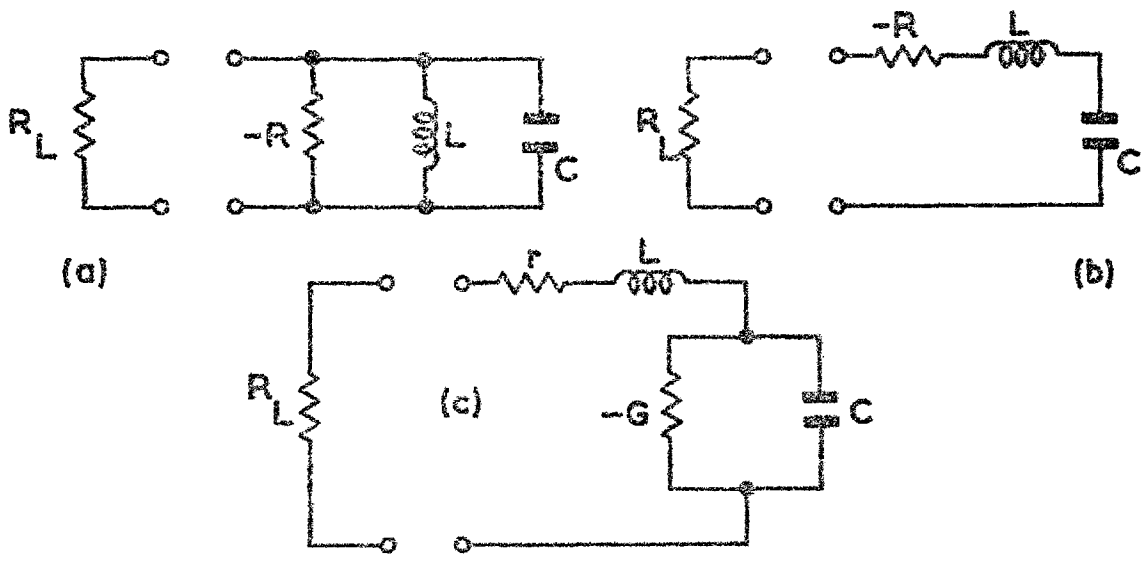

Fig. 1.3: Three circuits containing negative resistances.

It has been shown[9] that for potential stability of a TD, its parameters must satisfy (neglecting C_1)

$$\frac{L}{R^2C} < \frac{\theta^3}{1+\theta^2} \cdot \frac{1}{\theta - \tan^{-1}\theta} \qquad (1.10)$$

where

$$\theta = \frac{1}{2\pi RCf_R} = \sqrt{\frac{r}{R-r}} \quad . \qquad (1.11)$$

In the limit, as $r/R \rightarrow 0$

$$\frac{L}{R^2C} < 3. \qquad (1.12)$$

As stated in section 1.3, $L << R^2C$ for microwave TDs.

1.5 THE TDs USED IN THIS PROJECT

A sketch of the TD package used in TDA 1 (chapters 2 and 5) is shown in fig. 1.1 (d), and of the one used in TDA 2 (chapters 6 and 7) in fig. 1.1 (e). The latter is described

by Lee,[10] and the use of the former is reported by Easter.[8] Both TDs are made from germanium. Comments on their performance are made in chapter 8.

1.6 SCOPE OF THIS THESIS

The TD and many of the structures considered in this project are well-established in the microwave field. Consequently, relevant publications are referred to freely so as not to detract from the main treatise. Use of Nyquist-type stability criteria, and use of digital computers in circuit optimization are not quite so familiar to microwave engineers, thus they tend to be dealt with in some detail. Both techniques are of direct relevance to microwave networks exhibiting responses which are complicated functions of frequency and/or which are not commensurate.

1,7 ORIGINALITY

Except where the assistance of others is acknowledged, or where published material is referred to, the work reported in this thesis was independently devised by the author. Furthermore, the principal contents of the author's publications were believed to be original at the time of publication. Original contributions in this thesis include:

(i) the method of immittance-plane stability analysis involving successive inversions and determination of RH p-plane poles and zeros;

(ii) the simultaneous determination of gain and stability of reflection amplifiers on a redefined Smith chart (ρ-plane), and

(iii) the direct interpretation of stability in this plane;

(iv) the critical examination of McPhun's stability criterion;

(v) the application of a digital computer to the design of a coaxial-line band-rejection filter having sections with unequal lengths.

1.8 References

(1) L. Esaki, "New phenomenon in narrow germanium p-n junctions," Phys. Rev., Vol.109, pp. 603-604, 1958.

(2) K.K.N. Chang, "Parametric and tunnel diodes," Prentice-Hall, N.J., 1964.

(3) W.F. Chow, "Principles of tunnel diode circuits," Wiley, New York, 1964.

(4) J.O. Scanlan, "Analysis and synthesis of tunnel diode circuits," Wiley, London, 1966.

(5) Electronics and Communications in Japan (J.I.E.C.E.), special issue dealing with Esaki diode and its applications, Vol.47, April 1964.

(6) "Tunnel diode devices," product survey, Microwaves, Vol.4, pp. 32-37, July 1965.

(7) W.J. Getsinger, ref. (10) chap. 2.

(8) B. Easter, ref. (5) chap. 5.

(9) D.C. Youla and L.I. Smilen, "Stability criteria for tunnel diodes," Proc. IRE, Vol.49, pp.1206-1207, July 1961.

(10) M.A. Lee, ref. (6) chap. 5.

2

design of TDA 1

2.1 Introduction

For a considerable time during the early stages of this project it was found impossible to achieve a stable, predictable performance from a TD mounted in various ridged waveguide structures. The most fundamental problem which had to be overcome was that of stability. It was decided to design a reflection amplifier of a fairly conventional type in order to study this problem.

The TD was to be mounted in a reduced height section of an S-band rectangular waveguide, as shown in fig. 2.1. Matching to the full height waveguide was to be effected by a reasonably long exponential taper. The amplifier was to be rendered passive outside its operating band by a stabilizing network consisting of a radial-line band-rejection filter in a coaxial-line arrangement, and terminated by a resistive card. A circulator was to separate the reflected power from the incident power.

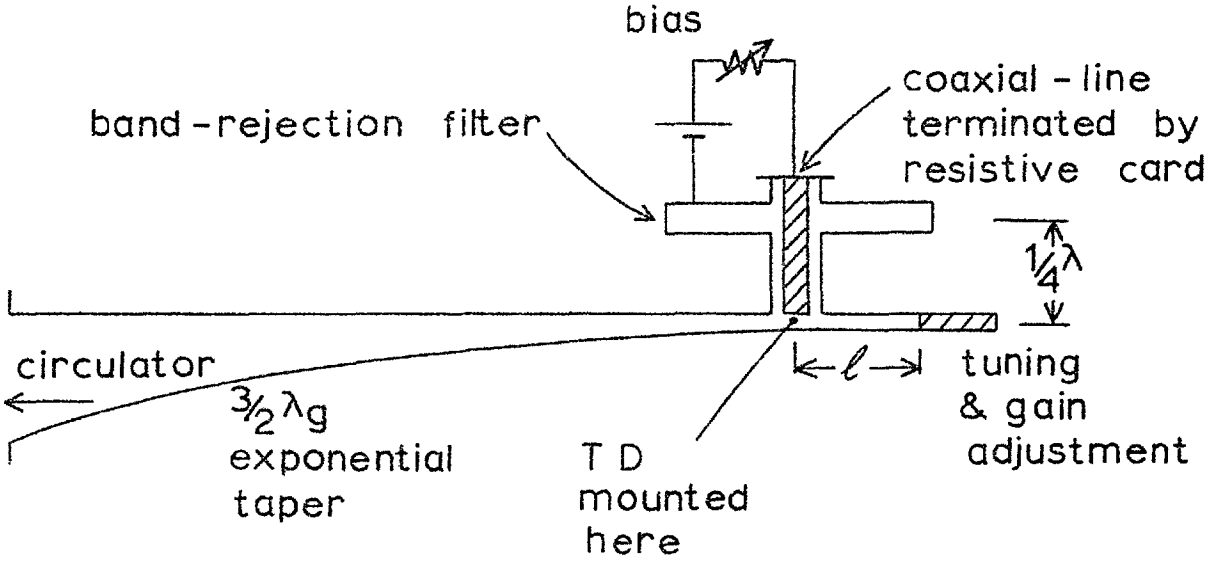

Fig. 2.1: Schematic of proposed amplifier.

This chapter describes all the relevant steps taken and the calculations made towards designing and constructing this TDA.

2.2 THE STABILIZING AND BIASING NETWORK

The radial-line

The short-circuited radial-line [1-3] was designed from curves given by Ramo and Whinnery.[3] Fig. 2.2 shows its dimensions, and its frequency response. The radial-line dimensions are determined by those of the coaxial-line which it interrupts. The impedance of the coaxial-line was chosen to be 40 Ω,* with a centre rod diameter of .110 in, the dia-

* For d.c. stability, a TD must be biased from a source whose resistance is less than the TD's negative resistance. For the TDs used, R_{min} was typically 50 Ω.

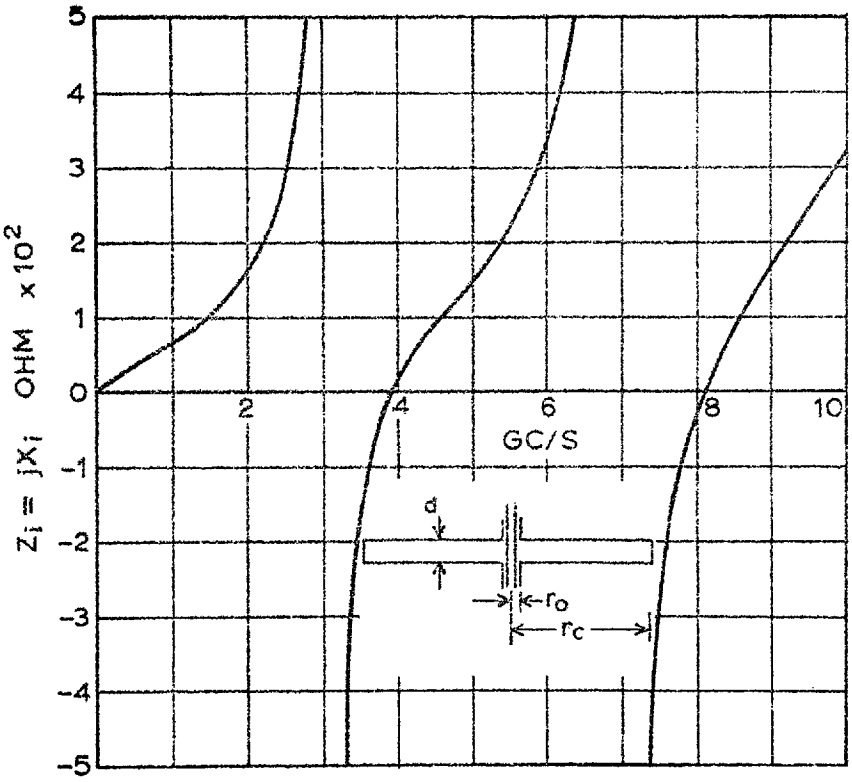

Fig. 2.2: The frequency response of the radial-line for r_o = .272 cm and r_c = 3.87 cm. Z_i is its wave impedance.

meter of the TD package. The first resonant frequency of the radial-line was required to be 3 Gc/s. Note from fig. 2.2 that its next resonance occurs at about 7 Gc/s.

The biasing circuit

The effective terminating resistance due to radiation of an open-ended coaxial-line having the dimensions of the present example was calculated from equations given by Harrington.[4] This resistance is very high, as shown in fig. 2.3. A resistive-film card* of resistance per square equal to Z_{fs} (the wave impedance of free space) terminating the 40 Ω line would, therefore, provide a good match from d.c. well into X-band. Wexler[5] has found that the value of the d.c.

*Very thin graphite on paxolin substrate made by the Morgan Crucible Company.

resistance of such cards can be carried over to microwave frequencies, i.e. the microwave resistance per square is substantially the same as the corresponding d.c. resistance.

Discontinuity and stray effects were, for simplicity, neglected. The effect, for instance, of attaching a bias lead to the centre conductor would be insignificant at the amplification band, due to the action of the radial-line.

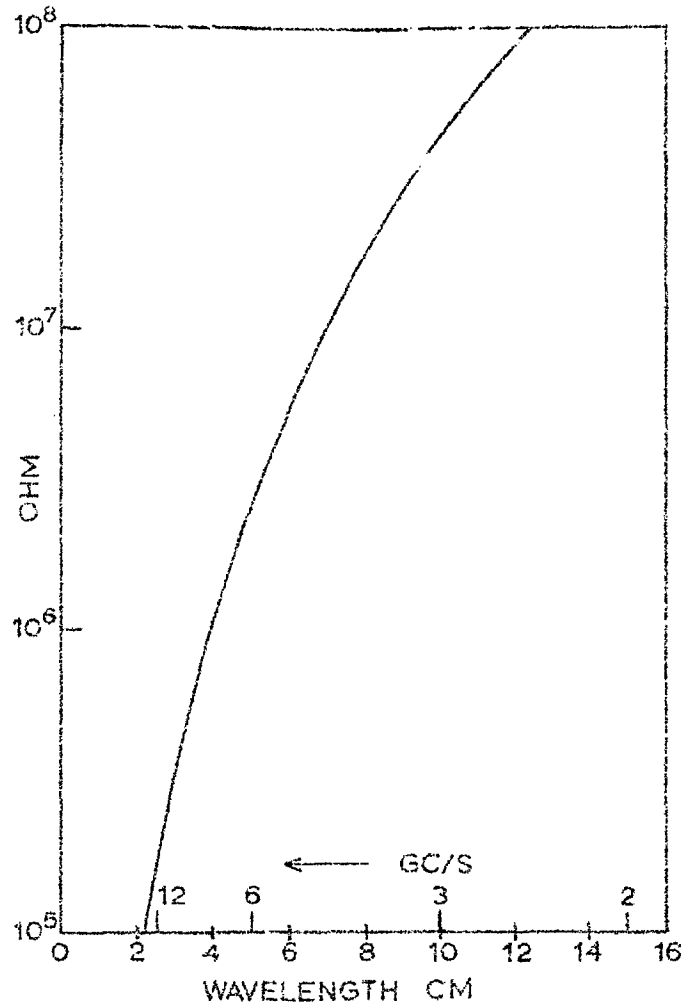

Fig.2.3: Radiation resistance of the 40 Ω coaxial-line.

The frequency response of the network

The total impedance $Z_{r\ell}$ presented by the radial-line is given by

$$Z_{r\ell} = jX_i \cdot \frac{d}{2\pi r_o} \qquad (2.1)$$

where X_i, r_o, and d are defined in fig. 2.2. The calculated input impedance Z_{in} to the band-rejection filter (see fig. 2.4) is plotted in fig. 2.5. The distance from the centre of the radial-line to the TD was made $\lambda/4$ at 3 Gc/s, i.e. 2.5 cm, so that a s.c. falls in series with the TD at this

frequency. At frequencies outside the amplification band, the filter was to eliminate the negative resistance of the TD. Fig.2.5 shows that at wavelengths above those at S-band the input resistance rises well above 40 Ω reaching a maximum of about 75 Ω around 1.5 Gc/s. Fig. 5.4 shows the result of adding this response in series with the experimental TD. At this stage it was hoped that instability would not be caused by the second resonance of the radial-line.

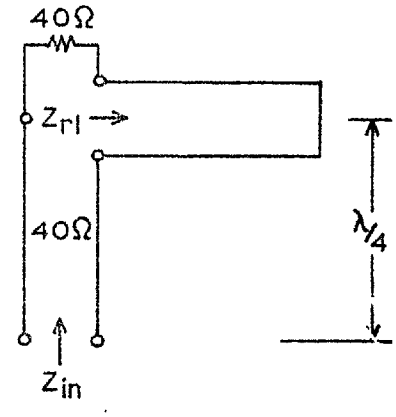

Fig.2.4: The band-rejection filter.

2.3 WAVEGUIDE IMPEDANCES SEEN BY TD

Experimental investigation to determine Z_0

Some tests were made to determine the characteristic impedance of a full height rectangular waveguide from the point of view of an obstacle mounted vertically and centrally in the waveguide. The obstacles used were narrow strips cut from resistive-film cards. Their width was about 1/20th of the waveguide broad dimension. Their ends were coated with silver paint, and they were clamped between two flanges. Their reactance was tuned out by a calibrated s.c., which terminated the set-up. The appropriate equivalent circuit[6] of the strips was assumed to be as shown in fig.2.6.

The position of the s.c. plunger was adjusted to produce the lowest possible VSWR. The distance ℓ of the plunger from the plane of the strip and the value s of the

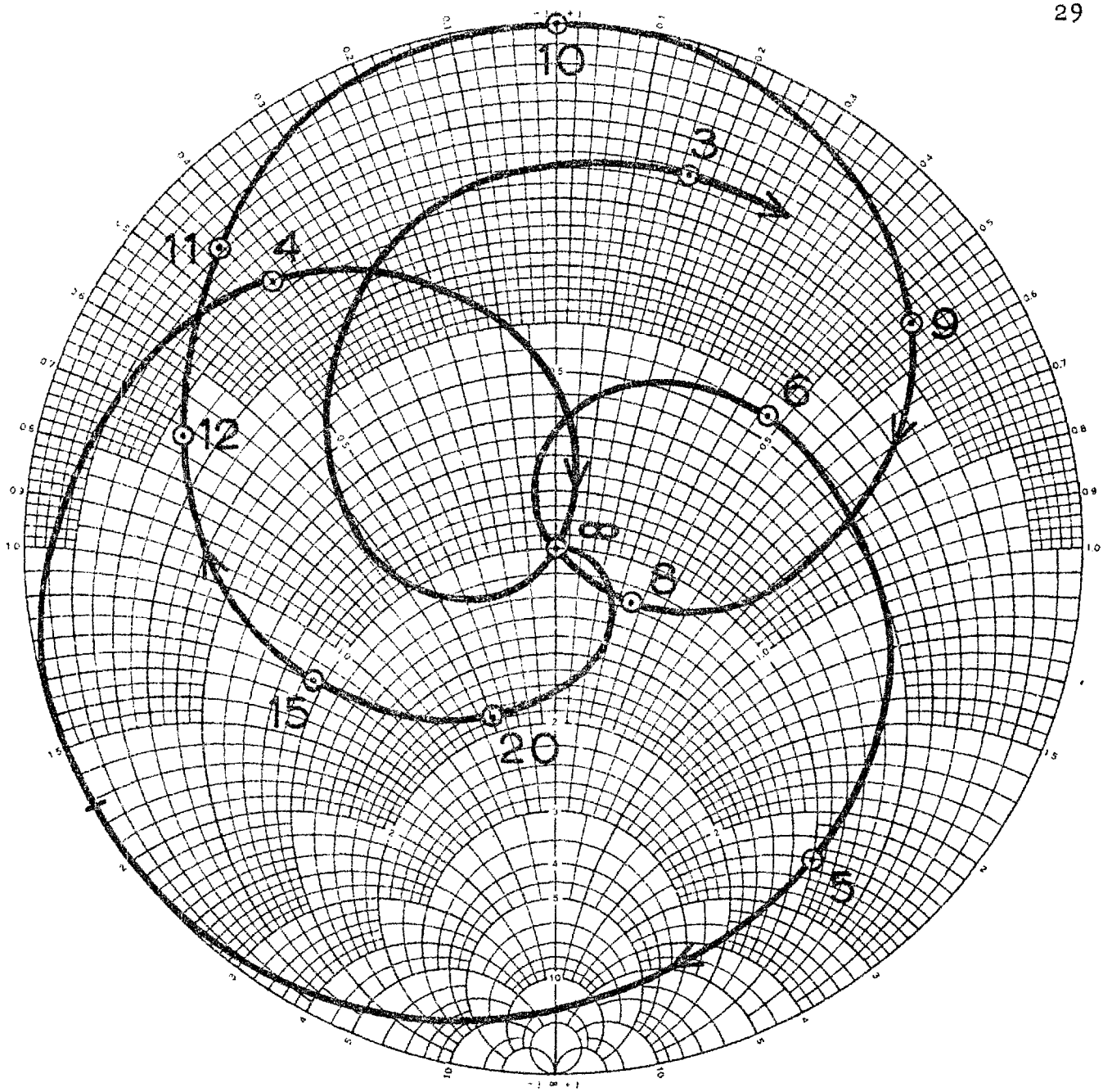

Fig. 2.5: Input impedance to band-rejection filter normalized to 40 Ω.

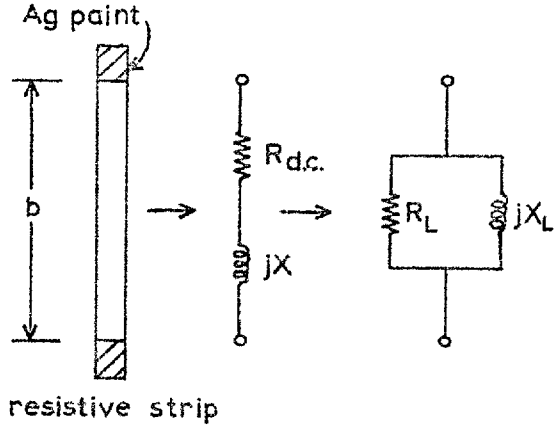

Fig.2.6: Microwave equivalent circuit of a resistive strip.

VSWR were recorded. λ_g was calculated from the positions of the minima in the usual way. The strip was then removed and R_{dc} was measured on a low frequency bridge.

Thus,

$$X_L = - Z_0 \tan \beta\ell \qquad (2.2)$$

and

$$\frac{R_L}{Z_0} = s \text{ or } \frac{1}{s} = r, \text{ say.} \qquad (2.3)$$

Therefore

$$Z_0 = \frac{r^2+\tan^2 \beta\ell}{r \tan^2 \beta\ell}.R_{dc} \qquad (2.4)$$

and

$$X = - \frac{r^2 \tan \beta\ell}{r^2+\tan^2 \beta\ell}.Z_0. \qquad (2.5)$$

Table 2.1 summarizes the result obtained from six strips at 3.047 Gc/s. The theoretical value was calculated from the voltage-power definition for the TE_{01}-mode,

$$Z_0 = Z_{fs}. \frac{2b}{a}. \frac{1}{\sqrt{(1 - (\lambda/2a)^2)}}. \qquad (2.6)$$

This experiment has confirmed the observations of other researchers,[6-10] that the appropriate characteristic impedance should be based on the voltage between the ends of the obstacle and the power flow through the waveguide. (In

Strip no.	R_{dc} Ω	tan $\beta\ell$	r	Z_0 Ω	X Ω
1	490	-2.29	1.40	481	226
2	410	-1.72	1.20	509	287
3	318	-1.36	1.045	484	244
4	302.5	-1.32	.95	484	218
5	300	-1.18	.98	517	250
6	249	-1.035	.833	491	200
	Experimental average			494	——
	Theoretical value			485	——
	Discrepancy			2%	

Table 2.1: Results of investigation to determine Z_0.

section 7.4 further experiments of a similar nature are described.) Reactive effects in the present context (final column in table 2.1) which are produced by mounting the TD in a reduced height waveguide are assumed to be accounted for by the TD's package capacitance and series inductance as given by the manufacturer.

Impedance levels and gain considerations

At 3 Gc/s Z_0 for a 3 in by 1.5 in waveguide is 493 Ω. If the parallel component of resistance of a TD (all parasi-

tics accounted for) at 3 Gc/s is, say, -40 Ω, then a load resistance of 25 Ω would produce a gain (see fig. 2.7 and section 4.2)

$$|\rho|^2 = G = \left(\frac{\frac{1}{25} + \frac{1}{40}}{\frac{1}{25} - \frac{1}{40}}\right)^2 = 18.8 \rightarrow 12.7 \text{ dB.}$$

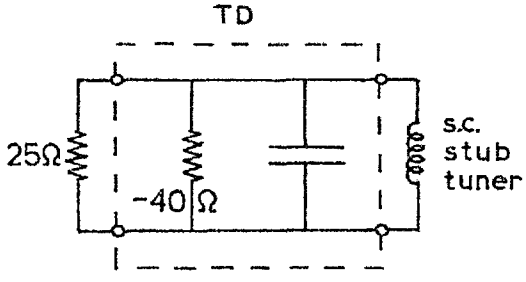

Fig. 2.7: Equivalent circuit for gain calculation.

A TD with -30 Ω produces a gain of 20.8 dB. The available TDs had resistances at 3 Gc/s typically within this range. 25 Ω was, therefore, taken as a suitable value for the TD to work into. The height b' of the reduced height section is then given by

$$b' = \frac{25}{493} \times 34.04 = 1.72 \text{ mm,}$$

where the full height b = 34.04 mm. The height of the TD pill was 1.27 mm. The difference was made up by bringing the centre rod of the coaxial-line .45 mm into the waveguide, and including this length as part of the coaxial-line structure, to a first approximation.

The exponential taper

A $3\lambda_g/2$ exponential taper[11-13] was considered a suitable transformer for this first amplifier, to transform from 493 Ω to 25 Ω. The theoretical VSWR[13] was less than 1.26 down to almost 2.4 Gc/s, and less than 1.1 from 2.91 to 3.09 Gc/s. Fig.2.8 shows the VSWR of the transformer calcu-

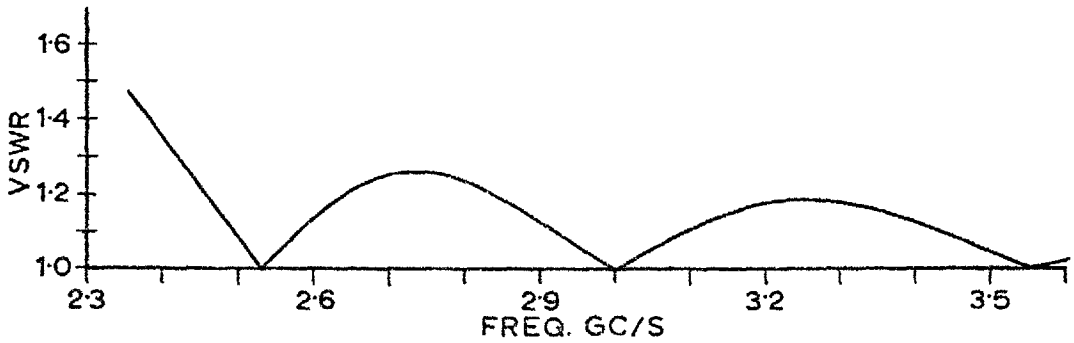

Fig. 2.8: Theoretical VSWR of the exponential taper.

lated by digital computer.* A scale drawing of the taper is shown in fig. 2.9. It was calculated from

$$b = 3.404\, e^{-\{\frac{2}{3\lambda_g} \log_e \frac{3.404}{1.72}\}z} \qquad (2.7)$$

where b is the internal height of the waveguide, z is the distance along the taper, and $\lambda_g = 13.85$ cm.

The s.c. stub

This component was to tune out the capacitive susceptance of the TD (see fig. 2.7). For convenience, Z_0 for the line containing the stub was taken as 25 Ω. (It should be noted that the best tuning element would be a lumped inductor. For s.c. lines, the higher the characteristic impedance and the shorter the line length, the closer is the approximation to the lumped case. One can not, for physical reasons, carry this argument to its logical conclusion.)

---

* The program was actually written after work on this amplifier had already ceased. It was used to calculate the input admittance to exponential lines from equations given by Bolinder.[11]

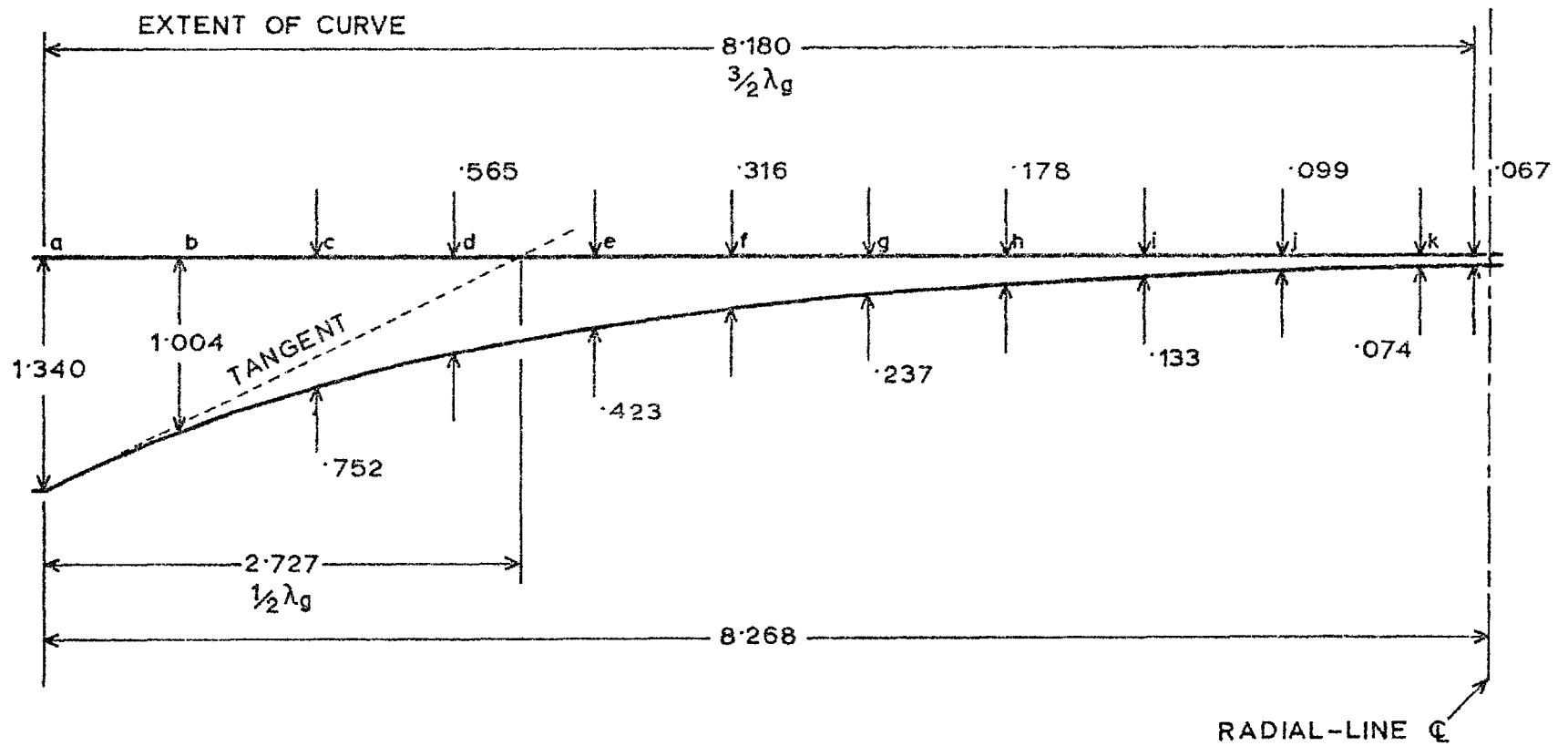

DISTANCES ab bc ... jk 2 cm

DIMENSIONS IN INCHES

Fig.2.9: The exponential taper.

2.4 CONSTRUCTIONAL DETAILS

A full size scale drawing of the important parts of the amplifier is given in fig. 2.10.

A .066 in brass plate was soldered to a 3 in by 1.5 in waveguide after a section in the shape of the exponential taper had been milled from it. To provide a rigid support during the soldering process, a 9/32 in brass plate was soldered to the top straight face (covering the whole area) of the waveguide. Another .066 plate, 7.214 cm wide, formed the adjustable s.c. stub plunger. Longitudinal 3/64 in slots were milled centrally in the top and bottom faces of the reduced height section, starting 1/4 in behind the TD position. Two 8 BA screws, flattened to fit the slots, passed through two holes in the sliding brass plate. Good contact between this plate and the waveguide could thus be achieved by tightening nuts at either end of the two screws, one of which was located as close to the leading edge of the plate as possible. The distance of a transverse line cut in the external part of the movable plate from the end of the waveguide indicated the distance of the leading edge from the TD position (coaxial-line centre-line).

The centre rod of the coaxial-line was supported and located, at one end by the resistive card, and the other by a thin polystyrene ring. Contact between the card and centre rod was maintained by a screw and washer of the same diameter as the centre rod, or smaller, the centre rod being tapped to contain the screw. The card was located by a special plate having a 1.5 in diameter recess, and fixed by three screws. The resistive-film side of the card was face down to the open-ended coaxial-line. The thickness of the card was about .017 in. A thin wire was soldered to the screw holding the card to the centre rod to link the microwave circuit to the

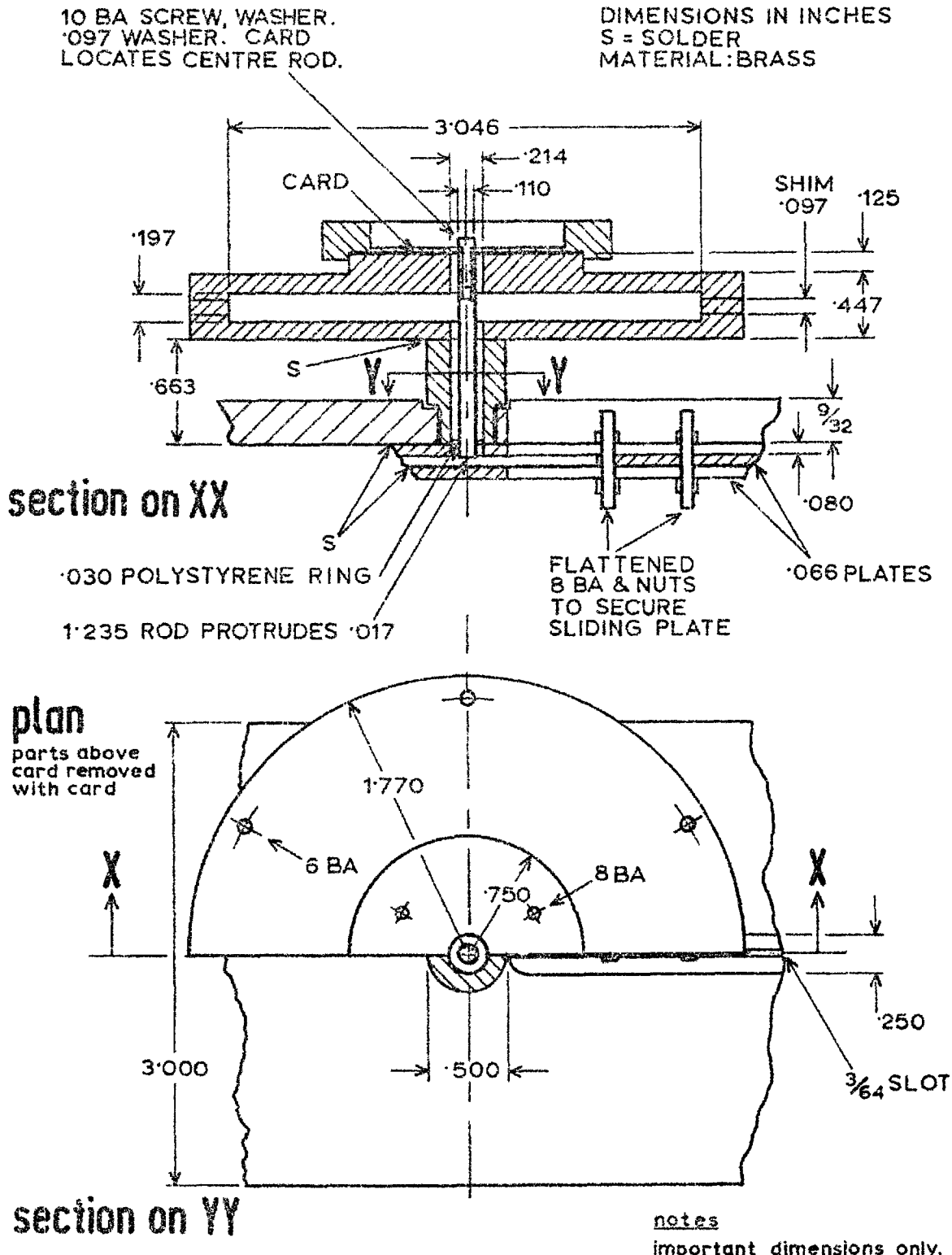

Fig.2.10: Part of S-band reflection amplifier (full size).

bias circuit.

Subsequent variation in dimensions was allowed for as follows. Some centre rods of greater diameter than the designed one were made to enable a lowering of the characteristic impedance of the coaxial-line. A number of shims for the radial-line, and washers of the same thickness for the coaxial-line (resistive card end) were made to increase or decrease the impedance of the radial-line by a small amount. Another shim to decrease the length of the radial-line, i.e. r_c, at the designed value of d by 2 mm was also made. A few 1.5 in diameter resistive cards including 400 and 200 Ω/square were prepared.

Fig.2.11 is a photograph of the final assembly.

2.5 Conclusion

Curves predicting the performance of the radial-line band-rejection filter have been given. The use of the voltage-power definition of Z_0 as the waveguide impedance seen by the TD for dominant mode propagation has been experimentally justified. The "centre frequency" gain for a typical range of TDs has been computed and found to be reasonable. Sufficient details of the design and construction of the S-band rectangular waveguide reflection amplifier have been presented. An account of its performance, both predicted and experimental, is found in chapter 5.

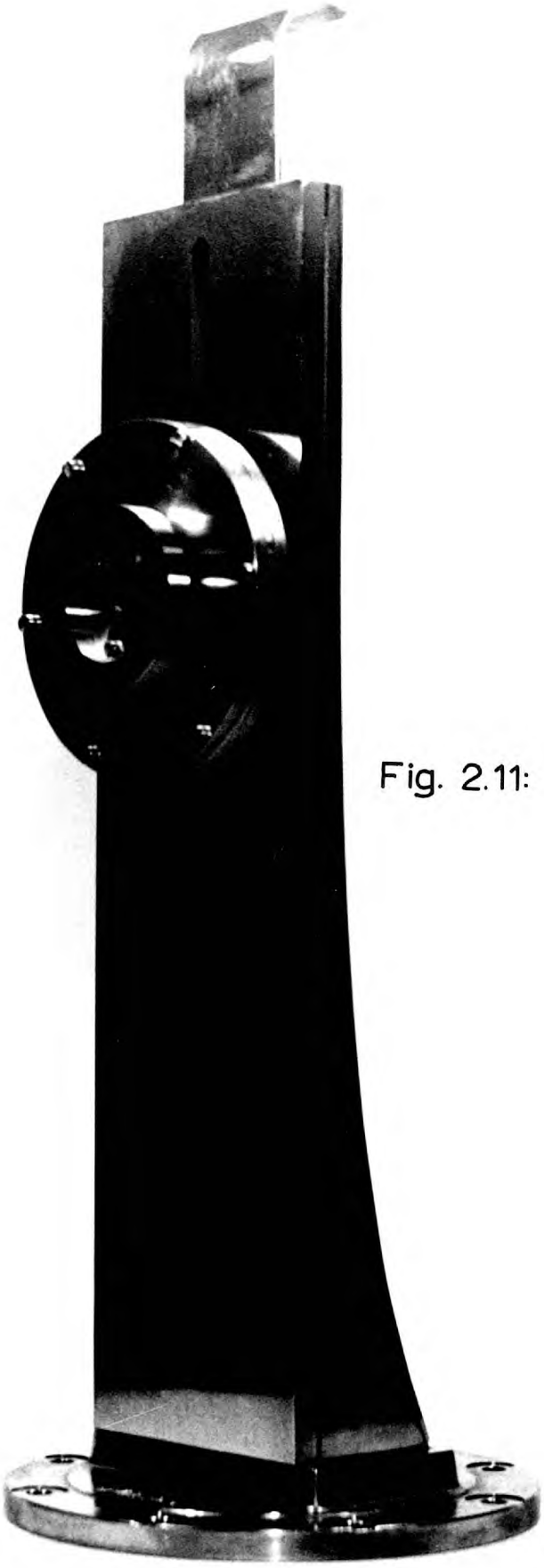

Fig. 2.11: TDA 1

2.6 References

(1) B.C. DeLoach Jr., "Radial line coaxial filters in the microwave region", IEEE Trans. Vol. MTT-11, pp.50-55, January 1963.

(2) M.A.R. Gunston, "An empirical formula for the design of radial line filters", IEEE Trans. Vol. MTT-12, pp.571-572, September 1964.

(3) S. Ramo and J.R. Whinnery, "Fields and waves in modern radio", Wiley, New York, 1953 (second edition), pp. 395-401.

(4) R.F. Harrington, "Time-harmonic electromagnetic fields", McGraw-Hill, New York, 1961, pp.110-113.

(5) A. Wexler, "Attenuating films in rectangular waveguide", Ph.D. thesis, University of London, 1966. Section (6.1).

(6) J. Brown, "Reactive effects in transverse-film bolometers in rectangular waveguides", Proc. IEE, Vol. 110, pp.77-78, January 1963.

(7) B.C. DeLoach, "A new microwave measurement technique to characterize diodes and an 800-Gc cutoff frequency varactor at zero volts bias", IEEE Trans. Vol. MTT-12, pp. 15-20, January 1964.

(8) J.A. Lane, "A physical interpretation of impedance for rectangular waveguides", Proc. Phys. Soc. Vol.70B, p. 1173, 1957.

(9) J.A. Lane and D.M.Evans, "The design and performance of transverse-film bolometers in rectangular waveguides", Proc. IEE, Vol.108B, pp.133-135, January 1961.

(10) W.J. Getsinger, "The packaged and mounted diode as a microwave circuit", IEEE Trans. Vol. MTT-14, pp.58-69, February 1966.

(11) F. Bolinder, "Fourier transforms in the theory of inhomogeneous transmission lines", Trans. of the Royal Inst. of Technology, Stockholm, No.48, 1951, pp.18-27.

(12) A.H. Hall, "Impedance matching by tapered or stepped transmission lines", Microwave J., Vol.9, pp.109-114, March 1966.

(13) "The microwave engineers handbook", Horizon House, USA, 1966, p.9.

3

stability analysis in the H-planes

3.1 Introduction

Using the Nyquist method, a technique is presented for predicting the stability of TDAs utilizing the immittance (i.e. impedance or admittance) planes. Publications of direct relevance are[1-17].

The technique* begins with a determination of the RH p-plane immittance poles and zeros associated with the TD

---

*The technique described in this chapter forms part of a paper published in the IEEE Transactions on Microwave Theory and Techniques[1]. After this work was done and submitted for publication, it was discovered that Henoch and Kvaerna had already considered the problem from a similar point of view. The reference to their Stanford University report[2] was obtained from Kvaerna's paper[4] published in Norway. Their previous correspondence[3] had given no indication of how they had considered the problem in general, apart from a useful stability criterion. There was, unfortunately, an inevitable time lag in sorting out the references and reading the large volume of literature on TDAs and related subjects.

equivalent circuit; a series of systematic inversions from impedance to admittance planes follows, a new circuit block being added after each inversion; the resulting RH p-plane poles and zeros are noted in conjunction with the relevant Nyquist-type plots each time a block is added. In this way, the necessary requirements for stability of TDAs can be predicted. The technique is especially useful in dealing with interconnections of microwave networks which may not, in general, have commensurate frequency responses, either with the TD or with each other.

3.2 THEORY OF NYQUIST-TYPE STABILITY CRITERION

A theorem

Chapters VII - IX of Bode's book[5] form an adequate background to the ensuing discourse. Only the most pertinent concepts are quoted here, for the sake of completeness. The following fundamental theorem derived from Cauchy's theory of analytic functions is found on page 149 of Bode:

> If a function f(z) is analytic, except for possible poles, within and on a given contour (in the z-plane)* the number of times the plot of f(z) encircles the origin of the f(z) plane (in the f(z)-plane) in the positive direction (i.e. counterclockwise), while z itself moves around the prescribed contour once in a clockwise direction, is equal to the number of poles of f(z) lying within the contour diminished by the number of zeros of f(z) within the contour, when each zero and pole is counted in accordance with its multiplicity.

For the purpose of analyzing the stability of electrical networks, the function f(z) often chosen is a characteristic immittance function H corresponding essentially to the characteristic differential equation of the network. The function may be denoted H(p), where $p = \sigma + j\omega$ is defined as

---

*The expressions in brackets are mine.

complex frequency; it can be obtained either by formulating the total impedance $Z_T(p)$ seen around a loop, or the total admittance $Y_T(p)$ seen between two terminals of the network. For stability, i.e. to ensure a decaying transient response to any applied signal or other electrical disturbance, no solutions for $H(p) = 0$ should exist for $\text{Real}(p) > 0$. In other words, $H(p)$ must have no zeros in the RH (right half) p-plane.

The contour for this analysis must, in general, enclose the entire RH p-plane (see fig. 3.1), so that p moves positively up the real frequency (i.e. $j\omega$) axis, avoiding singularities on this axis by small semicircular indentations into the RH plane, and clockwise (CW) around an infinite semicircle standing on the $j\omega$-axis, centred at the origin and lying in the RH p-plane. It is inconvenient, however, to deal with an infinite semicircle. This limitation can be alleviated by the following considerations. Suppose

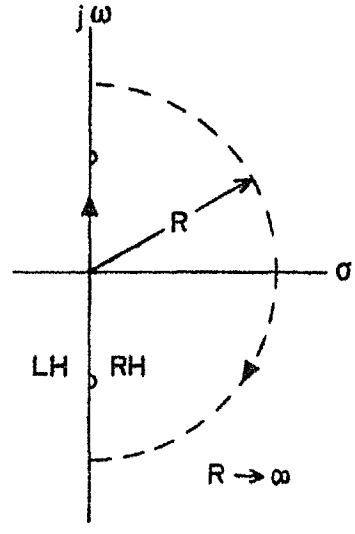

Fig. 3.1: p-plane.

$$Z(p)\Big|_{p \to \infty} \to \frac{1}{pC} \qquad (3.1)$$

then an infinite semicircular CW motion in the RH p-plane corresponds to an infinitessimal semicircular CCW motion in the RH Z(p)-plane. Suppose

$$Z(p)\Big|_{p \to \infty} \to R \qquad (3.2)$$

then the whole of the infinite semicircular arc in the RH p-plane coalesces into a single point in the RH Z(p)-plane. Suppose

$$Z(p)\Big|_{p \to \infty} \to pL \qquad (3.3)$$

then an infinite semicircular CW motion in the RH p-plane corresponds to a similar infinite motion in the RH Z(p)-plane.

Corresponding statements can be made about $Y(p)\Big|_{p\to\infty}$. These results are summarized in table 3.1.

function	limiting cases as $p \to \infty$		
Z(p)	$\frac{1}{pC}$	R	pL
Y(p)	$\frac{1}{pL}$	G	pC
closing loop in RH H(p)-plane	small CCW	single point	large CW

Table 3.1: Limiting cases in the transformation from p- to H(p)-plane.

Application to TDA stability

It is fortunate that part of the contour in the p-plane involves a steady-state real frequency response of the network under consideration, because

(i) in the case of a TDA it is required anyway,

(ii) it is a widely used and readily measured characteristic describing microwave networks of any complexity, and

(iii) it can be usefully displayed on a Smith chart.

The rest of the contour is accounted for by determining which of the limiting cases given by table 3.1 the circuit can be reduced to as p or $j\omega \to \infty$. The problem is further simplified by the fact that above ω_R no external negative resistance is exhibited by the TD, by definition of ω_R:

in this case all jω plots terminate somewhere in the RH H-plane*; and it is justified to draw an arbitrary loop from just above ω_R to just below $-\omega_R$ in the RH H-plane regardless of which of the three limiting cases the circuit is reducible to.

The number of CCW encirclements of the H-plane origin is equal to the number of poles minus the number of zeros of H(p) in the RH p-plane, consequently a stable network has an H(jω) which encircles the origin in a CCW manner as many times as it has poles in the RH p-plane. It follows from the even and odd symmetry of the real and imaginary components of H(jω), respectively, that a plot of H(jω) from $-j\infty$ to 0 is a mirror image of the plot from 0 to $+j\infty$ with respect to the real axis of the H-plane. In practice, therefore, H(jω) is computed for positive ω only - in the case of a TDA, to just above ω_R.

A stable TDA is one for which $Z_T(p)$ around any chosen loop, or $Y_T(p)$ between any chosen set of terminals has no zeros in the RHp-plane. If a certain amplifier configuration is liable to have such zeros, a special "stabilizing" network must be added to an appropriate part of the circuit to eliminate them. A knowledge of the poles of $Z_T(p)$ or $Y_T(p)$ in the RH p-plane and the corresponding responses $Z_T(j\omega)$ or $Y_T(j\omega)$ to just above ω_R is sufficient to deduce the number of relevant zeros, and hence the stability or otherwise of the amplifier.

---

*The terms H-, Z-, and Y-plane are used hereafter to avoid confusion of H(p)-, Z(p)-, and Y(p)-plane with H(jω)-, Z(jω)-, and Y(jω)-plane, respectively, the latter being strictly a special representation of functions of jω in the former planes.

3.3 TD EQUIVALENT CIRCUIT

It is reaffirmed that the TD equivalent circuit parameters are taken, for simplicity, to be frequency independent. Poles referred to as P and zeros referred to as Z are all contained within the RH p-plane.

Some simplified equivalent circuits

The equivalent circuit is often simplified to a parallel -G, C combination as shown in fig. 3.2(a), mainly in theoretical treatments of broadband TDAs.[18-21] This circuit has an impedance pole in the RH p-plane at

$$p = {}^{G}/_{C} \tag{3.4}$$

which is characteristic of the TD. It can be stabilized by the addition of a positive G', where

$$G' > G . \tag{3.5}$$

Note that G' can theoretically be infinite, hence the circuit is termed short-circuit (s.c.) stable.

In other theoretical treatments of broadband TDAs[22-24] the series inductance L is added as shown in fig. 3.2(b). This circuit is neither s.c. stable nor open-circuit (o.c.) stable. Its stability, when a positive resistor R' is added to it, is confined within the range

$$\frac{LG}{C} < R' < \frac{1}{G} \tag{3.6}$$

Fig. 3.2(c) shows L replaced by the series resistance r. This configuration is s.c. stable. It remains stable for added positive resistor R' if

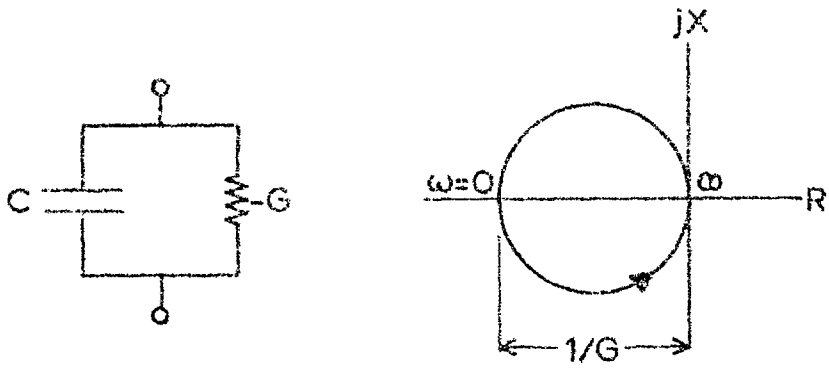

stability

P	Z	oc	sc
1	0	x	✓

(a)

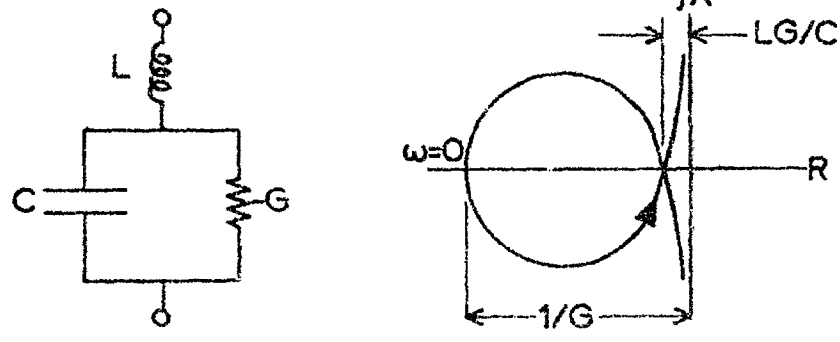

P	Z	oc	sc
1	2	x	x

(b)

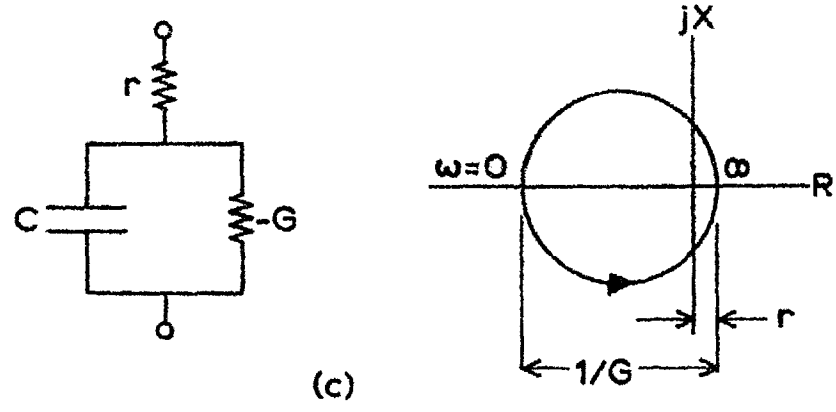

P	Z	oc	sc
1	0	x	✓

(c)

Fig.3.2: Simplified TD equivalent circuits. The numbers of poles and zeros associated with each circuit are given in columns 1 and 2, respectively; columns 3 and 4 indicate whether the circuits are o.c. and s.c. stable, respectively.

$$R' < \frac{1}{G} - r \qquad (3.7)$$

The complete equivalent circuit

This is reproduced in fig. 3.3. The impedance $Z_D(p)$ seen between its terminals is given by

$$Z_D(p) = r + pL + \frac{1}{-G + pC} . \qquad (3.8)$$

$Z_D(p)$ has an RH p-plane pole at $p = G/C$, and a pole at ∞.* The conditions for $Z_D(p) = 0$ to have no solutions for Real(p) > 0, i.e. the conditions for s.c. stability, are obtained from[6,9,25-29],**

$$p = -\frac{1}{2}\left(\frac{r}{L} - \frac{G}{C}\right) \pm \sqrt{\frac{1}{4}\left(\frac{r}{L} - \frac{G}{C}\right)^2 - \frac{1 - rG}{LC}} . \qquad (3.9)$$

These conditions are***

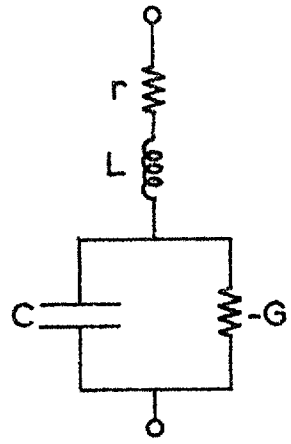

Fig. 3.3: TD equivalent circuit

---

*This pole does not directly influence stability. Its presence, however, permits the use of an arbitrary CW loop in the RH Z-plane joining the ends of the $Z_D(j\omega)$ plot (see fig. 3.4), in accordance with (3.3).

**Note that misprints have occurred in references[6,25-27] in this or one of the derived conditions given by (3.10) and (3.11).

***They are also valid in determining stability when external resistance R' and inductance L' are added (neglecting the package capacitance), in which case r + R' replaces r and L + L' replaces L.

$$\frac{r}{L} - \frac{G}{C} > 0 \tag{3.10}$$

and

$$1 - rG > 0 \tag{3.11}$$

or

$$\frac{LG}{C} < r < \frac{1}{G} \,. \tag{3.12}$$

Alternatively, this condition can be written as (see section 1.3 for definitions)

$$\omega_R < \omega_X \tag{3.13}$$

where both ω_R and ω_X must be real.* If

$$\omega_R > \omega_X \tag{3.14}$$

(with the above proviso) then

$$r < \frac{LG}{C} < \frac{1}{G} \,. \tag{3.15}$$

This TD has a conjugate pair of zeros in the RH p-plane, whose location is obtainable from (3.9).

Both types of TD can be used for microwave amplification when suitable external networks are provided. Their Nyquist-type impedance plots $Z_D(j\omega)$ are sketched in fig.3.4. Davidsohn et al.[6] and Blaeser[9] derive and discuss these and similar curves in the more general context of the addition of external series resistance and inductance, and the possible modes of instability.

It is noted that a practical TD is never o.c. stable, but it may or may not be s.c. stable according to whether its frequency response is like fig. 3.4 (b) or fig. 3.4 (a), respectively.

---

*In general, ω_R and ω_X can be either positive or imaginary only. The use of $\omega_R < 0$, or $\omega_X < 0$ or similar expressions in postulating modes of instability[6,25] is strictly erroneous.

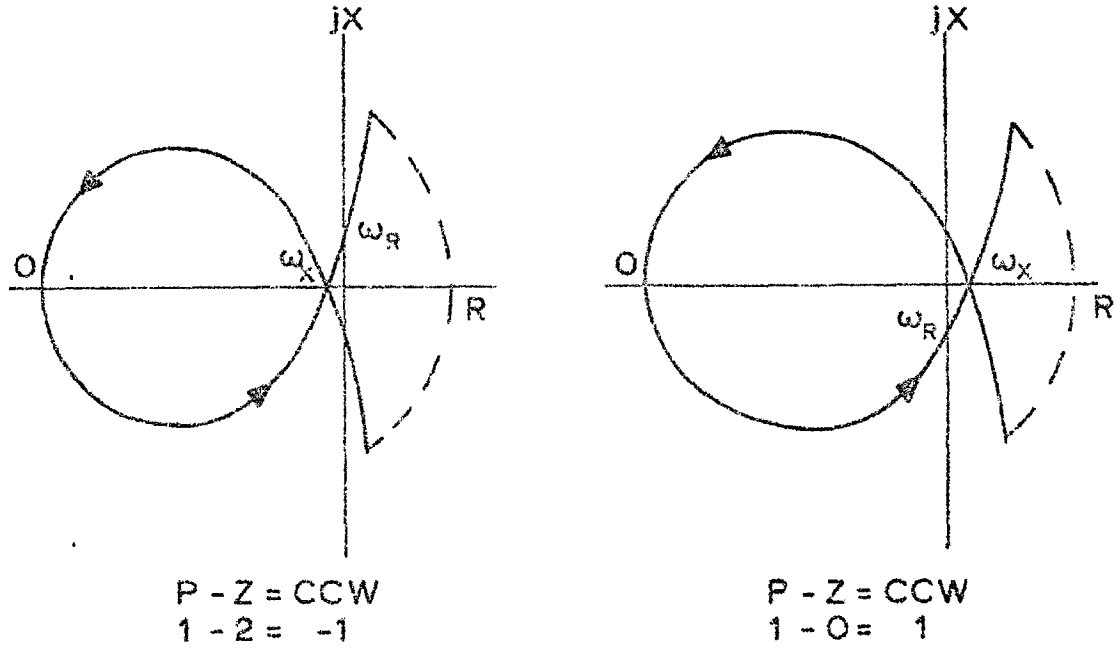

(a) $\omega_R > \omega_X$ (b) $\omega_R < \omega_X$

Fig. 3.4: TD impedance characteristics $Z_D(j\omega)$.

3.4 THE IDEAL STABILIZING NETWORK

For complicated microwave arrangements including band-limited circulators, it is usually necessary to unconditionally stabilize the amplifier over the whole frequency spectrum outside the desired amplification band. At this juncture, a definition of the ideal stabilizing network is in order:

The ideal stabilizing network when added to a tunnel-diode prevents instability at all frequencies except in the desired amplification band for an arbitrary variation in value of any component forming part of the source and load of the signals to be amplified. Within the amplification band (so as not to deteriorate the performance of the amplifier) it exhibits zero immittance.

With a series stabilizing network, for instance, unconditional stability above the amplification band is realized by providing enough resistance in series with the TD to lower, effectively, its resistive cut-off frequency. (If the same network is also used for biasing, (3.31) must hold. See also fig. 3.9.)

3.5 TYPES OF AMPLIFIER

There exist many ways of realizing microwave TDAs, whether reflection or transmission. It is convenient, for the present anlaysis, to classify them as in fig. 3.5. The microwave structures illustrated are not necessarily the simplest possible, nor the most complicated. They are proposed with three main provisos:

(i) any shunt element (resistor or s.c. line) must not be connected directly to the TD terminals 1 or 2,

(ii) the stabilizing (and biasing) network is distinct from the rest of the circuit, and

(iii) the TD parasitic or package capacitance is always present.

Restriction (i) can be overcome, geometry permitting; restriction (ii) if the resulting lack of flexibility can be tolerated; restriction (iii) to some extent by building the TD into the microwave structure.

More complicated realizations, e.g. with double tuning, can be conceived. There is, however, no loss of generality in describing the method of analyzing the stability of TDAs by choosing the configuration of fig. 3.5 (d). This type represents, essentially, the S-band reflection

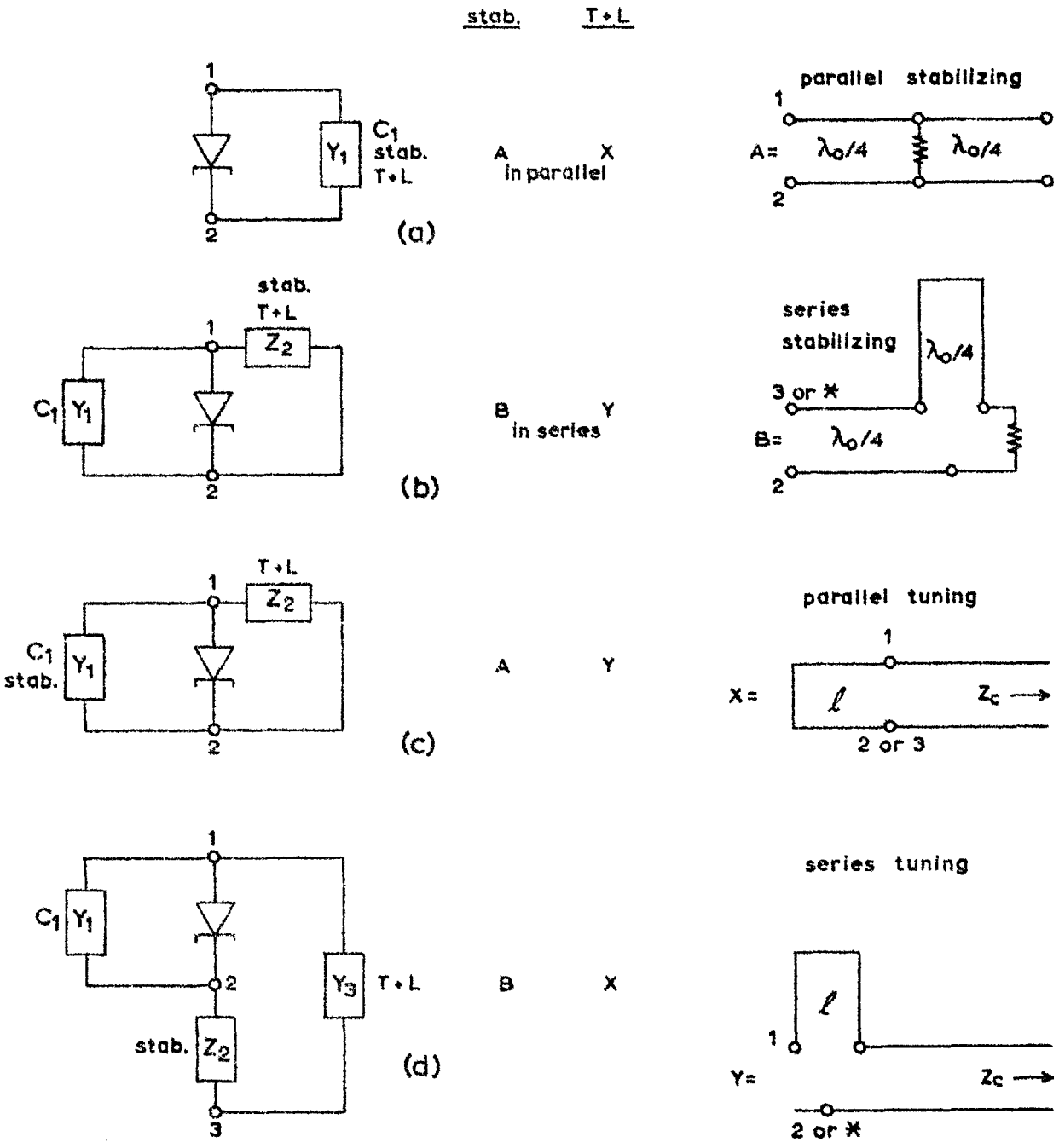

notes: stab. = stabilizing (and biasing) network
T+L = tuning and loading arrangement
stab. and T+L to be connected by the numbered terminals. $\ell < \lambda_o/4$.

Fig.3.5: Some configurations of TDA for stability analysis purposes; and simple microwave realizations. The stabilizing circuits A and B and the tuning and loading circuits X and Y have their terminals numbered so that their interconnections in the amplifier can be readily determined.

amplifier of chapter 2.

3.6 THE CONSEQUENCES OF ADDING THE PACKAGE CAPACITANCE

$Z_D(p)$ is inverted to give $Y_D(p)$:

$$Y_D(p) = \frac{1}{Z_D(p)} = \frac{pC - G}{p^2LC + p(rC - LG) + 1 - rG} . \tag{3.16}$$

The allowable forms of $Y_D(j\omega)$ are shown in fig. 3.6. Note that the poles and zeros of $Y_D(p)$ are given, respectively, by the zeros and poles of $Z_D(p)$. For the case of fig. 3.5 (d)

$$Y_1(p) = pC_1 . \tag{3.17}$$

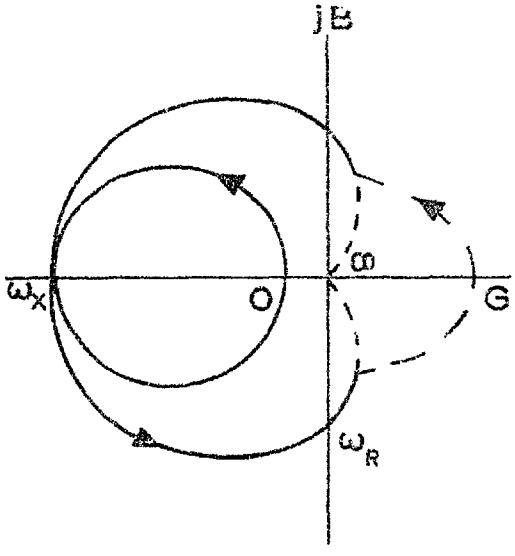

P - Z = CCW
2 - 1 = 1

(a)

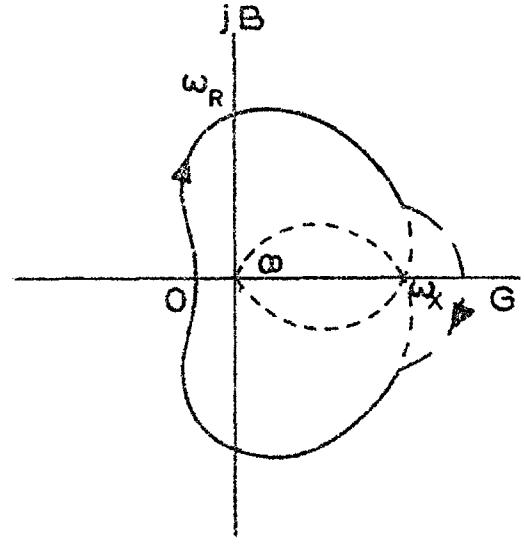

P - Z = CCW
0 - 1 = -1

(b)

Fig. 3.6: TD admittance characteristics $Y_D(j\omega)$.

Defining

$$Y_1' = Y_1 + Y_D \tag{3.18}$$

gives

$$Y_1'(p) = C_1\left[\frac{p^3 + p^2(rC-LG)/LC + p\{C + C_1(1-rG)\}/C_1LC - G/C_1LC}{p^2 + p(rC - LG)/LC + (1-rG)/LC}\right] \tag{3.19}$$

Clearly, the poles of $Y_1'(p)$ are identical to those of $Y_D(p)$, except for an added pole at ∞* given by

$$Y_1'(p)\Big|_{p\to\infty} \to pC_1 . \tag{3.20}$$

In general, the numerator of $Y_1'(p)$ has three roots:

(i) all roots real

(ii) all roots real; at least two are equal, and

(iii) one root real; the rest form a complex conjugate pair.

The plots of $Y_1(j\omega)$ shown in fig. 3.7, the only types possible, can be used to determine on which side of the jω-axis in the p-plane these roots, and hence the zeros of $Y_1'(p)$, fall. Note that since Y_1 is purely capacitive, the curves of fig. 3.6 are distorted only in the jB direction, thus ω_R remains unchanged. If the poles of $Y_1'(p)$ are located at p_1 and p_2, and the zeros at z_1, z_2, and z_3, it is interesting to observe that

$$z_1 + z_2 + z_3 = p_1 + p_2 = \frac{LG - rC}{LC} . \tag{3.21}$$

Since

$$p_1p_2 = \frac{1 - rG}{LC} \tag{3.22}$$

*Its significance is explained in section 3.2.

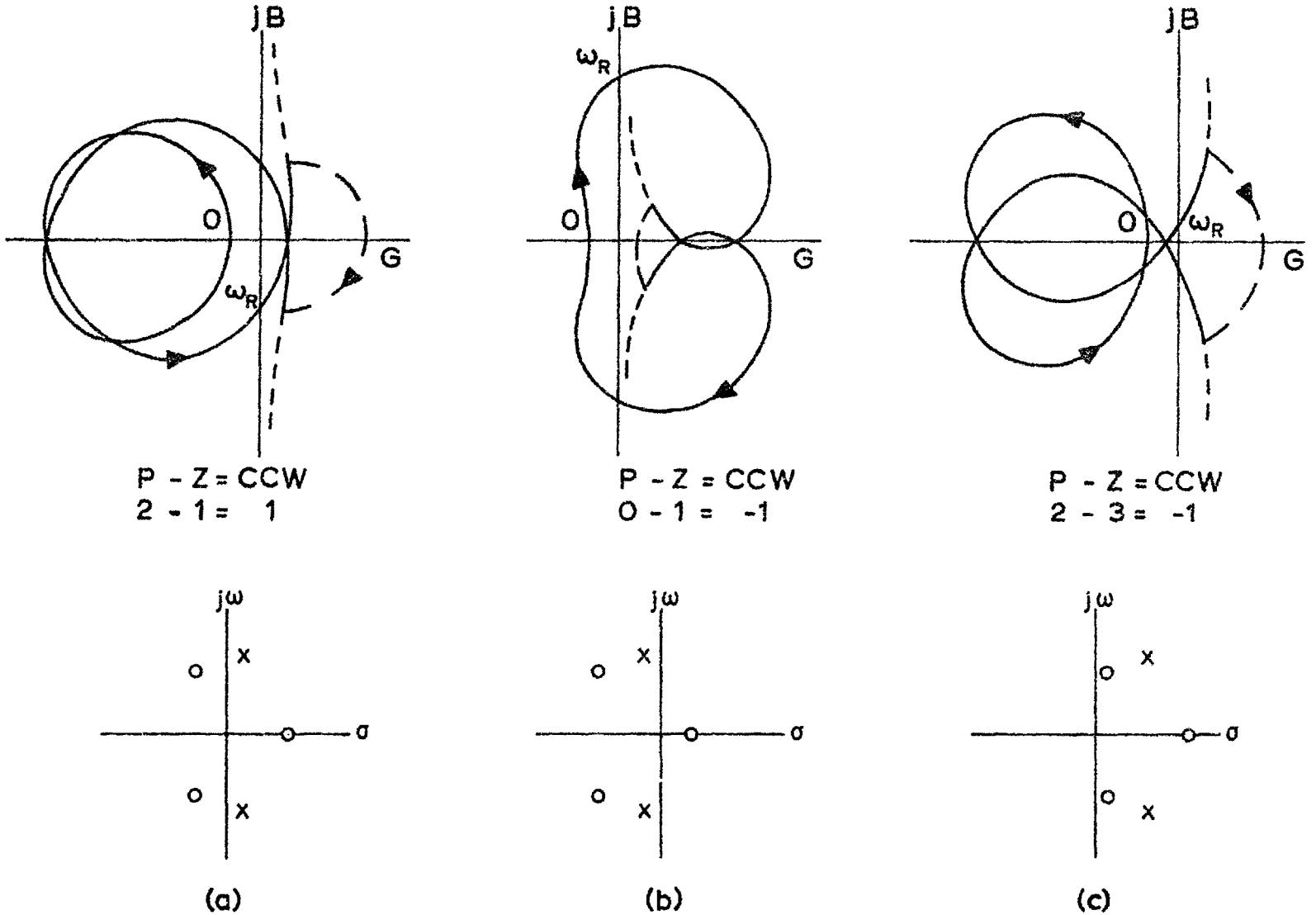

Fig.3.7: Y-plane sketches of $Y_1'(j\omega)$, and relative locations of the p-plane poles and zeros of $Y_1'(p)$.

and the only concern is with $r < 1/G$, p_1 and p_2 are found in the LH p-plane if $r > LG/C$ and in the RH p-plane if $r < LG/C$ (see section 3.3).

$$z_1 z_2 z_3 = \frac{G}{C_1 CL} \quad , \tag{3.23}$$

thus either we have two zeros in the LH p-plane and one in the RH p-plane, or all three in the RH p-plane. One possible arrangement of these poles and zeros is shown in fig. 3.7 under the corresponding $Y_1'(j\omega)$ curves.

$$\text{Now} \quad Y_1'(j\omega)\Big|_{\omega = \omega_R} = j\omega_R C_1 + \frac{1}{r + j\omega_R L + \frac{1}{-G + j\omega_R C}}$$

$$= j\omega_R C_1 + \frac{1}{j\omega_R L - \frac{j\omega_R Cr}{G}} \tag{3.24}$$

For

$$Y_1'(j\omega)\Big|_{\omega = \omega_R} < 0 \tag{3.25}$$

it follows that

$$C_1 < \frac{1}{\omega_R^2 (L - Cr/G)} \tag{3.26}$$

where

$$\omega_R = \frac{G}{C}\sqrt{\frac{1}{Gr} - 1} > 0 \text{ and real.} \tag{3.27}$$

Under these conditions the case of fig. 3.7(c) does not arise. If

$$r > LG/C \tag{3.28}$$

(see fig. 3.4 (b)) (3.25) can never be satisfied, hence (3.26) is invalid. In this case we obtain fig. 3.7 (b).

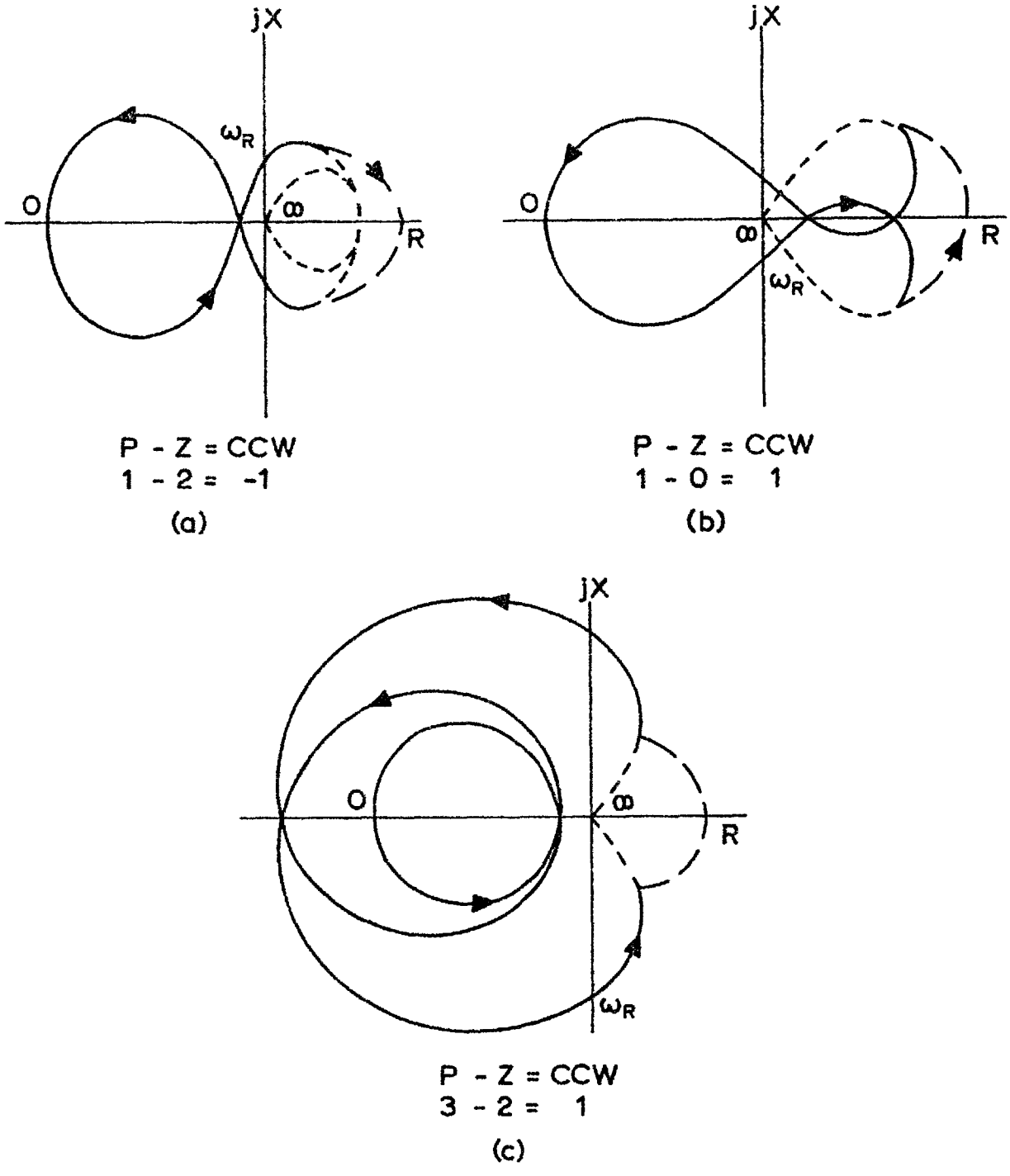

Fig.3.8: Z-plane sketches of $1/Y_1'(j\omega)$, the inversion of the curves of fig.3.7.

Now

$$Y_1'(j\omega)\Big|_{\omega = \omega_X} = j\omega_X C_1 + \frac{1}{r + j\omega_X L + \frac{1}{-G + j\omega_X C}}$$

$$= j\omega_X C_1 + \frac{1}{r - \frac{GL}{C}} \quad . \tag{3.29}$$

By definition of ω_X (see section 1.3), the imaginary component of $Y_1'(j\omega)$ for $\omega < \omega_X$ is always capacitive, thus the effect of C_1 is actually to increase the effective "ω_X" of the TD.*

3.7 ADDITION OF STABILIZING NETWORK

The curves of fig. 3.7 are next inverted into the Z-plane, resulting in fig. 3.8. Notice that the general form of the curves between $\omega = 0$ and the first cut-off frequency is, as expected, much the same as those of fig. 3.4.

The impedance Z_2' between terminals 1 and 3 of fig. 3.5 (d) is given by

$$Z_2' = Z_2 + 1/Y_1' \quad . \tag{3.30}$$

Fig.3.9 shows two simple forms $Z_2'(j\omega)$ can take.** The

---

*This fact is of no use in the design of broadband TDAs. C_1 limits the potential bandwidth, as discussed by Getsinger,[30] so it should, in practice be minimized as much as possible along with r, L, and C. There is, therefore, no point in formulating the new "ω_X" value: it is not important as a design parameter.

**For clarity, the curves for $-\omega$ will not be shown from now on.

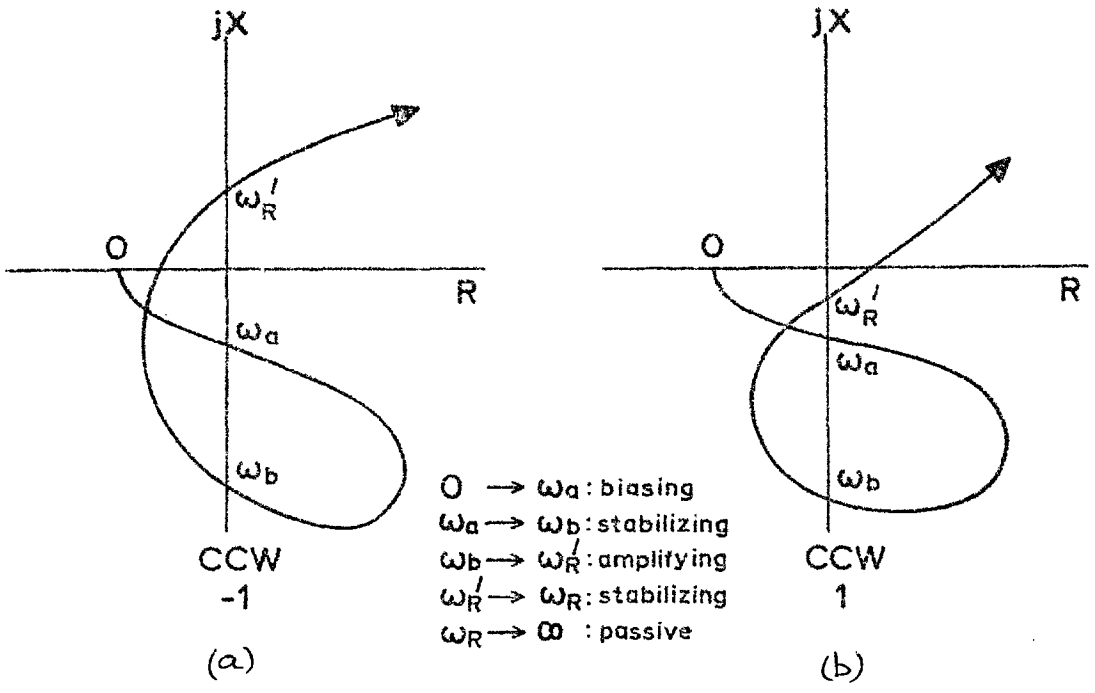

Fig. 3.9: Z-plane sketches of $Z_2'(j\omega)$.

p-plane poles associated with fig. 3.8 are carried through, and the resulting pole-zero arrangement associated with fig. 3.9 is summarized in table 3.2.

Fig.	Poles	Zeros Z	
	P	3.9 (a)	3.9 (b)
3.8 (a)	1	2	0
3.8 (b)	1	2	0
3.8 (c)	3	4	2

Table 3.2: RH p-plane poles and zeros of $Z_2'(p)$

The curve of fig. 3.8 (c) is seen to have 3 RH p-plane poles associated with it (given by z_1, z_2, and z_3, the

zeros of $Y_1'(p)$). It is not obvious what will happen to the locus in the region in the LH Z-plane where the magnitude of the real component is greater than its d.c. value, the nature of the encirclements and hence stability being in some doubt. In fig. 3.9 and table 3.2, further encirclements above ω_R' are assumed nonexistent.

Now the TD has one RH p-plane pole. If it is connected in series with any passive network (C_1 forming part of it), which itself has neither poles nor zeros in the RH p-plane (by definition of passive), the nature of this pole is unchanged. Since the stability of the complete loop depends on eliminating RH p-plane zeros, the Nyquist plot of $Z(j\omega)$ around the loop must encircle the Z-plane origin once in a CCW direction.* This can only be realized if the plot starts in the LH Z-plane at $\omega = 0$ (since it ends in the RH Z-plane), as illustrated by fig. 3.10. Hence, the total d.c. resistance external to the TD, R_b say, must satisfy

$$R_b < \frac{1}{G} - r \qquad (3.31)$$

for stability.

---

*Henoch and Kvaerna's basic stability criterion[2-4] is: "A tunnel-diode amplifier is stable if and only if the sum of the diode impedance and the connected network impedance plotted as a function of frequency encircles the origin once in a counter-clockwise direction when the plot is closed with an arbitrary line in the right-half Z-plane between the positive and negative diode cut-off frequency. The diode cartridge capacitance is considered to belong to the network connected to the diode."

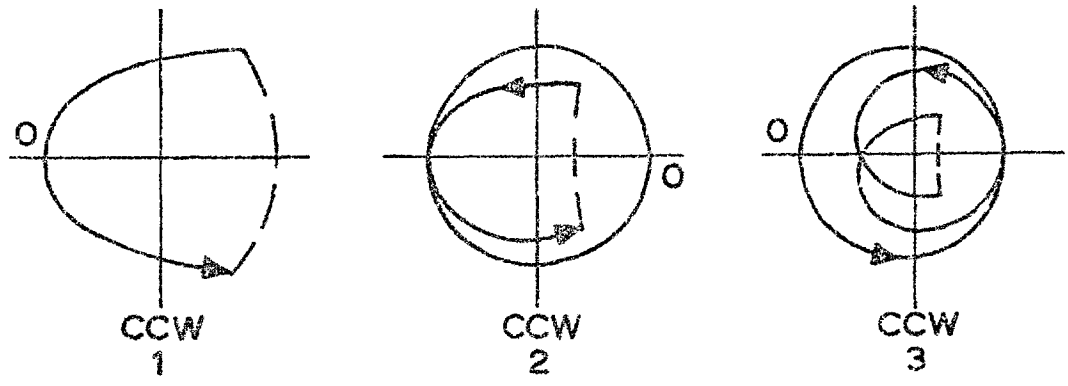

Fig. 3.10: Counterclockwise encirclements.

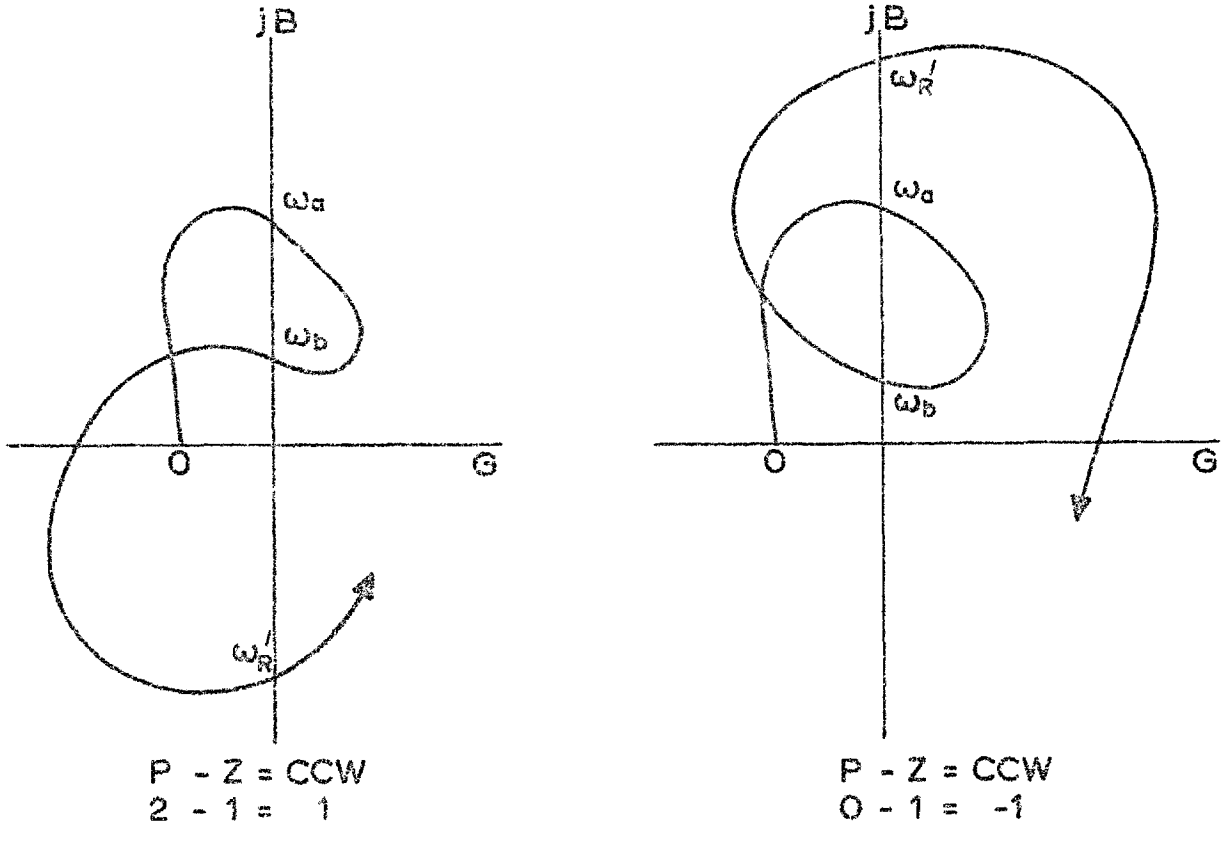

(a) (b)

Fig. 3.11: Inversion of curves of fig. 3.9 to give $Y_2'(j\omega)$.

3.8 THE CONNECTED AMPLIFIER

The remaining discussion considers the cases of figs. 3.8 (a) and (b) only.

The poles and zeros of $Z_2'(p)$ transform to the zeros and poles of $Y_2'(p)$, respectively: fig. 3.11 shows sketches of $Y_2'(j\omega)$. For final stability of the connected amplifier $Y_3(p)$ (see fig. 3.5 (d)) must ensure that

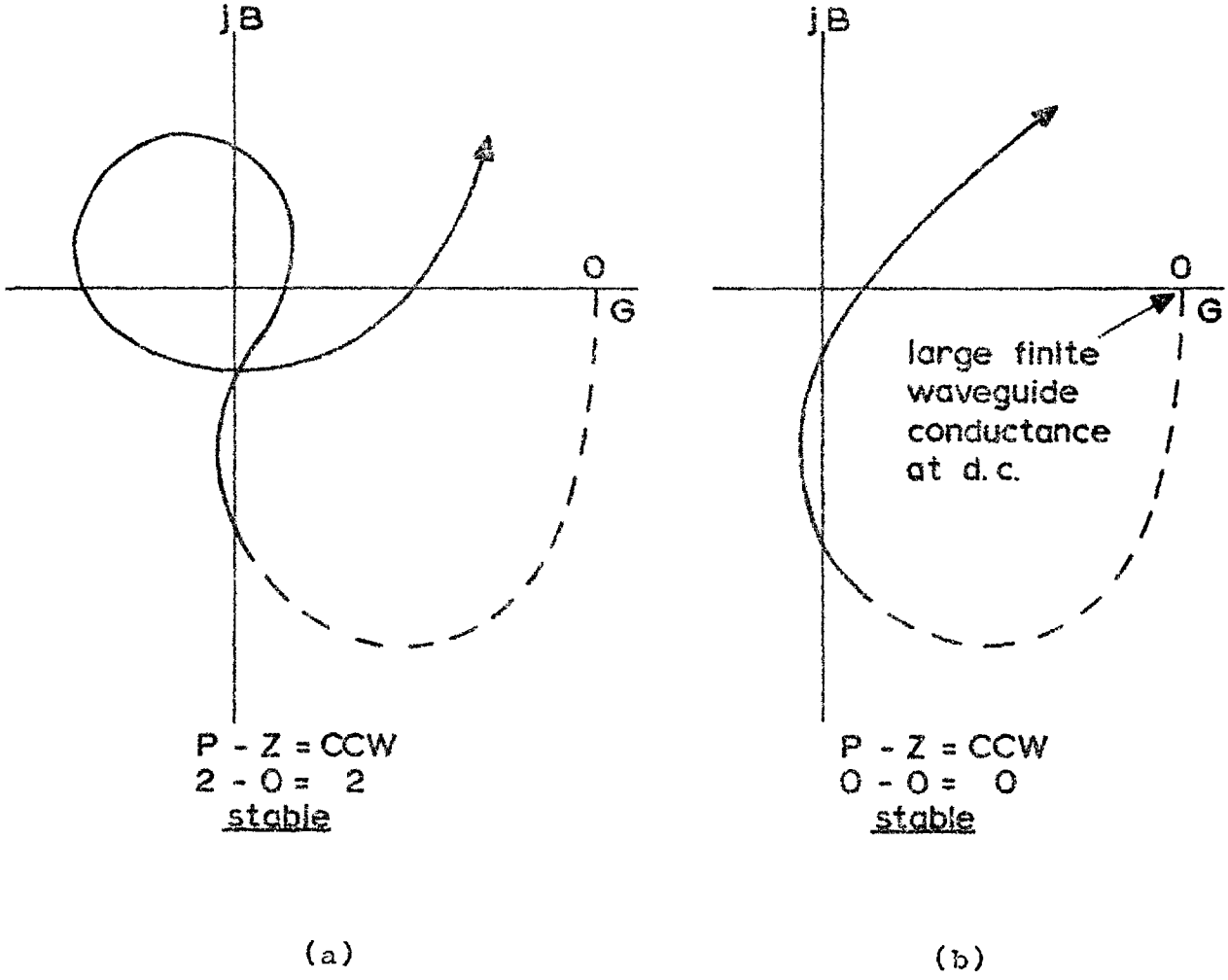

(a) (b)

Fig. 3.12: $Y_T(j\omega)$ when $Y_3(j\omega)$ is defined for a simple rectangular waveguide system such as shown in fig. 2.1.

$$Y_T(p) = Y_2'(p) + Y_3(p) \qquad (3.32)$$

is free from zeros in the RH p-plane. Since the poles of $Y_2'(p)$ are carried through, $Y_T(j\omega)$ must encircle the Y-plane origin in a CCW manner as many times as $Y_2'(p)$ has RH p-plane poles. Examples in which a simple rectangular waveguide system defines $Y_3(j\omega)$ are sketched in fig. 3.12.

3.9 Conclusion

The stability of the amplifier configuration of fig. 3.5 (d), containing one TD, has been investigated. The technique described is general and can be extended to more complicated arrangements. Particular attention has been paid to the effects of the parasitic package capacitance.

A knowledge of the number of RH p-plane poles P for H(p) at any appropriate part of the amplifier, together with the number of CCW encirclements of the H-plane origin by $H(j\omega)$, the plot being closed by an arbitrary loop in the RH H-plane from ω_R to $-\omega_R$, is sufficient to determine the number of RH p-plane zeros of H(p) given by

$$Z = P - CCW.$$

These zeros become the poles of $1/H(p)$, which are carried through when the next block of the amplifier is added. This process is continued until all blocks of the amplifier have been connected. The stability for the final connected network is assured when

$$CCW = P$$

i.e. when the relevant $H_T(p)$ has no RH p-plane zeros.

3.10 References

(1) J.W. Bandler, "Stability and gain prediction of microwave tunnel-diode reflection amplifiers", IEEE Trans. Vol. MfT-13, pp.814-819, November 1965.

(2) B.T.Henoch and Y. Kvaerna, "Broadband tunnel-diode amplifiers", Stanford University, August 1962; AD 299 284.

(3) B.T. Henoch and Y. Kvaerna, "Stability criteria for tunnel-diode amplifiers", IRE Trans. Vol. MTT-10, pp. 397-398, September 1962.

(4) Y. Kvaerna, "Tunnel-diode amplifier at 3 Gc/s", Elektroteknisk Tidsskrift, Norway, Vol.76, pp. 459-463, 15 October 1963.

(5) H.W. Bode, "Network analysis and feedback amplifier design", Van Nostrand, Princeton, N.J., 1945.

(6) U.S. Davidsohn, Y.C. Hwang and G.B. Ober, "Designing with tunnel diodes, part 1", Electronic Design, Vol.8, pp.50-55, 3 February 1961.

(7) G.L. Millican and L.F. Jelsma, "Radar electronic circuitry utilizing tunnel diodes, final report", Texas Instruments Inc., Dallas, Tex., 10 October 1961; AD 276 391.

(8) R.B. Whitson, "Impedance mapping in tunnel diode stability analysis", IEEE Trans. Vol. CT-10, pp.111-113, March 1963.

(9) G.H. Blaeser, "Tunnel diodes at microwave frequencies", Air Force Cambridge Research Laboratories, Mass., September 1962; AD 291 737.

(10) H.H. Meinke, "Antenna with tunnel diode", Technische Hochschule, Munich, 31 March 1963; AD 404 714.

(11) J.H. Lepoff, "The design of broad-band tunnel diode amplifiers", Sylvania Electric Products Inc., Cal., 21 October 1963; AD 430 257.

(12) J.H. Lepoff, "How to design stable, broadband TD amplifiers", Microwaves, Vol.3, pp.38-45, November 1964.

(13) C.S. Kim and A. Brandli, "High-frequency high-power operation of tunnel diodes", IRE Trans. Vol. CT-8, pp. 416-425, December 1961.

(14) E.G. Cristal, "A proposed technique for stabilization of tunnel diodes", Microwave J., Vol.5, pp. 108-113, April 1962.

(15) J. Hamasaki, "A low-noise and wide-band Esaki diode amplifier with a comparatively high negative conductance at 1.3 Gc/s", IEEE Trans. Vol. MTT-13, pp.213-223, March 1965.

(16) H.C. Okean, "Synthesis of negative resistance reflection amplifiers employing band-limited circulators", IEEE Trans. Vol. MTT-14, pp. 323-337, July 1966.

(17) H. Plutchok, "Octave-bandwidth tunnel-diode amplifier design", Proc. Nat. Elect. Conf., Vol.21, pp.119-124, 1965.

(18) A.S. Clorfeine, "Unconditional stability in tunnel-diode amplifiers", RCA Review, Vol.25, pp. 94-104, March 1963.

(19) J.O. Scanlan and J.T. Lim, "A design theory for optimum broadband reflection amplifiers", IEEE Trans. Vol. MTT-12, pp. 504-511, September 1964.

(20) E.S. Kuh and J.D. Patterson, "Design theory of optimum negative-resistance amplifiers", University of California, 6 December 1960; AD 253 241.

(21) L.I. Smilen and D.C. Youla, "Exact theory and synthesis of a class of tunnel diode amplifiers", Proc. Nat. Elect. Conf., Vol.16, pp. 376-404, 1960. Also "A theory for broadband tunnel diode amplifiers"; AD 277 194.

(22) G.I. Zysman, "Design of broadband transmission line equilizers", Polytechnic Institute of Brooklyn, 5 June 1962; AD 282 247.

(23) W. Kohler and H.J. Carlin, "Equiripple transmission line networks", Polytechnic Institute of Brooklyn, 24 January 1963; AD 297 373.

(24) J.O. Scanlan and J.T. Lim, "The effect of parasitic elements on reflection type tunnel diode amplifier performance", IEEE Trans. Vol. MTT-13, pp.827-836, November 1965.

(25) H.R. Lowry, J. Giorgis, E. Gottlieb and R.C. Weischedel, "General Electric tunnel diode manual", General Electric Co., Liverpool, N.Y., 1961; p.22.

(26) K.K.N. Chang, "Parametric and tunnel diodes", Prentice-Hall, Englewood Cliffs, N.J., 1964; p.59.

(27) J.O. Scanlan, "Properties of the tunnel diode", Electronic Technology, Vol.39, pp. 269-276, July 1962.

(28) W.F. Chow, "Principles of tunnel diode circuits", Wiley, New York, 1964; p.79.

(29) M.E. Hines, "High-frequency negative-resistance circuit principles for Esaki diode applications", Bell System Tech. J., Vol.39, pp. 477-513, May 1960.

(30) W.J. Getsinger, "Prototypes for use in broadbanding reflection amplifiers", IEEE Trans. Vol. MTT-11, pp. 486-497, November 1963.

4

stability analysis in the ρ-plane

4.1 Introduction

Some form of negative resistance Smith chart or reflection coefficient representation has been used by many researchers[1-25] (also references 10, 13 and 17 of chapter 3) to portray active loads. In this chapter the Nyquist approach to stability is developed into a form suitable for representation on a chart having conventional Smith chart scales. It is shown how the gain and stability of negative conductance reflection amplifiers can be simultaneously predicted on this chart.* Various stability criteria for use

---

*The derivation of the ρ'-plane (section 4.3) and the application of a Nyquist-type stability criterion (section 4.4), and also the discussion of the reflection amplifier connected to a mismatched transmission-line (section 4.7) have been published by the author.[1] Some months after submission of the manuscript, the original P.H. Smith showed qualitatively[2] how his chart could be adpated to display immittances with negative real parts.

The present chapter includes some further work on stability in the reflection coefficient plane: a direct interpretation of stability in the plane (section 4.5).

in conjunction with the Smith chart are rigorously presented. Predominantly graphical computations are involved, as in chapter 3, from which some of the H-plane ideas are carried over.

This chapter also includes a description of the stability criterion of Henoch and Kvaerna[3,4] (section 4.7) pertaining to reflection amplifiers connected to a mismatched transmission-line, and a critical examination of the criterion proposed by McPhun[5-7] (section 4.8) which involves the magnitude of the reflection coefficient only.

4.2 TRANSMISSION-LINE WITH NEGATIVE CONDUCTANCE LOAD

Define a transmission-line load $Y_L(j\omega)$ as

$$Y_L(j\omega) = -G_L + jB_L \tag{4.1}$$

where $-G_L$ and B_L are functions of ω. Then the voltage reflection coefficient $\rho(j\omega)$ is given by

$$\rho(j\omega) = \frac{Y_0(\omega) + G_L - jB_L}{Y_0(\omega) - G_L + jB_L} \tag{4.2}$$

where $Y_0(\omega)$ is the characteristic admittance of the transmission-line.* The power gain $G(\omega)$ of the load, i.e. the ratio of reflected power to incident power, is defined by

$$G(\omega) = |\rho(j\omega)|^2 = \frac{(Y_0(\omega) + G_L)^2 + B_L^2}{(Y_0(\omega) - G_L)^2 + B_L^2} \quad . \tag{4.3}$$

---

*Dependence of Y_0 on ω is assumed, e.g. to allow for rectangular waveguides. Furthermore, it is written $Y_0(\omega)$ rather than $Y_0(j\omega)$, since we are interested in propagating waveguides for which the characteristic admittance is real.

(4.3) shows that $G(\omega) > 1$ for any load having a negative conductance component. On differentiating, we obtain

$$\frac{dG(\omega)}{d\omega} = \frac{\left[4B_L^2\left[Y_O(\omega)\frac{dG_L}{d\omega} + G_L\frac{dY_O(\omega)}{d\omega}\right] - 8Y_O(\omega)G_LB_L\frac{dB_L}{d\omega}\right.}{\left.+\ 4(Y_O^2(\omega) - G_L^2)\cdot\left[Y_O(\omega)\frac{dG_L}{d\omega} - G_L\frac{dY_O(\omega)}{d\omega}\right]\right]} \cdot$$

$$[(Y_O(\omega) - G_L)^2 + B_L^2]^2 \qquad (4.4)$$

At the "centre" frequency ω_o, $B_L = 0$. For this case

$$\left.\frac{dG(\omega)}{d\omega}\right|_{\omega_o} = \left.\frac{4(Y_O(\omega) + G_L)\cdot\left[Y_O(\omega)\frac{dG_L}{d\omega} - G_L\frac{dY_O(\omega)}{d\omega}\right]}{(Y_O(\omega) - G_L)^3}\right|_{\omega_o} . \qquad (4.5)$$

The non-trivial ($Y_O(\omega) \neq 0$, $G_L \neq 0$, and $Y_O(\omega) + G_L \neq 0$), and stable ($Y_O(\omega) - G_L \neq 0$) condition for G_{max} to occur at ω_o is given by

$$Y_O(\omega)\left.\frac{dG_L}{d\omega}\right|_{\omega_o} = G_L\left.\frac{dY_O(\omega)}{d\omega}\right|_{\omega_o} . \qquad (4.6)$$

For a practical TD

$$\frac{dG_L}{d\omega} \neq 0 \qquad (4.7)$$

in general, and for a rectangular waveguide propagating the dominant mode

$$\frac{dY_0(\omega)}{d\omega} \neq 0. \tag{4.8}$$

Thus, the gain of the load will not, in general, reach a maximum at the frequency of zero susceptance.[26]

4.3 REPRESENTATION OF IMMITTANCES WITH NEGATIVE REAL PARTS ON THE SMITH CHART

The complete ρ-plane

$|\rho(j\omega)| > 1$ for reflection amplifiers; it follows that the associated VSWR $s(\omega)$ given by

$$s(\omega) = \frac{1 + |\rho(j\omega)|}{1 - |\rho(j\omega)|} \tag{4.9}$$

is negative.[8,*] If one extends the families of circles which constitute the conventional Smith chart beyond the bounding unit circle by including immittances with negative real parts, [9-11] fig. 4.1 is arrived at.**

The ρ'-plane: a transformed ρ-plane

This extention (fig. 4.1) is quite impractical, apart from its availability, for displaying, for example, the

---

*A standing wave detector alone can not distinguish between positive and negative VSWR. A directional coupler could, for example, be used to establish whether the reflected power exceeded the incident power by comparing the former with the power returning from a s.c. termination.

**The equations describing the constant resistance and constant reactance circles are given in many text books, e.g. Ramo and Whinnery.[27]

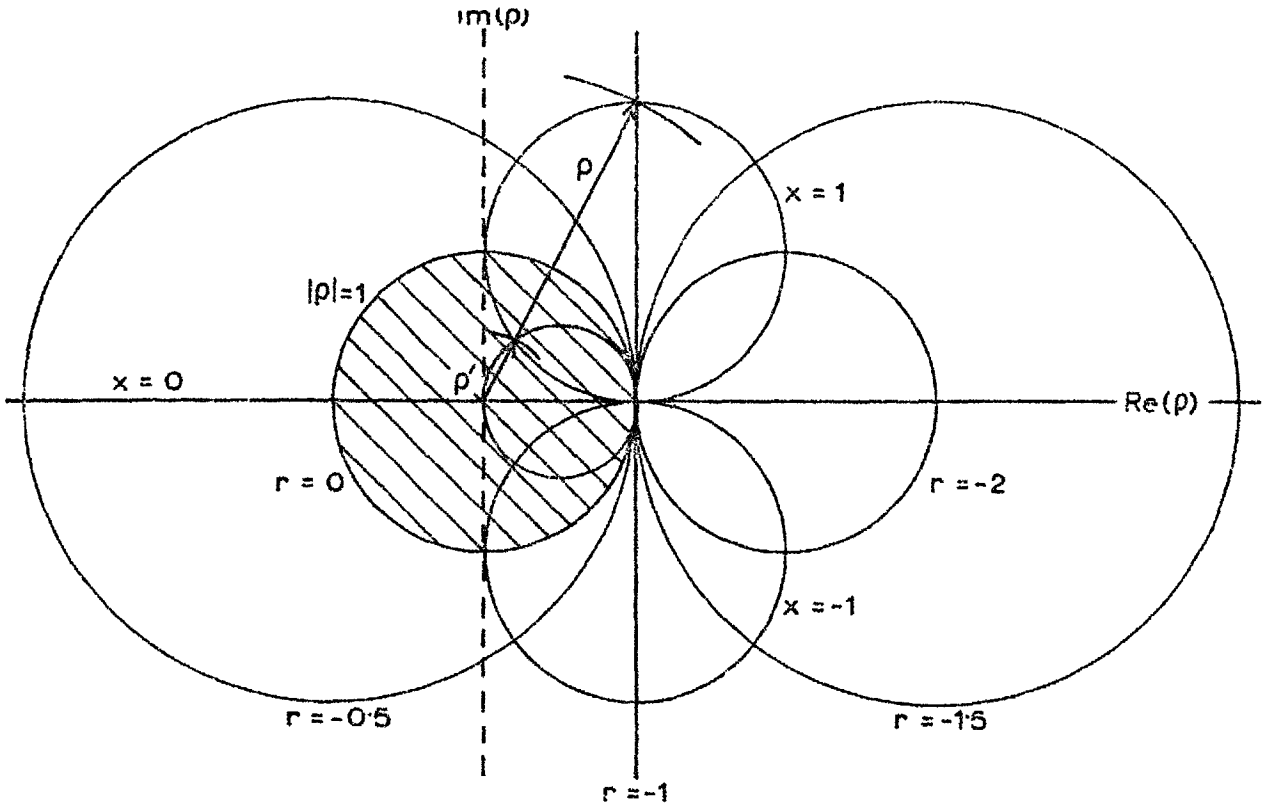

Fig. 4.1: Complete ρ-plane of which the conventional Smith chart (shaded area) forms a part.

frequency response of negative conductance amplifiers. A simple transformation, however, brings the negative conductance (or resistance) region into the conventional Smith chart,* and consequently facilitates its use with the minimum of alteration.

Define a transmission-line load $Y_L'(j\omega)$ as

$$Y_L'(j\omega) = G_L' + jB_L'. \tag{4.10}$$

Then

$$\rho'(j\omega) = \frac{Y_0'(\omega) - G_L' - jB_L'}{Y_0'(\omega) + G_L' + jB_L'}. \tag{4.11}$$

*The transformation has also been independently proposed by Chow.[12]

Compare (4.11) with (4.2) such that

$$Y_O'(\omega) = Y_O(\omega); \quad B_L' = B_L; \quad \text{and } G_L' = G_L . \tag{4.12}$$

In this case

$$\rho'(j\omega) = \frac{1}{\rho^*(j\omega)} = \frac{\rho(j\omega)}{\rho^*(j\omega).\rho(j\omega)} = \frac{\rho(j\omega)}{|\rho(j\omega)|^2} \tag{4.13}$$

where $\rho^*(j\omega)$ is the complex conjugate of $\rho(j\omega)$. In polar co-ordinates

$$\rho(j\omega) \equiv |\rho(j\omega)| e^{j\theta(\omega)} \tag{4.14}$$

and

$$\rho'(j\omega) \equiv |\rho'(j\omega)| e^{j\theta'(\omega)}. \tag{4.15}$$

Thus

$$\theta'(\omega) = \theta(\omega) \tag{4.16}$$

and

$$|\rho'(j\omega)| = \frac{1}{|\rho(j\omega)|} . \tag{4.17}$$

Vectors ρ' and ρ lie in the same line on the chart (see fig. 4.1). They rotate in the same sense when considered functions of position along the transmission-line since

$$\rho'(j\omega)e^{-j2\beta z} = \frac{\rho(j\omega)}{|\rho(j\omega)|^2} e^{-j2\beta z} \tag{4.18}$$

where z is the distance measured towards the generator.

The centre of the transformed plane corresponds to infinite gain, and constant ρ' circles correspond to constant

gain.* Note that the only fundamental change to the conventional Smith chart is the change of sign of the constant conductance (or resistance) circles.

4.4 ADAPTING H-PLANE STABILITY ANALYSIS TO THE ρ'-PLANE

Let

$$H_L(j\omega) = H_T(j\omega) - H_0(\omega) \tag{4.19}$$

where H_T is defined in section 3.2. Thus, an otherwise physically present matched transmission-line (or pure resistance) has been "extracted" from H_T. Hence,

$$\frac{H_L(j\omega)}{H_0(\omega)} = \frac{H_T(j\omega)}{H_0(\omega)} - 1 \quad . \tag{4.20}$$

The critical point in stability analysis using H_T is (0,j0); using H_L/H_0 the critical point becomes (-1,j0), i.e. the centre of the transformed Smith chart. CCW loci around the H-plane origin become CW about the ρ'-plane origin (or vice versa), as explained by fig. 4.2, which also illustrates the consequences of the transformation of ρ. The ρ'-plane accounts for the whole of the LH H-plane, plus the part of the RH H-plane from the imaginary axis to $H_0(\omega)$ only when $H_0(\omega)$ is physically present in the connected circuit. The Smith chart is a simple distortion of the H-planes and is symmetrical about the real axis, therefore all the concepts discussed in chapter 3 concerning real frequency responses, e.g. arbitrary closing loops above ω_R, can be carried over without ambiguity.

---

*Return "gain" in dB replaces return "loss" in dB.

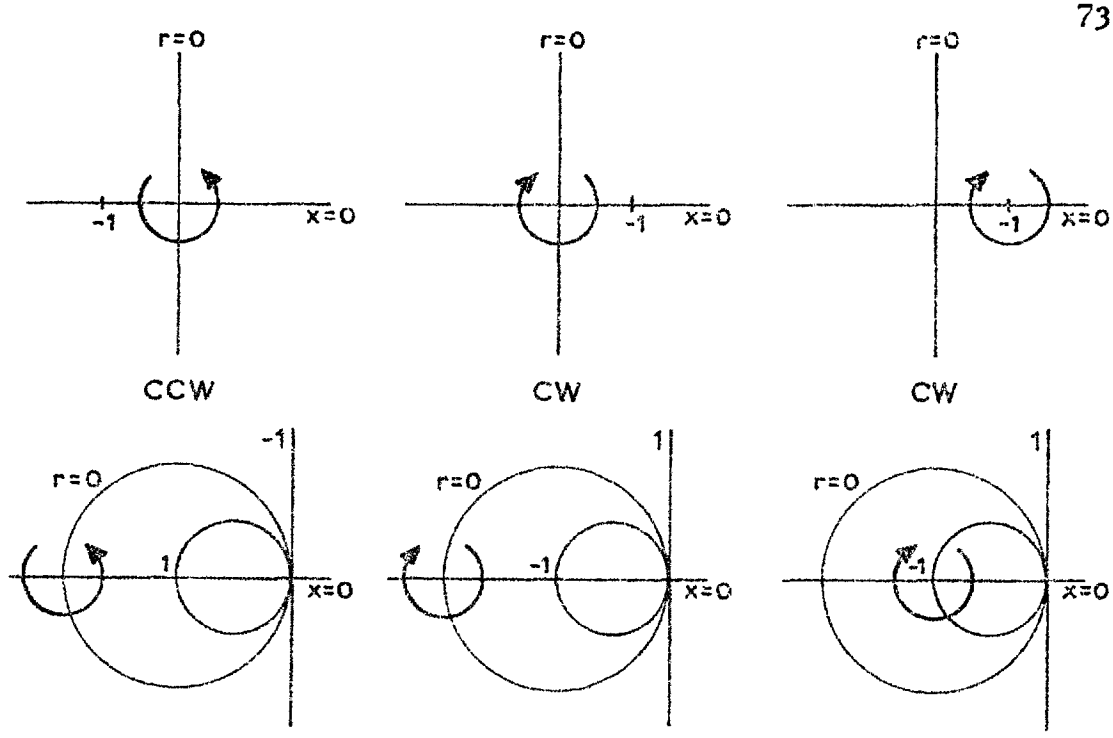

Fig.4.2: Transformations and associated senses of rotation. The development of the senses of rotation in the transformed Smith chart is shown in parallel with the corresponding ones in the H-plane.

4.5 DIRECT INTERPRETATION OF STABILITY IN THE ρ'-PLANE

The stability criterion

Stability requires that RH p-plane poles be absent from $\rho(p)$: only then will $|\rho(j\omega)|^2$ represent the magnitude of the finite power gain of a stable reflection amplifier. Now if

$$H^*(j\omega) = H(-j\omega) \qquad (4.21)$$

then

$$\rho^*(j\omega) = \rho(-j\omega) \quad . \qquad (4.22)$$

Substituting p for jω in (4.13),

$$\rho'(-p) = \frac{1}{\rho(p)} . \qquad (4.23)$$

Hence, $\rho'(-p)$ should have no RH p-plane zeros; alternatively, $\rho'(p)$ should have no LH p-plane zeros for stability.

To comply with the theorem quoted in section 3.2, the p-plane contour required for the present analysis must enclose the entire LH p-plane. The motion is again positive up the $j\omega$ axis, avoiding singularities on the axis by small semicircular indentations into the LH plane, but this time CCW around an infinite semicircle standing on the $j\omega$ axis, centred at the origin and lying in the LH p-plane (see fig. 4.3). The plot of $\rho'(j\omega)$ must encircle the ρ'-plane origin as many times in a CW manner as $\rho(p)$ has zeros (given by the zeros of its numerator) in the RH p-plane.

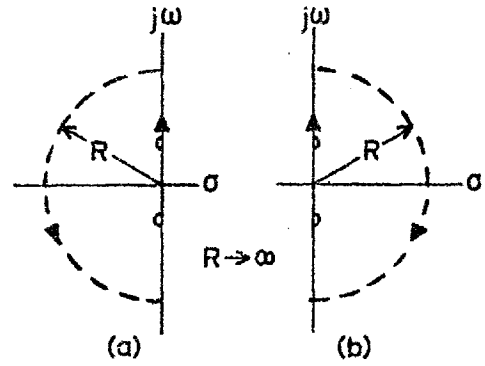

Fig.4.3: p-plane, (a) a CCW encirclement in the LH, (b) a CW encirclement in the RH.

Limiting cases for $\rho'(p)$ as $p \to \infty$

$$\rho'(p) = \frac{1}{\rho(-p)} = \frac{Z_L(-p) + Z_0}{Z_L(-p) - Z_0} . \qquad (4.24)$$

If $Z_L(p)\big|_{p\to\infty} \to \frac{1}{pC}$ then

$$\rho'(p)\big|_{p\to\infty} \to -1 . \qquad (4.25)$$

If $Z_L(p)\big|_{p\to\infty} \to R$ then

$$\rho'(p)\big|_{p\to\infty} \to \frac{R + Z_0}{R - Z_0} . \qquad (4.26)$$

If $Z_L(p)\big|_{p\to\infty} \to pL$ then

$$\rho'(p)\big|_{p\to\infty} \to 1. \qquad (4.27)$$

The infinite CCW semicircle in the LH p-plane will, therefore, coalesce into a single point on the real ρ or ρ' axis, according to table 4.1.

function	C	R	L
$\rho(p)$	-1	$\frac{R - Z_0}{R + Z_0}$	1
$\rho'(p)$		$\frac{R + Z_0}{R - Z_0}$	

Table 4.1: Limiting cases in the transformation from p- to ρ- and ρ'-planes.

The arbitrary closing loop

The question of where an arbitrary loop from just above ω_R to just below $-\omega_R$ can be drawn presents some difficulty here. It is important to distinguish between whether the Smith chart is being used with the stability criterion in terms of immittance or in terms of voltage reflection coefficient. Fig. 4.4 illustrates the difficulty with the aid of table 4.1 and the ideas of section 3.2. Note that for an H-plane criterion the closing loop is drawn, as expected, through the region of the H-plane origin.

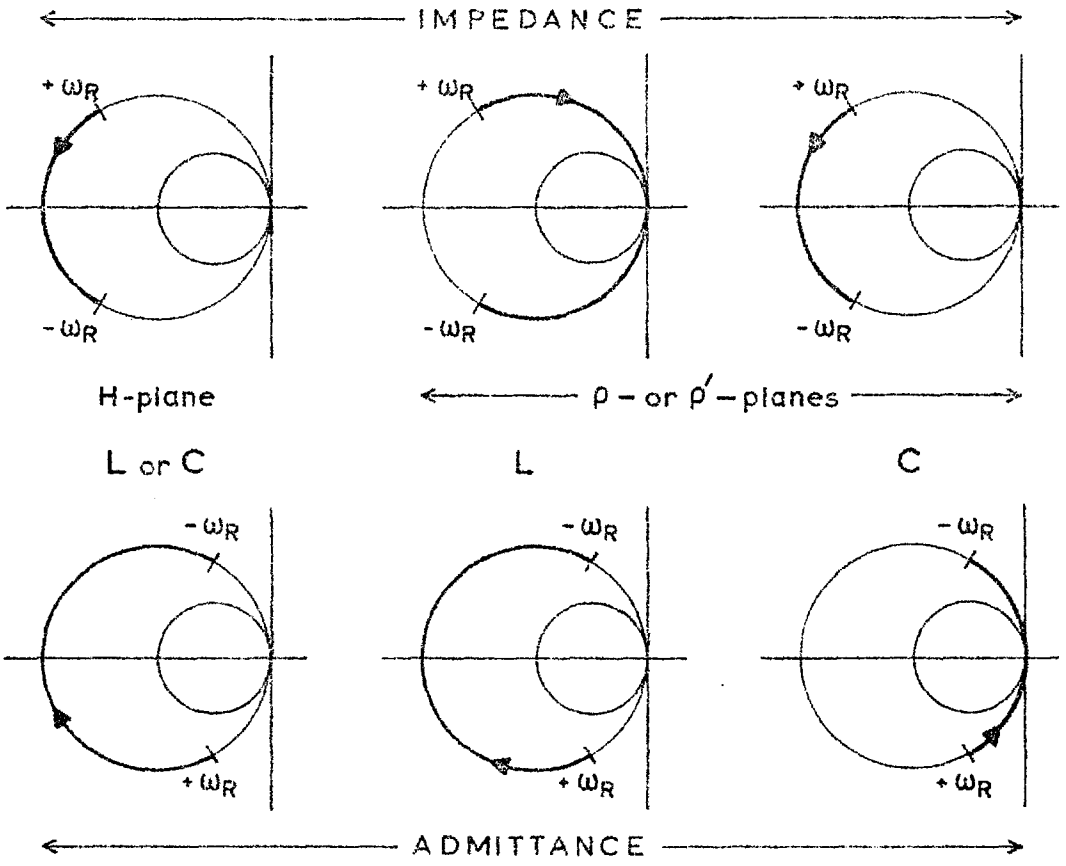

Fig. 4.4: Some arbitrary closing loops on the Smith chart applicable to TDs. The loops are drawn as arcs of the unit circle for convenience.

Concluding comments

A stability criterion in terms of ρ' is both more complicated than one in terms of H, and unnecessary in practice, for the following reasons:*

(i) the denominator of ρ'(p) may have zeros in the LH p-plane other than "active" ones which would have to be determined,

(ii) the arbitrary closing loop in the ρ'-plane can not be so easily dismissed (see fig. 4.4) as in the H-plane, and

(iii) no further information on stability is forthcoming by considering ρ' rather than H.

---

*As an academic exercise one could formulate the conditions for stability in terms of ρ' and the number of CW encirclements of the ρ'-plane origin in parallel with the method of chapter 3.

It is recommended, therefore, that when using the Smith chart for predicting simultaneously the stability and gain of reflection amplifiers, the stability criterion itself should be formulated in terms of H, as explained in chapter 3 and section 4.4. Practical examples of this are found in chapters 5 and 6.

4.6 ANOTHER TYPE OF NEGATIVE SMITH CHART

A number of authors[5,8,13,14] have employed a transformation of the form

$$\rho'' = -\frac{1}{\rho} \tag{4.28}$$

to obtain a negative Smith chart for $|\rho(j\omega)| > 1$. For stability $\rho''(p)$ must have no RH p-plane zeros, therefore $\rho''(j\omega)$ must encircle the ρ''-plane origin as many times in a CCW direction as $\rho''(p)$ has RH p-plane poles. This negative Smith chart has some practical disadvantages, viz.

(i) the inversion process results in a chart which is a mirror image of the conventional chart with respect to the imaginary ρ axis,

(ii) transformations towards load or generator are opposed in sense to those on the conventional chart, and

(iii) plots of frequency responses of immittances having positive and negative real components would be discontinuous if both conventional and negative charts have to be used at the same time.

4.7 REFLECTION AMPLIFIER CONNECTED TO MISMATCHED LINE

Stability criterion in terms of amplifier and source reflection coefficients

Let ρ_C be the reflection coefficient of the mismatched line (the mismatch being due to a practical circulator, say) referred to the terminals of a reflection amplifier whose reflection coefficient is ρ_A (see fig. 4.5). Henoch and Kvaerna[3,4] have shown that

$$1 - \rho_A(p).\rho_C(p) = 0 \qquad (4.29)$$

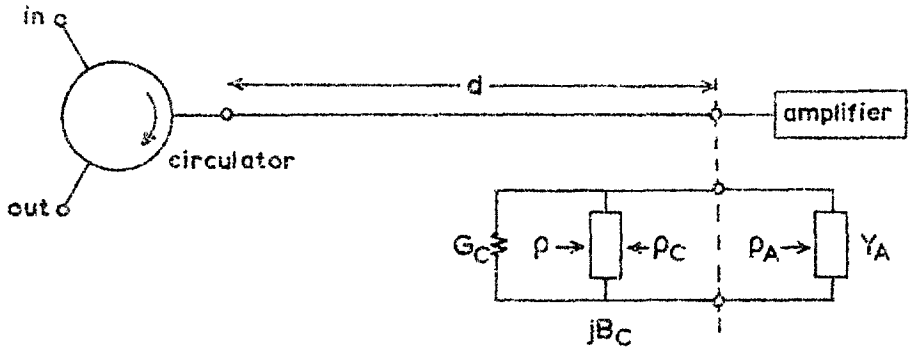

Fig.4.5: Non-ideal circulator representation at amplifier terminals.

must have no solutions in the RH p-plane for stability. For $\rho_A(p)$ to represent an inherently stable amplifier it must have no RH p-plane poles, and since $\rho_C(p)$ represents a passive device, $1 - \rho_A(p).\rho_C(p)$ has no RH p-plane poles. Therefore, a plot of $1 - \rho_A(j\omega).\rho_C(j\omega)$ must not encircle the origin of the ρ-plane, i.e. the centre of the conventional Smith chart (1,j0) for stability. This is equivalent to stating that

$\rho_A(j\omega).\rho_C(j\omega)$ must not encircle the point +1 which (assuming voltage reflection coefficients) is $(\infty, j\infty)$ for impedance co-ordinates or $(0,j0)$ for admittance co-ordinates. A new vector standing on $(1,j0)$ is obtained, and its rotation about the critical point is investigated. If

$$|\rho_A(j\omega)| \cdot |\rho_C(j\omega)| < 1 \qquad (4.30)$$

the connected circuit isstable and independent of the relative phases of $\rho_A(j\omega)$ and $\rho_C(j\omega)$, since encirclements of the critical point (i.e. +1) do not arise. Graphically represented, this requires that the plot of $\rho_A(j\omega).\rho_C(j\omega)$ be totally contained within the conventional Smith chart.

Stability criterion in terms of gain equation

The methods just described do not provide a "gain equation" from which information on both gain and stability can be derived simultaneously, e.g. from a Smith chart plot. If Y_C is the circulator admittance referred to the amplifier's terminals (see fig. 4.5), then

$$\rho(j\omega) = \frac{Y_C^*(j\omega) - Y_A(j\omega)}{Y_C(j\omega) + Y_A(j\omega)} \qquad (4.31)$$

gives the actual gain response. $\rho(j\omega)$ is obtained in practice by extracting $G_C(\omega)$ from $Y_C(j\omega) + Y_A(j\omega)$ and plotting the remaining admittance normalized to $G_C(\omega)$ on the Smith chart. The encirclements of the centre of the chart $(-1,j0)$ are investigated in the manner which has been explained.

In this context it is important to note that if a TD reflection amplifier is known to be stable when connected to a certain matched transmission-line, it will remain stable when the line is mismatched if the new frequency response of the amplifier has the same net encirclements of the critical

point as for the matched line. This fact is a simple, and yet powerful, consequence of the foregoing arguments.

4.8 McPHUN'S STABILITY CRITERION[5-7]

McPhun[5] has proposed a stability criterion for TD circuits based on the magnitude of the voltage reflection coefficient. A discussion of the implications of this criterion is relevant to this chapter.*

The criterion

The amplifier is divided into any two parts: an active part containing the TD, and the remaining passive part (see fig. 4.6). $|\rho(j\omega)|$ is computed from d.c. to ω_R for $R = R_{min}$, the minimum negative resistance of the TD junction. R is increased slightly and $|\rho(j\omega)|$ is recomputed. If this increase in negative resistance results in an increase in $|\rho(j\omega)|$ then the amplifier is unstable, otherwise it is stable. This criterion was derived "intuitively".

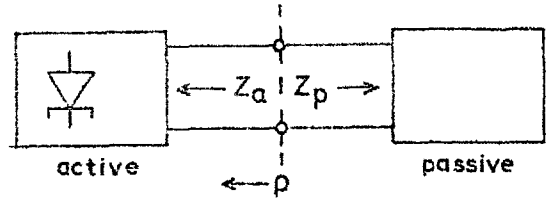

Fig. 4.6: The divided amplifier.

Its application to a particular case

Consider the network of fig. 4.7. By considerations of the conservation of energy, the power gain of the

---

*Comments on the criterion have been published by the present author,[6] also a rebuttal by McPhun.[7] Only the important concepts which emerged from the correspondence are reported here.

amplifier is the same[28] for any reference plane between 1 and 2; it is given by $|\rho(j\omega)|^2$, where

$$\rho(j\omega) = \frac{Z_a(j\omega) - Z_p^*(j\omega)}{Z_a(j\omega) + Z_p(j\omega)} = \frac{N(j\omega)}{D(j\omega)} \qquad (4.32)$$

and where Z_a and Z_p are as shown in fig. 4.7. Since $|\rho(j\omega)|$

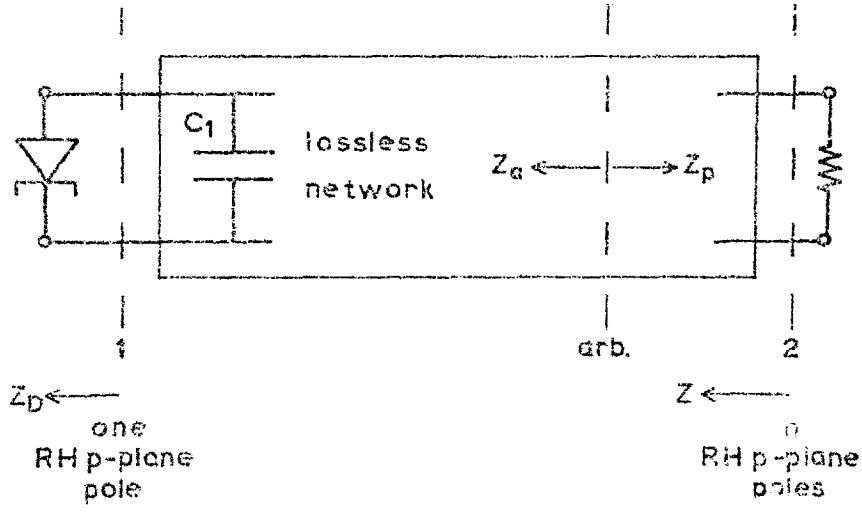

Fig. 4.7: Amplifier representation: choice of reference plane.

is independent of the reference plane chosen, let us consider the one nearest -R, as shown in Fig.4.8. The TD series resistance r must, under the present restrictions, be regarded as part of Z_a.

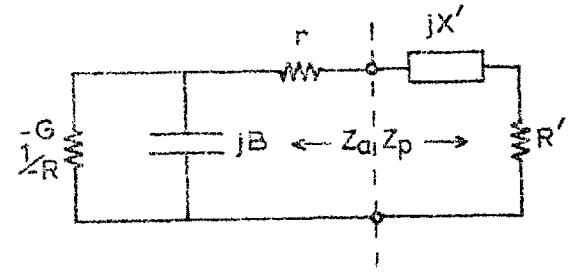

Fig.4.8: Reference plane nearest -R.

Let

$$R_S = -\frac{G}{B^2 + G^2} \qquad (4.33)$$

and

$$X_S = -\frac{B}{B^2 + G^2} \tag{4.34}$$

where B and G are shown in fig. 4.8. For a fixed frequency,

$$\frac{dR_S}{dG} = \frac{G^2 - B^2}{(B^2 + G^2)^2} \tag{4.35}$$

and

$$\frac{dX_S}{dG} = \frac{2BG}{(B^2 + G^2)^2} \quad . \tag{4.36}$$

Assume, for example, that B > G. Then

$$\frac{dR_S}{dG} < 0 \tag{4.37}$$

$$\frac{dX_S}{dG} > 0 \; ; \tag{4.38}$$

i.e. as R increases, R_S increases and X_S decreases. From fig. 4.9 (a) it is clear that a point in quadrant 2 of the Z-plane moves closer to the origin. Thus $|D(j\omega)|$ decreases. Since a corresponding point of $N(j\omega)$ is displaced laterally to the left by 2R',

$$|N(j\omega)| > |D(j\omega)| \quad . \tag{4.39}$$

Now

$$\frac{d\,|\rho(j\omega)|}{dR} = \frac{|D(j\omega)|\,\frac{d|N(j\omega)|}{dR} - |N(j\omega)|\,\frac{d|D(j\omega)|}{dR}}{|D(j\omega)|^2} \; ; \tag{4.40}$$

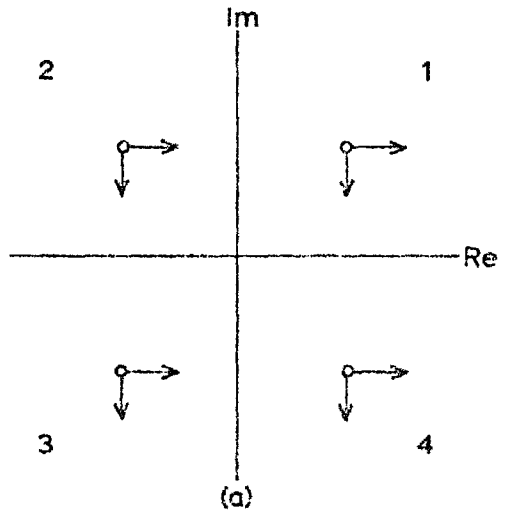

B > G

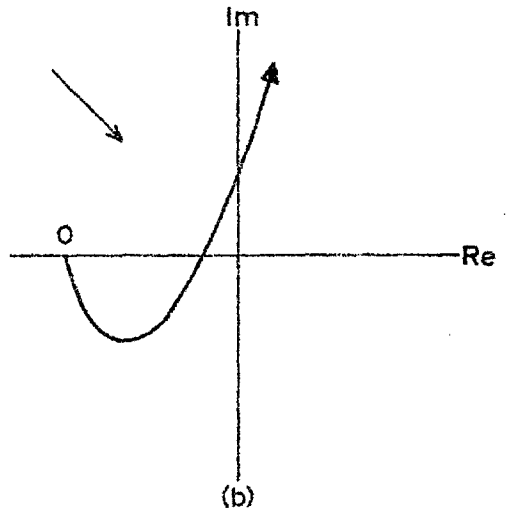

Unstable (criterion valid)

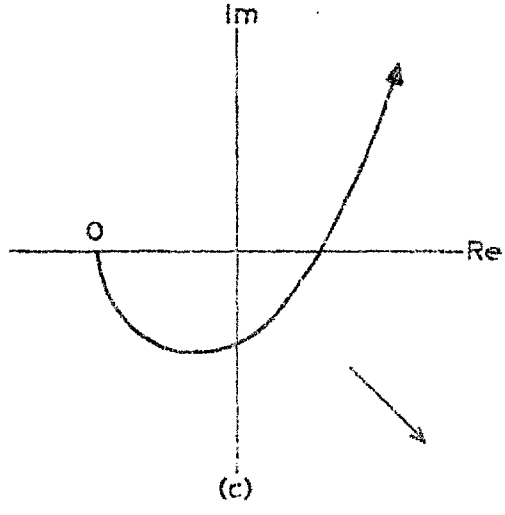

Stable (criterion valid)

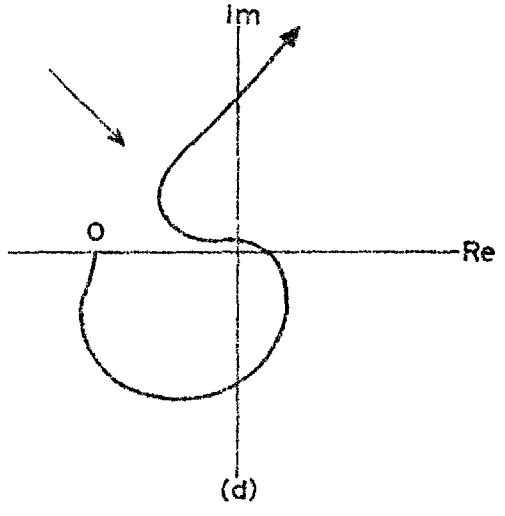

Stable (criterion invalid)

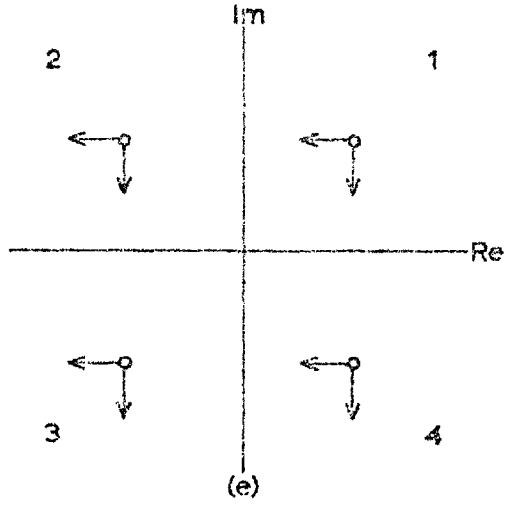

B < G

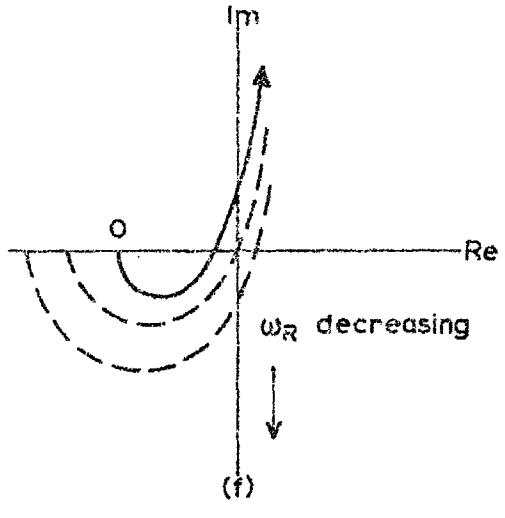

$Z_D(j\omega)$

Fig.4.9: Effects in the Z-plane of increasing R.

but

$$\frac{d|N(j\omega)|}{dR} < 0 \qquad (4.41)$$

and

$$\frac{d|D(j\omega)|}{dR} < 0 \ , \qquad (4.42)$$

and if

$$\left|\frac{d|N(j\omega)|}{dR}\right| \leqslant \left|\frac{d|D(j\omega)|}{dR}\right| \qquad (4.43)$$

then

$$\frac{d|\rho(j\omega)|}{dR} > 0 \ . \qquad (4.44)$$

Depending on how much greater than unity $|\rho(j\omega)|$ is (4.44) will also be true even when (4.43) is violated. The circuit is often unstable when $Z_a(j\omega) + Z_p(j\omega)$ passes through quadrant 2, as there may not be one CCW encirclement of the origin as a result. McPhun's criterion is valid in this case; e.g. see fig. 4.9 (b): as R increases this locus passes through the origin (gain infinite), and then becomes stable (gain falls), leading to fig. 4.9 (c).

Fig. 4.9 (d) represents a possible exception to the criterion, since $|\rho(j\omega)|$ could increase with R, and yet the circuit is stable. This ambiguity has arisen because the phase of $\rho(j\omega)$ has not been taken into account in the criterion.

The tendencies for a point in the Z-plane when B < G are shown in fig. 4.9 (e). Fig. 4.9 (f) shows the effect of increasing R on a TD impedance plot $Z_D(j\omega)$; the combined effects of figs. 4.9 (a) and (e) are clearly demonstrated.

The plot of $Z_a(j\omega) + Z_p(j\omega)$ must start in the LH Z-plane for stability since it ends in the RH plane and one CCW encirclement is required. The d.c. starting point tends to the left as R increases (fig. 4.9 (e)), so that if the plot starts in the RH Z-plane it represents an unstable circuit whose $|\rho(j\omega)|$ increases with R, conforming to the criterion.

4.9 Conclusion

For a matched transmission-line (or the real part of its immittance if it is mismatched) acting as both source and load of a reflection amplifier, the gain and stability can be simultaneously predicted on a conventionally arranged Smith chart whose resistance or conductance scales assume negative values. The matched line is extracted from H_T and the remaining immittance is plotted (normalized) on the chart. Both RH and LH H-planes can be mapped into the Smith chart, CCW encirclements of the critical point, the chart centre, in the former case remaining CCW, but becoming CW in the latter case. The sense of the encirclements is the same whether the criterion is in terms of H or ρ', although, for the reasons given in section 4.5, it may often be preferable to formulate it in terms of H.

The application of McPhun's stability criterion to a particular circuit has not only brought to light the fact that a criterion in terms of $|\rho(j\omega)|$ alone is not infallible, but also some interesting effects and their consequences on Z-plane loci of changing the bias of the TD.

4.10 References

(1) J.W.Bandler, "Stability and gain prediction of microwave tunnel-diode reflection amplifiers", IEEE Trans. Vol. MTT-13, pp. 814-819, November 1965.

(2) P.H. Smith, "A new negative resistance Smith chart", Microwave J., Vol.8, pp. 83-92, June 1965.

(3) B.T. Henoch and Y. Kvaerna, "Broadband tunnel-diode amplifiers", Stanford University, August 1962; AD 299 284.

(4) B.T. Henoch and Y. Kvaerna, "Stability criteria for tunnel-diode amplifiers", IRE Trans. Vol. MTT-10, pp. 397-398, September 1962.

(5) M.K. McPhun, "Practical stability criterion for tunnel-diode circuits", Electronics Letters, Vol.1, pp. 167-168, August 1965.

(6) J.W. Bandler, "Practical stability criterion for tunnel-diode circuits", ibid, Vol.1, pp. 262-264, November 1965.

(7) M.K. McPhun, "Practical stability criterion for tunnel-diode circuits", ibid, Vol.1, p. 289, December 1965.

(8) H.F. Lenzing and C. D'Elio, "Transmission line parameters with negative conductance loads and the 'negative' Smith Chart", Proc. IEEE, Vol.51, pp. 481-482, March 1963.

(9) H. Rothe, "Verstärkung und Bandbreite des Reflexionsmasers (amplification and bandwidth of the reflection maser)", Archiv der Elektrischen Übertragung (Germany), Vol.16, pp. 486-494, October 1962.

(10) N.M. Sovetov, "Generalization of impedance circular diagrams to the case of microwave channels with negative resistance", Radio Engineering and Electronic Physics (translation from Russian), Vol.6, pp. 329-332, March 1961.

(11) L.J. Kaplan and D.J.R. Stock, "An extension of the reflection coefficient chart to include active networks", IRE Trans. Vol. MTT-7, pp. 298-299, April 1959.

(12) W.F. Chow, "Principles of tunnel diode circuits", Wiley, New York, 1964; p. 116.

(13) R.L. Kyhl, "Plotting impedances with negative resistive components", IRE Trans. Vol. MTT-8, p. 377, May 1960.

(14) L.J. Kaplan and D.J.R. Stock, "Some comments on the method of Kyhl", IRE Trans. Vol. MTT-8, p. 668, November 1960.

(15) D.J.R. Stock and L.J. Kaplan, "The representation of impedances with negative real parts in the projective chart", IRE Trans. Vol. MTT-7, p. 475, October 1959.

(16) G.L. Suchkin, "The measurement of active impedances", Radio Engineering and Electronics (translation from Russian), Vol. 4, pp. 202-204, December 1959.

(17) B. Rosen, "Transformation of impedances having a negative real part and the stability of negative resistance devices", Proc. IRE, Vol. 48, p. 1660, September 1960.

(18) C.T. Stelzried, "Interpretation of the transmission line parameters with a negative-conductance load and application to negative-conductance amplifiers", Proc. IRE, Vol. 49, pp. 812-813, April 1961.

(19) J.C. Hoover, "Practical problems in the design of tunnel diode amplifiers", IRE WESCON Conv. Re ord, Vol.6, Pt.1, Paper 7.4, 1962.

(20) R.D. Hall, "Microwave tunnel diode devices", Electronic Defense Labs. (Sylvania), U.S.A., 20 March 1964; AD 601 577.

(21) T. Kitsuregawa, K. Shirahata, and D.Taketomi, "Wide-band circulator type Esaki diode amplifier", Mitsubishi Denki Lab. Reports (Japan), Vol.5, pp. 355-370, July 1964.

(22) R.D. Gallagher, "A microwave tunnel diode amplifier ", Microwave J., Vol.8, pp. 62-68, February 1965.

(23) H. Yunoki, Y. Ito, T. Kudo, and H. Komizo, "Integrated tunnel diode amplifier for broad-band radio communication in case of f_{ro} being higher than f_{xo}", IEEE Int. Conv. Record, Vol.14, Pt.5, pp. 124-132, 1966.

(24) R.C. Havens, "An X-band strip transmission line tunnel diode amplifier", Microwave J., Vol.9, pp. 49-54, May 1966.

(25) M.K. McPhun, "Measurement of negative resistance using a Z-g diagraph", Proc. IEEE, Vol.54, pp. 910-911, June 1966.

(26) J.O. Scanlan and J.T. Lim, "A design theory for optimum broad-band reflection amplifiers", IEEE Trans. Vol.MTT-12, pp. 504-511, September 1964.

(27) S. Ramo and J.R. Whinnery, "Fields and waves in modern radio", Wiley, New York, 1953 (second edition); pp. 34-38.

(28) H.J. Carlin and A.B. Giordano, "Network theory", Prentice-Hall, Englewood Cliffs, N.J., 1964; pp. 331-334.

5

predicted and experimental performance of TDA 1

5.1 Introduction

The theory of chapters 3 and 4 is used to predict the performance of TDA 1, the design of which is reported in chapter 2. Attention is focussed mainly on stable operation. The variation of gain with s.c. stub length (fig. 2.1) is predicted, and also the gain of the amplifier when the band-rejection filter is considered ideal (section 3.4). The approximation that the circulator and exponential taper are perfectly non-reflecting is made in both cases. Initially, a procedure is outlined for constructing immittance curves on a Smith chart for the TD equivalent circuit, viewed either as a series or as a parallel arrangement.

Experimental results are presented, in particular the gain variation with s.c. stub length at a constant bias voltage, and the variation of gain with bias voltage for a s.c. stub

length. An attempt to approach the predicted performance under ideal band-rejection filter conditions was made experimentally by reducing the characteristic impedance of the coaxial-line, increasing the resistance per square of the terminating card, and (since this was also found necessary) decreasing the r_c dimension (fig. 2.2) of the radial-line.

Some of the results reported in this chapter have been included in reference 1 of chapters 3 and 4.

5.2 TD SMITH CHART NOMOGRAM

The Smith chart is first calibrated for the range of TD equivalent circuit element values required, so that this range is adequately displayed over the chart: C, L, -R and -G being set out along the centre line, and X and B being set out around the imaginary axis (see fig. 5.1). The frequency scale is set out as follows.

If a straightedge is placed on the chart, then the product of the two numbers given by the points of intersection of the straightedge with the outer (imaginary) axis will be found at the corresponding point of intersection of the straightedge with the centre line (real) axis. Let the normalized scale on the chart read n. Assume that the B and C scales have been decided upon, and marked out. It is required to calculate

$$B = \omega C = 2\pi f C \qquad (5.1)$$

when f and C are given. Then

$$knB = C \qquad (5.2)$$

where k is a constant scale factor. Thus

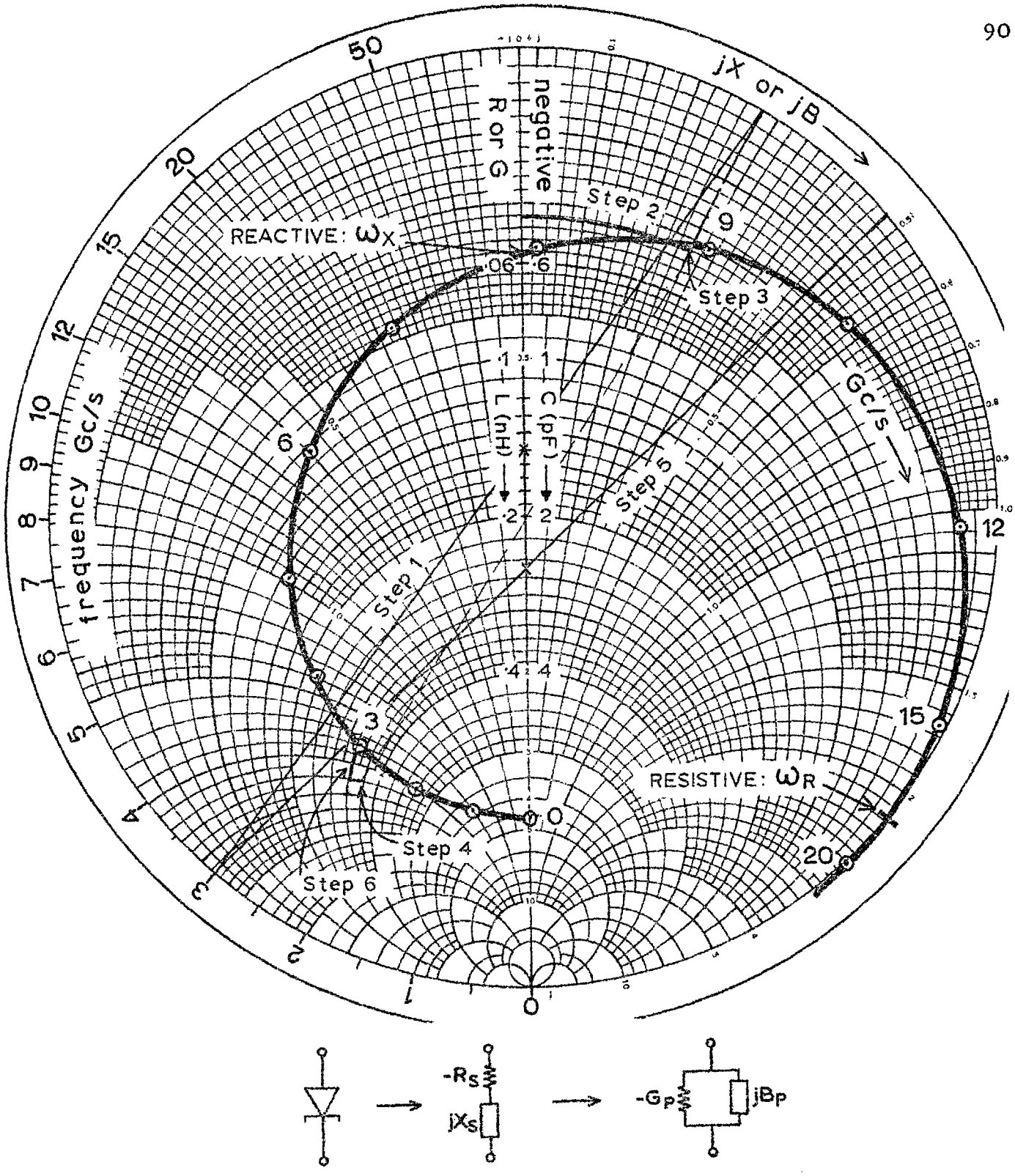

Fig. 5.1: Tunnel-diode chart normalized to 10 Ω or 100 m℧.
Example: R = 47 Ω, C = 1.5 pF, r = 0.75 Ω, L = 0.25 nH.

$$\text{Im} = \frac{1}{\omega} = \frac{1}{2\pi f} \quad . \tag{5.3}$$

Therefore

$$n = \frac{1}{2\pi f k} \quad . \tag{5.4}$$

Choose convenient values of B and C, and obtain the corresponding n by a straightedge; hence k is known from (5.2). The frequency scale is then generated from (5.4) by inserting values for f and marking the n scale appropriately.

Referring to fig. 5.1, let B = 100 m℧ and C = 2 pF. Then n = 1.0. From (5.2):

$$k = \frac{2}{1.0 \times 100} = \frac{1}{50} \text{ second/radian/unit} \times 10^{-9}.$$

From (5.4), with f in Gc/s,

$$n = \frac{50}{2\pi f} = \frac{7.95}{f} \text{ units.}$$

This whole process is repeated in a similar manner to calculate X = ωL, but, with a certain amount of trial and error, all the scales can be adjusted so that they neatly fit in with each other. All the operations are carried out with a straightedge, a pair of dividers, and a pencil. The processes of inversion and addition, and so on, on a Smith chart are the familiar ones.

A summary of the instructions for using the nomogram follows:

1) Locate f, C; find jB
2) Invert -R to give -G
3) Add -G + jB
4) Invert to give -R' + jX'
5) Locate f, L; find jX

6) Add r + jX to 4) to give $-R_S + jX_S$

7) Invert to give $-G_P + jB_P$

8) Invert $-G_P$, jB_P to give $-R_P$, jX_P

9) Continue ..

Fig. 5.1 provides an example of the method, culminating in a TD impedance plot $Z_D(j\omega)$, i.e. as far as step 6.

5.3 THEORETICAL CALCULATIONS

The parameter values of the TD (Mullard type 49AAY) used in the amplifier are

$R = 47\ \Omega$, $C = 1.5$ pF, $r = 0.75\ \Omega$, $L = 0.25$ nH, and

$$C_1 = 1.0 \text{ pF}.$$

An initial calculation showed that its susceptance would be tuned out at 3 Gc/s (resonant frequency of the stabilizing network) by a s.c. stub length (see fig. 2.1) of 15 mm; $-35.4\ \Omega$ would be left facing the $25\ \Omega$ waveguide at this frequency resulting in a gain of

$$G = \left(\frac{\frac{1}{25} + \frac{1}{35.4}}{\frac{1}{25} - \frac{1}{35.4}} \right) = 33.7 \rightarrow 15 \text{ dB}.$$

Addition of package capacitance

Inverting the curve of fig. 5.1 (step 7) leads to $Y_D(j\omega)$ — curve (a) of fig. 5.2. Since no effort was made to build the TD into the waveguide structure, its package capacitance of 1 pF was assumed to be present in full. Adding C_1

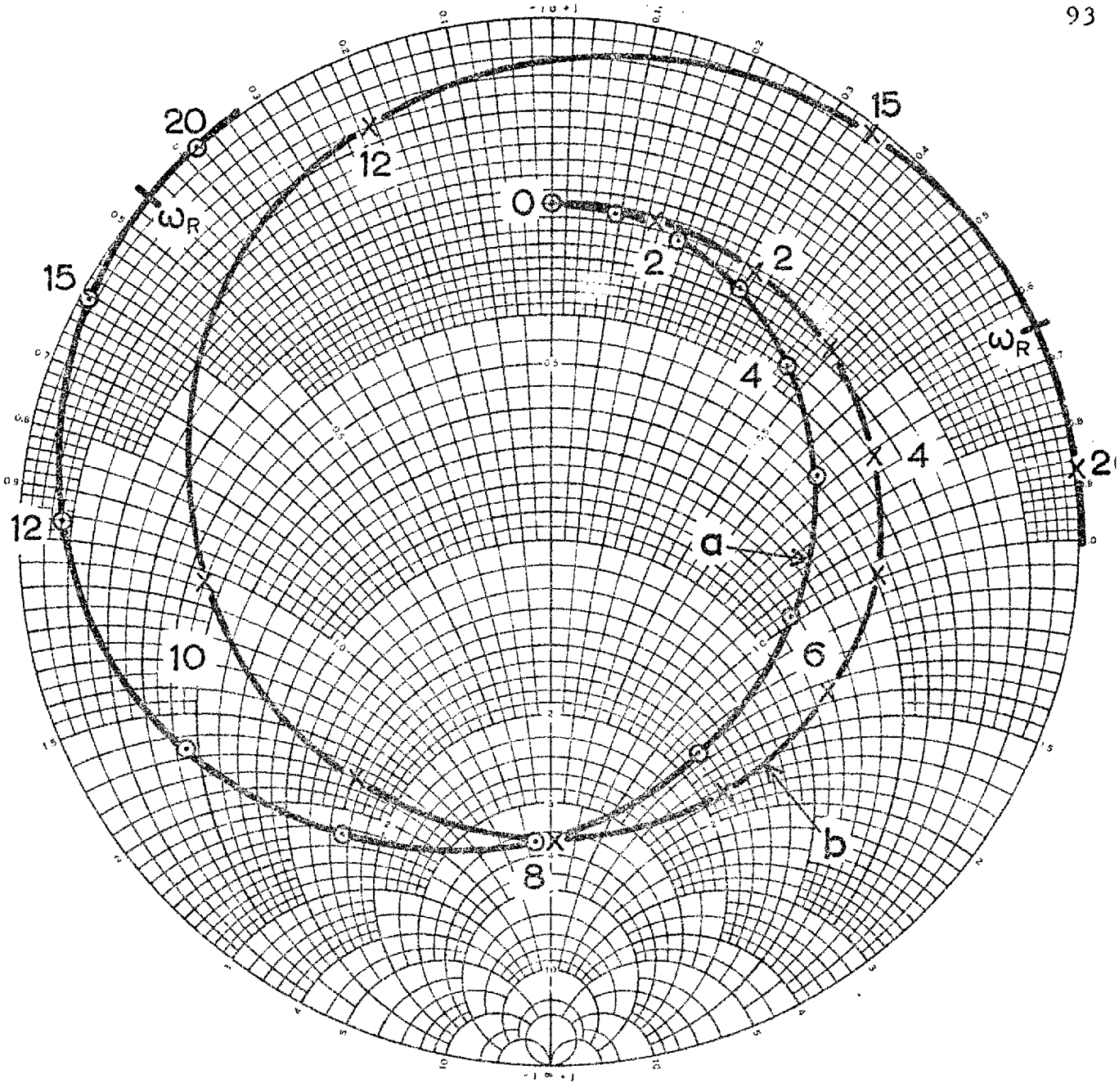

Fig.5.2: Admittance plots normalized to 100 m℧; (a) inversion of curve of fig. 5.1, (b) addition of $j\omega C_1$ to (a).

to $Y_D(j\omega)$ gives $Y_1'(j\omega)$, depicted by curve (b) of fig. 5.2. A study of this curve reveals that it corresponds to the case of fig. 3.7 (c) which leads to fig. 3.8 (c), and apparently has an unpleasant set of RH p-plane poles and zeros (see fig. 3.7 (c)). On inserting the parameter values for the TD for which f_R = 17.7 Gc/s and f_X = 7.9 Gc/s into (3.26), we find this inequality to be violated. The right hand side, which will be referred to as C_1' is .4 pF. The use here of the stability criterion as for fig. 3.7 (a) is justified as follows:

(i) The negative resistance component corresponding to the third zero reactance point of fig. 3.8 (c) is in the region of -240 Ω. If reasonable positive resistance values given by the stabilizing network are added, the resulting resistance may remain substantially negative, and, owing to the large and very rapidly changing reactance in this frequency region and to the fact that the arrangement under consideration corresponds to fig. 3.9 (a) (see also fig. 5.4), a net CCW encirclement of the Z-plane origin could actually occur for fig. 3.9 (a). In this case only 2 RH p-plane zeros arise and not 4 (see table 3.2).

(ii) Alternatively, the problem does not arise if the TD is already cut off, or more nearly so, in this region, in which the series resistance is a very critical parameter, as illustrated by fig. 5.3. Kim and Lee[1] have found r to increase markedly with frequency, and attribute this phenomenon to skin effect. Fukui[2] has also observed r to increase with frequency. McPhun,[3] on the other hand, reports that R decreases with frequency while the other parameters remain substantially constant. Recent discussions with colleagues in the field of microwave applications of TDs suggest that it is very likely that f_R is not as high as low frequency measurements imply. As seen from fig. 5.3, r would need to be barely

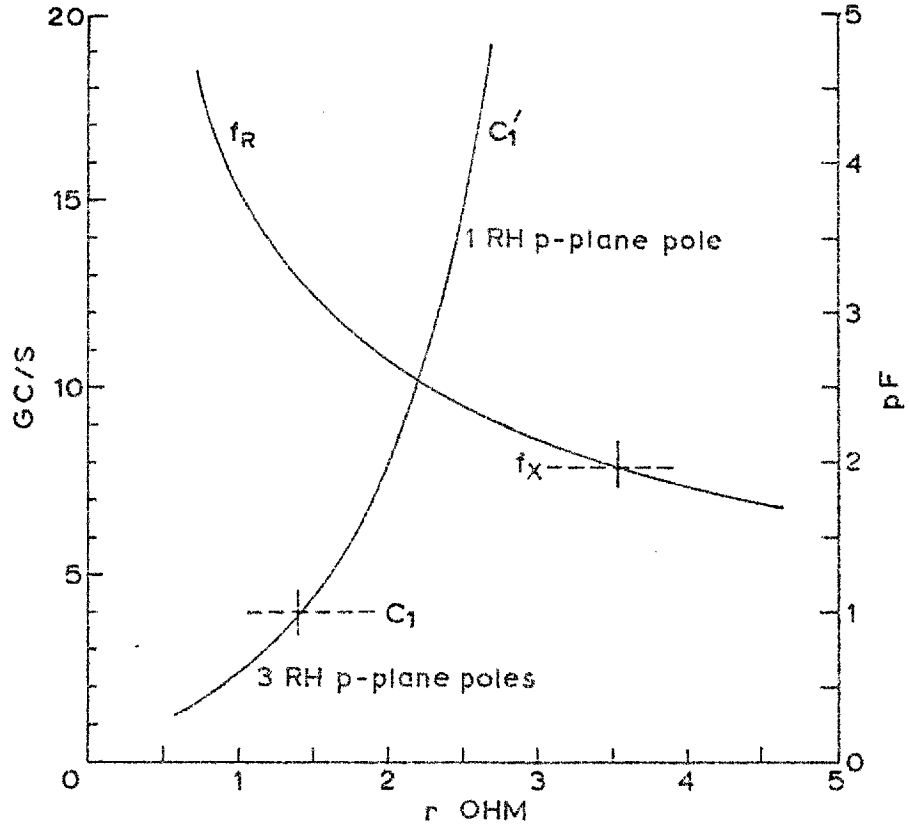

Fig. 5.3: f_R and C_1' as a function of r for the TD.

double its low frequency value at about 13 Gc/s for (3.26) to be satisfied.

(iii) The third argument is that should the amplifier turn out to be unstable at R = 47 Ω, which is R_{min} for this TD, the bias can be altered to increase R and hence lower f_R. Since R/r >>1, the functional dependence of f_R and C_1' on R is very similar to that on r.

Addition of stabilizing network

Fig. 5.4 is the impedance as seen between terminals 1 and 3 of fig. 3.5 (d). It was obtained by adding the stabilizing network impedance plotted in fig. 2.5 to the inversion of curve (b) of fig. 5.2. Fig. 5.4 combines both

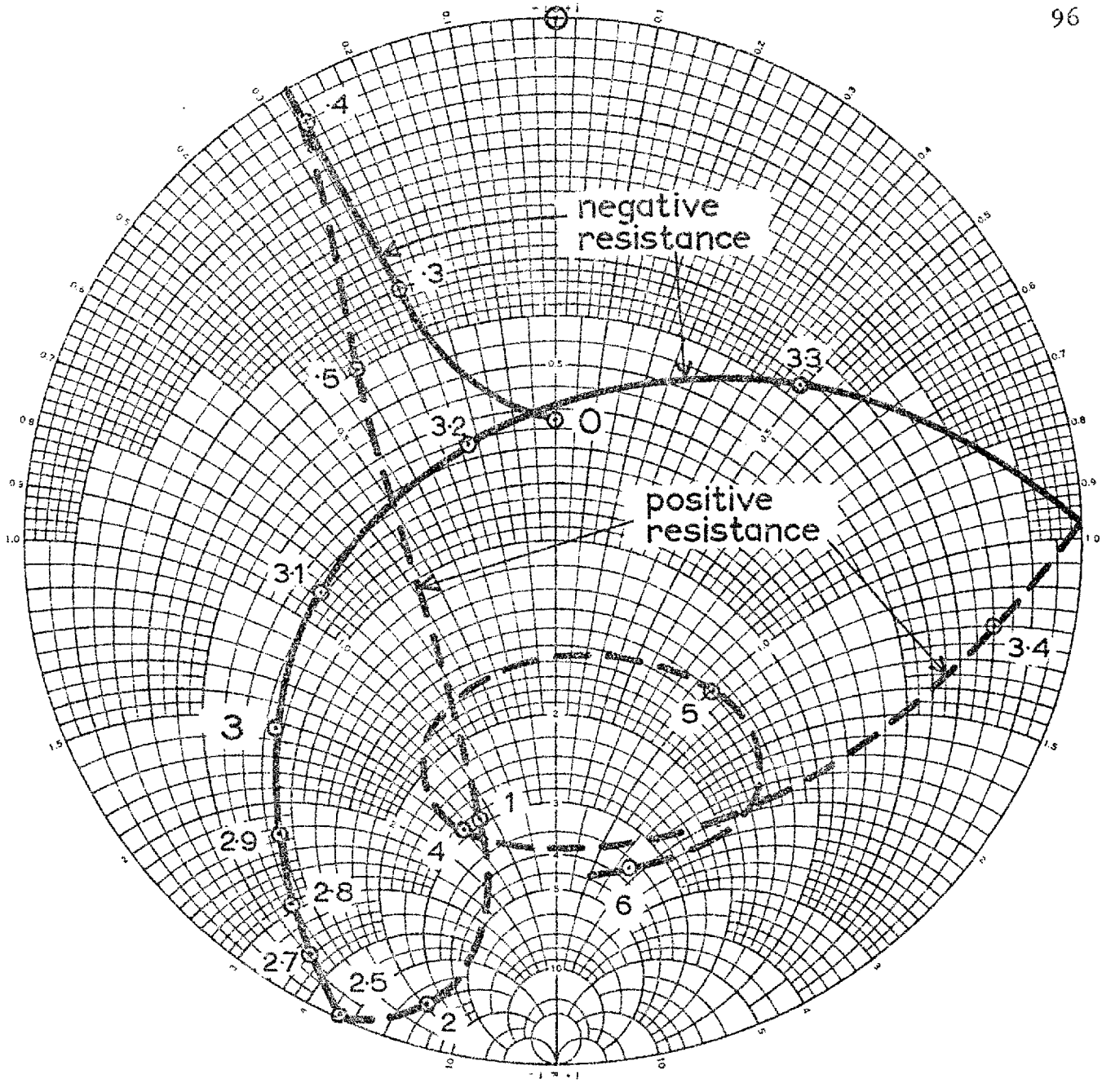

Fig. 5.4: Impedance between terminals 1 and 3 of fig. 3.5 (d), normalized to 10 Ω.

conventional and negative resistance Smith charts; the behaviour of this locus is like that of fig. 3.9 (a). Apart from the negative resistance portion of the locus at low frequencies (see (3.31)), the only "active" frequency region is within S-band.

The connected amplifier

This negative resistance portion is inverted into the admittance chart and normalized to $Y_0(\omega)$, the reduced height waveguide characteristic admittance (fig. 5.5 (a)). The s.c. stub tuning susceptance $jB_{sc}(\omega)$ (fig. 5.5 (b)) is added to give $Y_L(j\omega)$ for three different stub lengths ℓ. From fig. 3.12 (a) and section 4.4 it is known that stable operation prevails only when $Y_L(j\omega)$ encircles the critical point (the centre of the chart) twice in a CW direction, i.e. once in a CW direction for positive ω only. Thus, only the continuous curves of fig. 5.6 indicate stability. Notice that the predicted gain for ℓ = 15 mm reaches a peak of about 19 dB above the "centre" frequency 3 Gc/s (see section 4.2). The curve marked "ideal" shows the calculated gain of the amplifier based on an ideal band-rejection filter as defined in section 3.4: one whose input impedance at the TD terminals is identically zero in the frequency range of interest. It was obtained by normalizing curve (b) of fig. 5.2 and adding $jB_{sc}(\omega)$ for ℓ = 15 mm. The bandwidth for this case was limited mainly by the s.c. stub (see section 2.3). See also curve (iv) of fig. 5.13.

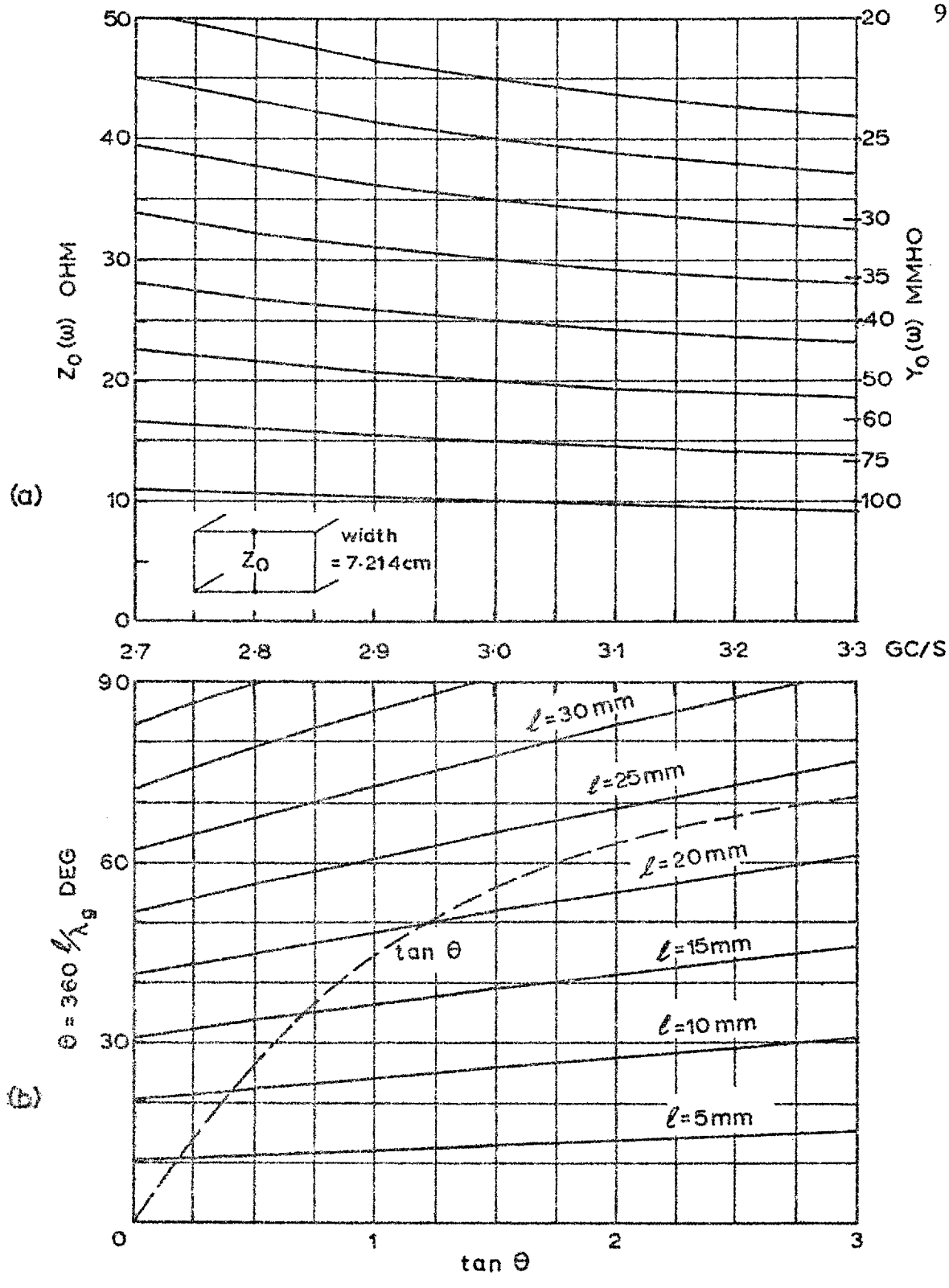

Fig.5.5: S-band rectangular waveguide immittances, (a) matched termination, (b) s.c. termination.

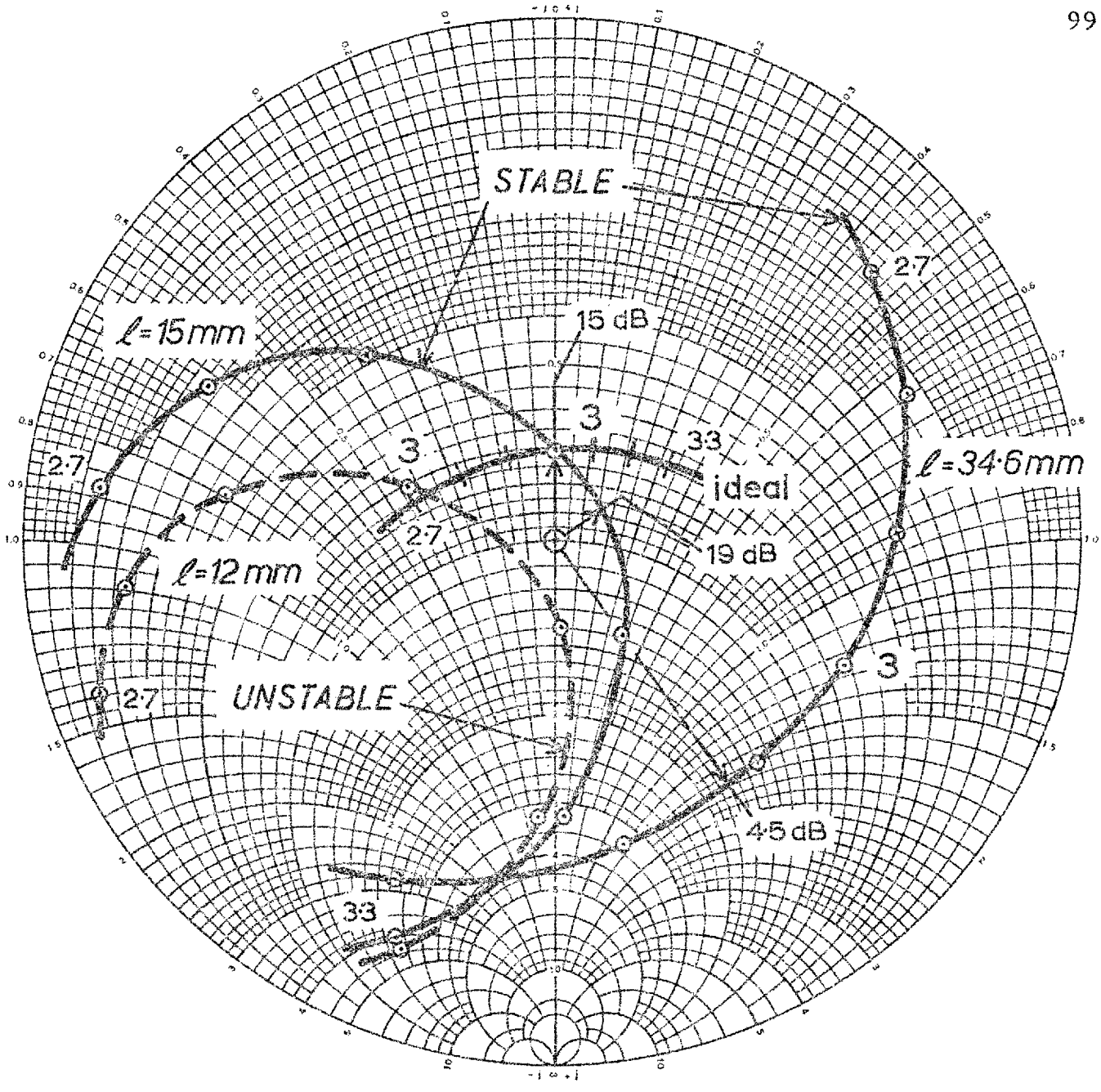

Fig. 5.6: Amplifier gain and stability given by the encirclements of the centre of the chart of the amplifier's admittance normalized to $Y_0(\omega)$, the rectangular waveguide characteristic admittance.

5.4 EXPERIMENTAL RESULTS

Circulator response

Relevant response curves exhibited by the circulator* used with the amplifier are plotted in fig. 5.7. The VSWR at

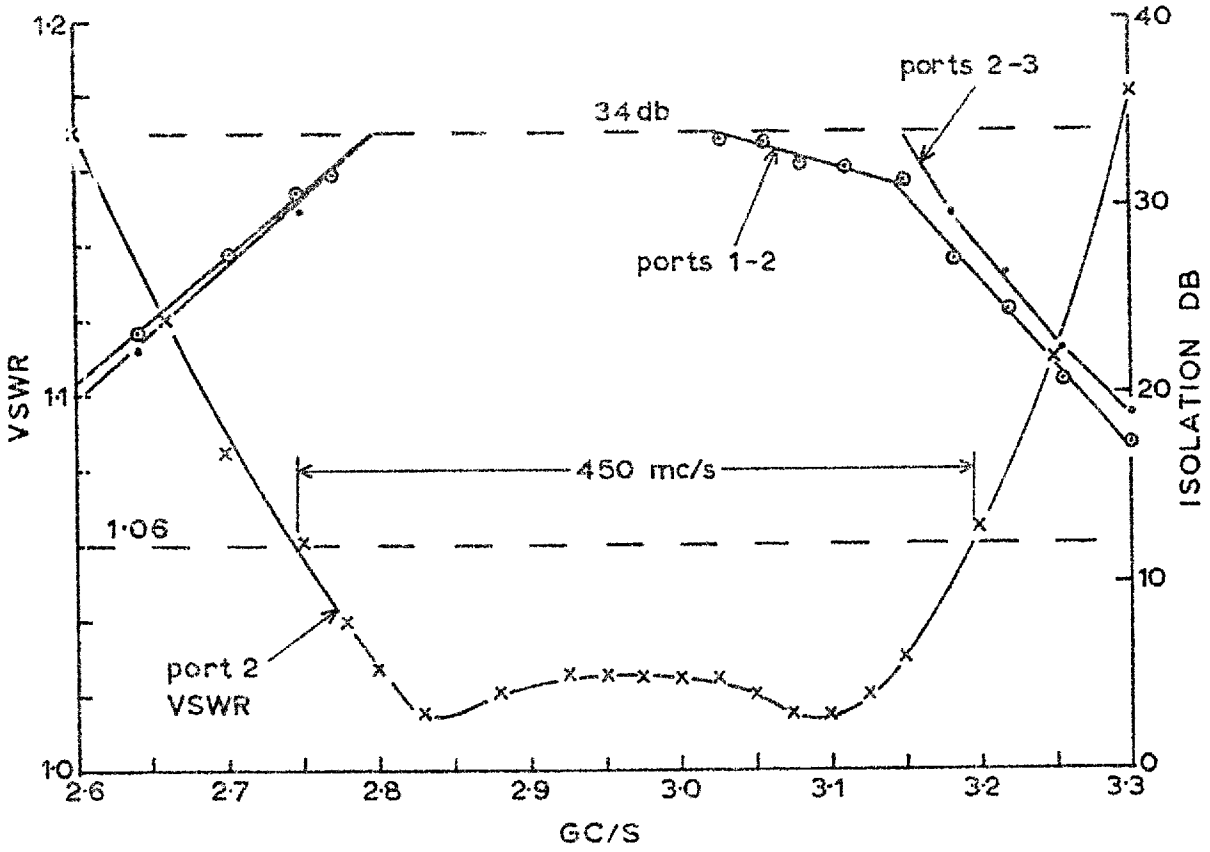

Fig. 5.7: The performance of the circulator.

---

*Marconi three-port rectangular waveguide Y circulator type F1038-01; No.107; frequency 3 Gc/s. The manufacturer's specifications were checked experimentally, and found to be correct. They are:

(i)	over 10% band:	isolation	30 dB min
		insertion loss	0.3 dB max
		VSWR	1.06
(ii)	over 20% band:	isolation	20 dB min
		insertion loss	0.4 dB max
		VSWR	1.2

port 2 was measured with ports 1 and 3 matched. The reverse isolation between ports 1 and 2 and ports 2 and 3 were measured by the substitution method.[4] The forward loss between successive ports was ascertained by the same method to be less than .4 dB from 2.6 to 3.3 Gc/s.

Experimental set-up

A block diagram of the general arrangement of the apparatus is shown in fig. 5.8. The following preliminary

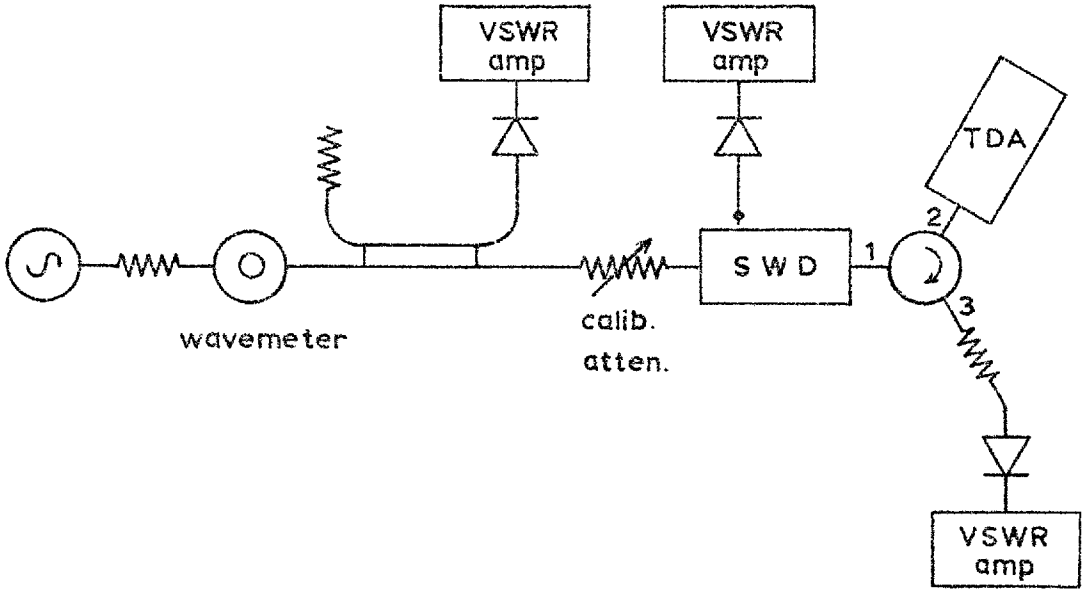

Fig. 5.8: Block diagram of apparatus.

VSWR measurements were made on the TDA connected directly to the SWD. At the frequency of maximum gain the input power was increased until the negative VSWR began to increase, indicating a decrease in return gain. The power level was then reduced by about 10 dB to avoid this gain compression. The gain of the TDA was measured by the substitution method,[4] as follows. With the circulator and TDA removed, i.e. with the

load detector directly receiving the input power, the precision calibrated attenuator was adjusted (at a given frequency) to produce a given deflection on the VSWR amplifier of the load detector. This procedure was repeated at 10 or 20 Mc/s intervals to cover the frequency range of interest; the frequency and the corresponding attenuator reading were recorded. The source power was adjusted throughout to a level giving a constant reference deflection on the directional coupler VSWR amplifier. When the circulator and TDA were reconnected, the gain for any parameter setting of the TDA was given by the increase in dB of the attenuation necessary to produce the required deflection on the load detector VSWR amplifier, after adjusting the power level to produce the reference deflection on the directional coupler VSWR amplifier.

A simple circuit (fig. 5.9) for biasing the TD was constructed. See also section 2.2. for further details. A

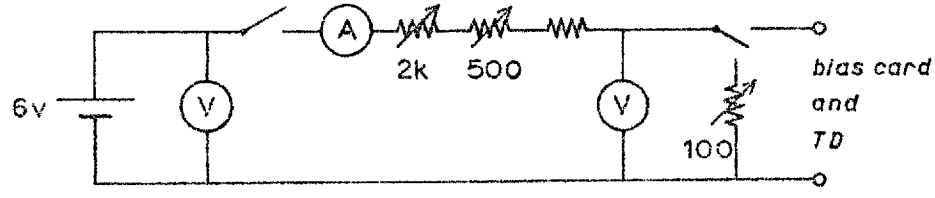

Fig. 5.9: The biasing circuit.

200 Ω per square card was used rather than a 400 Ω per square card as it produced a biasing resistance close to 40 Ω, namely 38 Ω. Difficulties encountered in obtaining the designed value of biasing resistance are attributed to the small working area of the card and to the contact between the card and the centre rod.

The TD was lightly attached to the centre rod of the band-rejection filter with a dab of silver paint. The whole unit was then screwed into the waveguide structure (fig. 2.10).

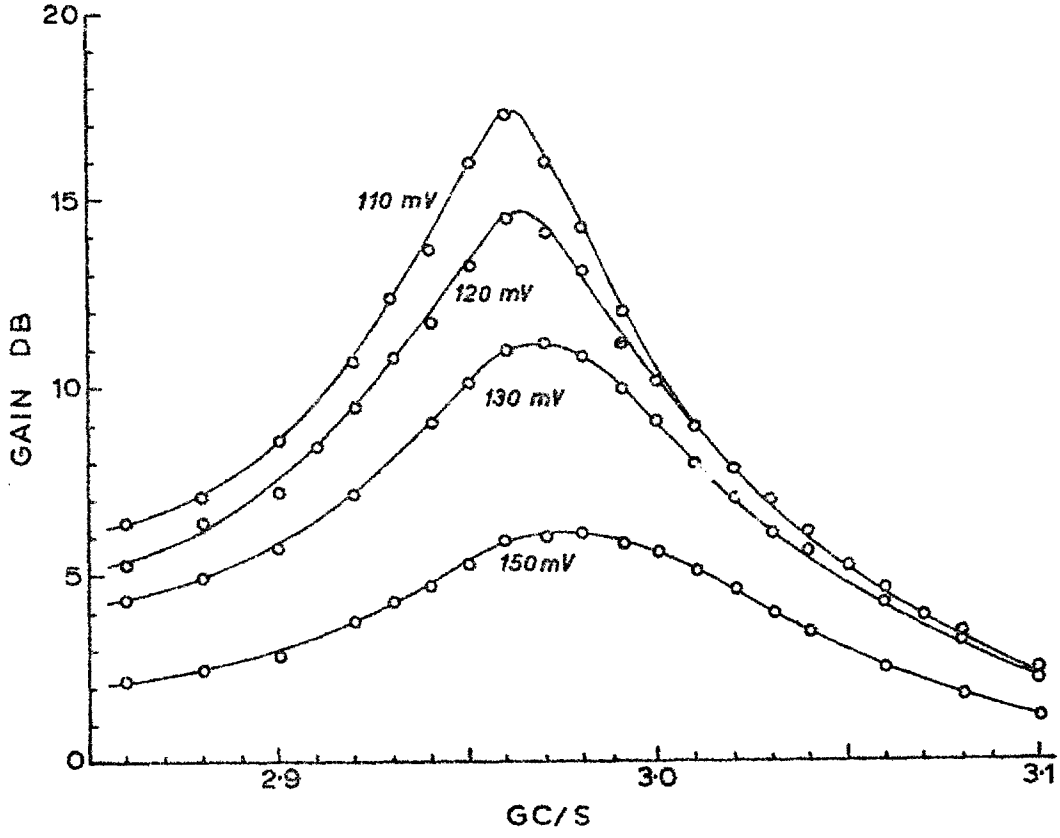

Fig.5.10: Gain vs. frequency at certain bias voltages, for ℓ = 15 mm.

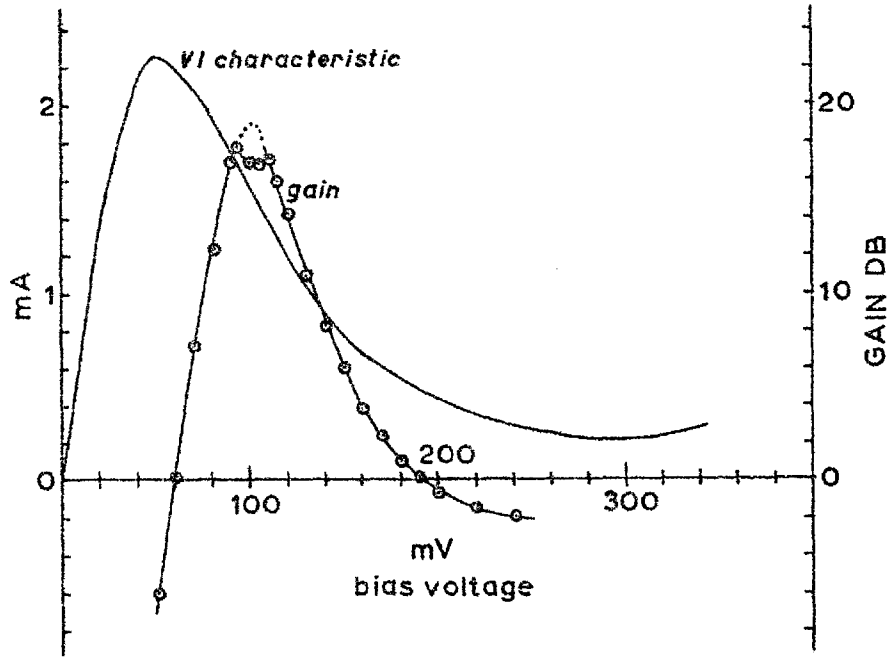

Fig.5.11: Gain vs. bias voltage at 2.96 Gc/s, for ℓ = 15 mm.

The other face of the TD made contact with a small, thin, indented disc of phosphor bronze to prevent excessive force from being applied to it, and to provide a simple means of springing.

Amplifier performance

Note that circulator losses are included in the measured gain curves.

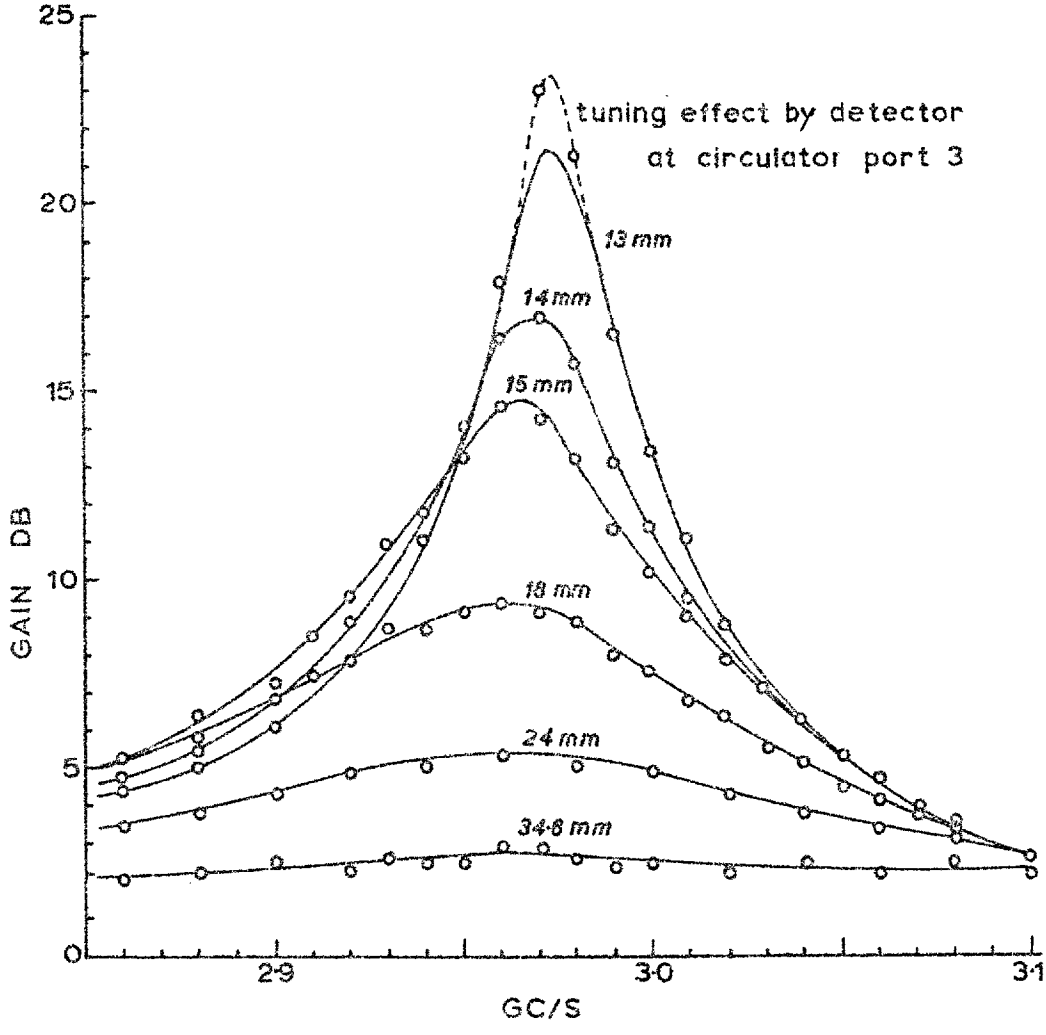

Fig. 5.12: Gain vs. frequency at certain stub lengths, for 120 mV.

Figs. 5.10 and 5.11 show the measured gain for a s.c. stub length ℓ of 15 mm. The band-rejection filter dimensions were as shown in fig. 2.10. Gain vs. bias voltage is plotted in fig. 5.11, superimposed on the VI characteristic of the TD, which was deduced from a curve tracer.

Fig. 5.12 shows the results of varying the stub length at a bias voltage of 120 mV. As noted in the figure, the gain for 13 mm could be affected by mismatches at port 3 of the circulator. 34.6 mm corresponds to $\lambda/4$ at 3 Gc/s, i.e. an o.c. is thrown across the TD at "centre" frequency. An overall gain of 2 dB was observed at this setting.

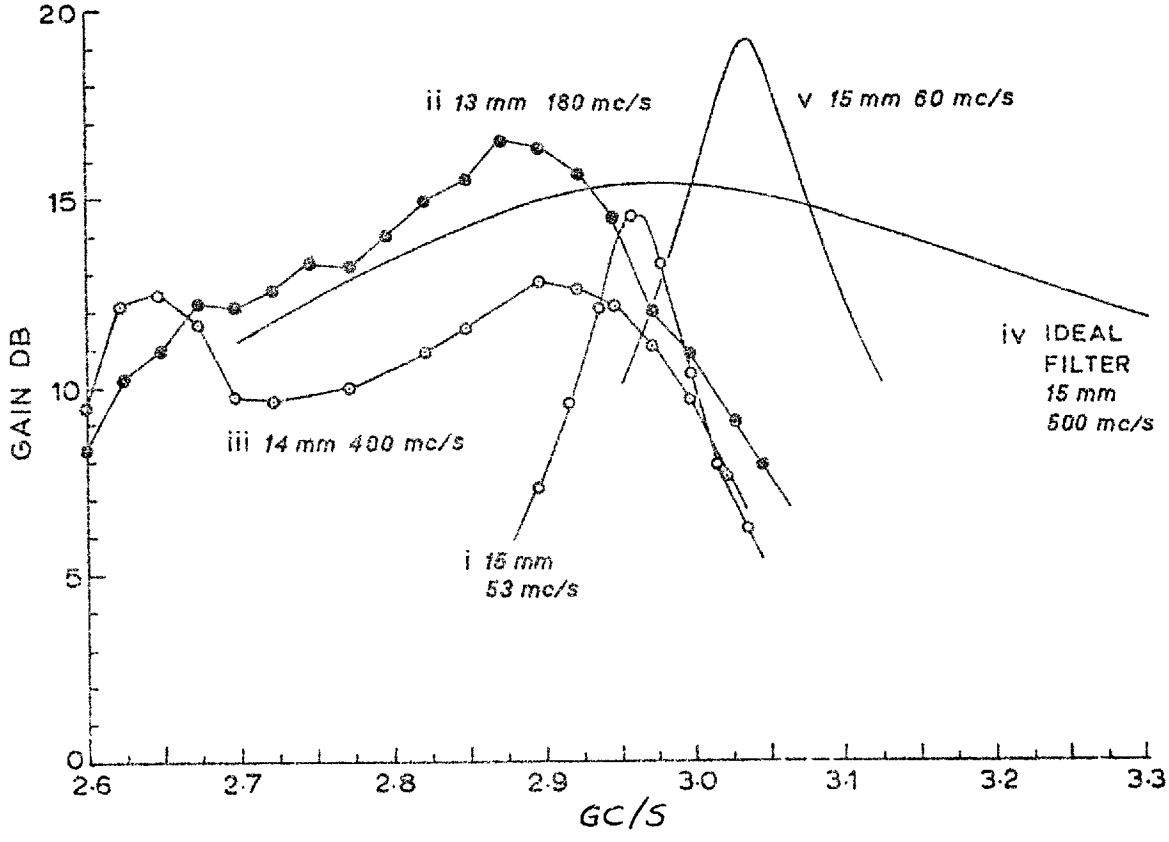

Fig. 5.13: Before and after attempts at broadbanding, and comparison with theory.

5.5 COMPARISON OF PREDICTED WITH EXPERIMENTAL RESULTS

Amplifier as designed

Refer to fig. 5.11. It is seen that there is a small depression in the gain curve just above 100 mV, where $R = R_{min} = 47\ \Omega$. Figs. 5.6 and 5.13 predict a maximum of 19 dB. An out of band parasitic oscillation could have been responsible for this depression, possibly at about 7 Gc/s (see section 2.2). As indicated by the dotted interpolation, the gain should have reached about 19 dB. In practice, for minimum noise,[5] the TD would be operated at a bias voltage above that at R_{min}: 120 mV being suitable for this particular TD.[5,6] For this reason and because the amplifier was absolutely stable at 120 mV, the performance at this bias voltage was thought to provide a fairer comparison with the theoretical prediction. The experimental curves of figs. 5.12 and 5.13 were thus taken at 120 mV. Predicted curve (v) of fig. 5.13 has a maximum of 3.03 Gc/s, experimental curve (i) has a maximum at 2.96 Gc/s; discrepancy: 2.5%.

Stable amplification at $R = R_{min}$ was impossible for $\ell \leqslant 13$ mm. Oscillations were detected at the circulator output arm (port 3) when the source was switched off. This fact confirms the prediction of fig. 5.6. The package capacitance effect (fig. 5.3) is not thought to be responsible for the depression in gain at R_{min}.

Broadbanded amplifier

Two attempts at broadbanding the amplifier experimentally are presented in fig. 5.13: curves (ii) and (iii). To achieve the remarkable increase in bandwidth the following adjustments to the band-rejection filter were necessary (see section 2.4):

(i) The centre rod was replaced by one whose diameter was .181 inches to give a 10 Ω characteristic impedance.

(ii) The resistive card was replaced by one whose resistance per square was 400 Ω.

(iii) The outer radius r_c of the radial-line (fig. 2.2) was decreased by 2 mm by inserting a brass ring into the line. Without this ring the amplifier became unstable in the region of 2.6 Gc/s. Its presence would tend to increase the resonant frequency of the radial-line.

(iv) It was not found necessary to alter the height of the radial-line, i.e. the d dimension.

The predicted gain under ideal band-rejection filter conditions is given by curve (iv) of fig. 5.13. It is emphasized that no account of the actual frequency responses of either the exponential taper or the circulator was taken. This is because no reference to the transformation of complex loads through exponential lines was found. The approximation was therefore made that the TD faced a non-reflecting load. The ideal band-rejection filter could not, of course, be realized because out of band resistive loading of the TD would have been removed, and biasing can not be effected through a 0 Ω transmission-line.

5.6 Conclusion

Making extensive use of the Smith chart, the performance of the S-band TDA has been predicted. The stability problems arising from the addition of the package capacitance has been discussed; possible ways of overcoming the associated theoretical difficulty have been put forward. The predicted gain and stability of the amplifier (fig. 5.6) compares

favourably with the experimental results. Successful attempts at broadbanding (fig. 5.13) have been made: the best produced at 12.7 dB maximum gain a 3 dB bandwidth of 32% (a frequency bandwidth of 14%) based on λ_g.

5.7 References

(1) C.S. Kim and C.W. Lee, "Microwave measurement of tunnel diodes," Microwaves, Vol.3, pp. 18-21, November 1964.

(2) H. Fukui, "The characteristics of Esaki diodes at microwave frequencies," 1961 Int. Solid-State Circuits Conf., Digest of Technical Papers pp. 16-17.

(3) M.K. McPhun, "The equivalent circuit of the tunnel diode," Proc. IEEE, Vol.52, p. 1754, December 1964.

(4) E.L. Ginzton, "Microwave measurements," McGraw-Hill, New York, 1957; pp. 467-469.

(5) B. Easter, "The performance and limitations of low-level amplifiers employing tunnel diodes," Electronic Engineering, Vol.37, pp. 520-523, August 1965.

(6) M.A. Lee, "Tunnel diodes for low-noise amplifiers," Industrial Electronics, Vol.3, pp. 584-586, December 1965.

6

design and theoretical performance of TDA 2

6.1 Introduction

A simple reflection amplifier (TDA 1) was successfully designed, constructed, and tested. It was desired next to investigate the design of another TDA, again with the TD mounted in S-band rectangular waveguide. Waveguide structures more readily amenable to exact frequency response characterization were to be included. In particular, the radial-line band-rejection filter was to be replaced with one composed of coaxial-lines. A quarter wave transformer was to replace the exponential taper. It turned out that a suitable configuration could be used both as a reflection and a transmission amplifier. The latter type of TDA has been considered by several authors.[1-8] See section 1.3.

A digital computer was essential in designing this amplifier. This is because of the non-commensurate nature of the constituent parts, viz. circulator, quarter wave transformer, and inductive iris tuning in rectangular waveguide;

coaxial-line stabilizing and biasing network; and the lumped TD equivalent circuit. It would be a prohibitive task to formulate an exact synthesis technique, as several authors have done for commensurate networks,[1,2,9-11] for such a combination. Extensive use of a digital computer is also preferable to graphical or approximate calculations in this case.*

An account of all the steps taken in designing and constructing the S-band reflection/transmission amplifier is given in this chapter. The optimization of the stabilizing network by computer is described.** A program (the details of which have been published by the author[13]) which produces a digital reflection coefficient plot was frequently used, and is introduced in this chapter. The theoretical gain and stability performance of the amplifier is reported.

6.2 CHOICE OF AMPLIFIER CONFIGURATION

The most natural mount for a TD in a rectangular waveguide is a symmetrical one in a reduced height section, with its terminals effectively connected to the broad faces of the waveguide. A compatible stabilizing and biasing system must, as in the previous amplifier, be in series with the TD.

---

*All computer programs written by the author were in FORTRAN IV, for use on the IBM 7090 digital computer.

**An increasing interest is being shown by network designers into the ideas of mathematical programming[12] as a basis for designing complicated networks by computer to have specified or optimized responses. No publication on the application of these ideas to microwave network synthesis has, however, been brought to the author's attention. For this reason, the present techniques tend to be straightforward in nature.

In the envisaged coaxial-line network, the second resonance would occur at a frequency three times the first one. As no insurmountable difficulties were experienced previously by using resistive-film cards for biasing (section 2.2), these were to be used again.

Quarter wave transformers can be made superior to exponential tapers of the same overall length in impedance matching.[14-20] The possibility exists of changing the response by altering the Z_0 values for the individual sections, and any complex load admittance, e.g. a circulator's response, can readily be transformed theoretically through the transformer.

The disadvantages associated with the use of a s.c. stub for inductive tuning has been discussed in section 2.3. The variation with frequency of the reactance of a rectangular waveguide symmetrical inductive iris[21] is, however, almost linear over a substantial frequency band. This structure can be realized in a plane intersecting the TD. Using such an iris for tuning permits the TD to be backed either

(i) by a s.c. line of high Z_0 and of length $\lambda_{go}/4$, in which case the TDA is of the reflection type, or

(ii) by a quarter wave transformer having one section and leading to a full height waveguide which can then be used as the input end of a transmission TDA.

The requirements for (i) and (ii) can be readily combined: the reflection amplifier would have a removable plate short-circuiting the input of the transmission amplifier. Furthermore, the Z_0 of the section in question can be such as to provide a nominal match at the input port.*

---

*As pointed out in section 1.3, the matched transmission amplifier is inferior to the reflection amplifier. In view of this and because of the relatively low cost and availability of low loss broadband circulators, and the fact that isolation of the output port of the transmission amplifier is required anyway, its practical application is not foreseen.

6.3 FREQUENCY RESPONSES IN THE ρ-PLANE PLOTTED BY DIGITAL COMPUTER[13]

It is very often necessary to predict changes in reflection coefficient ρ or VSWR or input H as a function of frequency, say, caused by adjustment of some variable in the load of a transmission-line, or its transformation towards the generator. For an active load, e.g. a TDA, information on gain and stability is required. The task is generally tedious if done manually.

In appendix A1 details are given of a computer program which provides a plot of active or passive real frequency immittances as on a Smith chart, utilizing the complete ρ-plane, i.e. including the ρ'-plane. It takes the form of a subroutine into which Z or Y values are fed as calculated by the main program, and which generates a print-out of voltage or current reflection coefficient, respectively. It was designed both as an extension of the ideas of section 4.3, and for application to transmission-line problems generally.

The program was invaluable during the design of TDA 2. A glance at the print-out was sufficient in determining stability, and the effects of parameter variation on the shape of the response could be rapidly observed. See section 6.9. The program is referred to hereafter by its name CHART1. Examples of computer print-outs are figs 6.1, 6.9, and 6.14.

6.4 ONE-PORT PROGRAM AND CIRCULATOR RESPONSE

It is important to know the circulator performance when designing broadband TDAs: the stabilizing network must fit in with the circulator, or vice versa. Pertinent to this section is a brief account of a program useful in obtaining the input parameters of any transmission-line load,

determined by experiment.[22] This is found in appendix A2. The experimental procedure is described at the same time.

Standing wave measurements were carried out on port 2 of the circulator (see section 5.4), and the relevant readings fed into the computer. Figs. 6.1 and 6.2 are the results of interest here. The first shows a print-out of $y_c(j\omega)$ instructed by CHART1 (section 6.3); the second shows corresponding plots of $g_c(\omega)$, $b_c(\omega)$, and VSWR as a function of frequency.

It was found convenient to take 2.6 and 3.3 Gc/s as the lower and upper frequency limits, respectively, of the amplification band. As seen in fig. 6.2, the circulator VSWR is less than 1.2 over this band. The "centre" frequency in S-band rectangular waveguide is shown in section 6.8 to be 2.93 Gc/s.

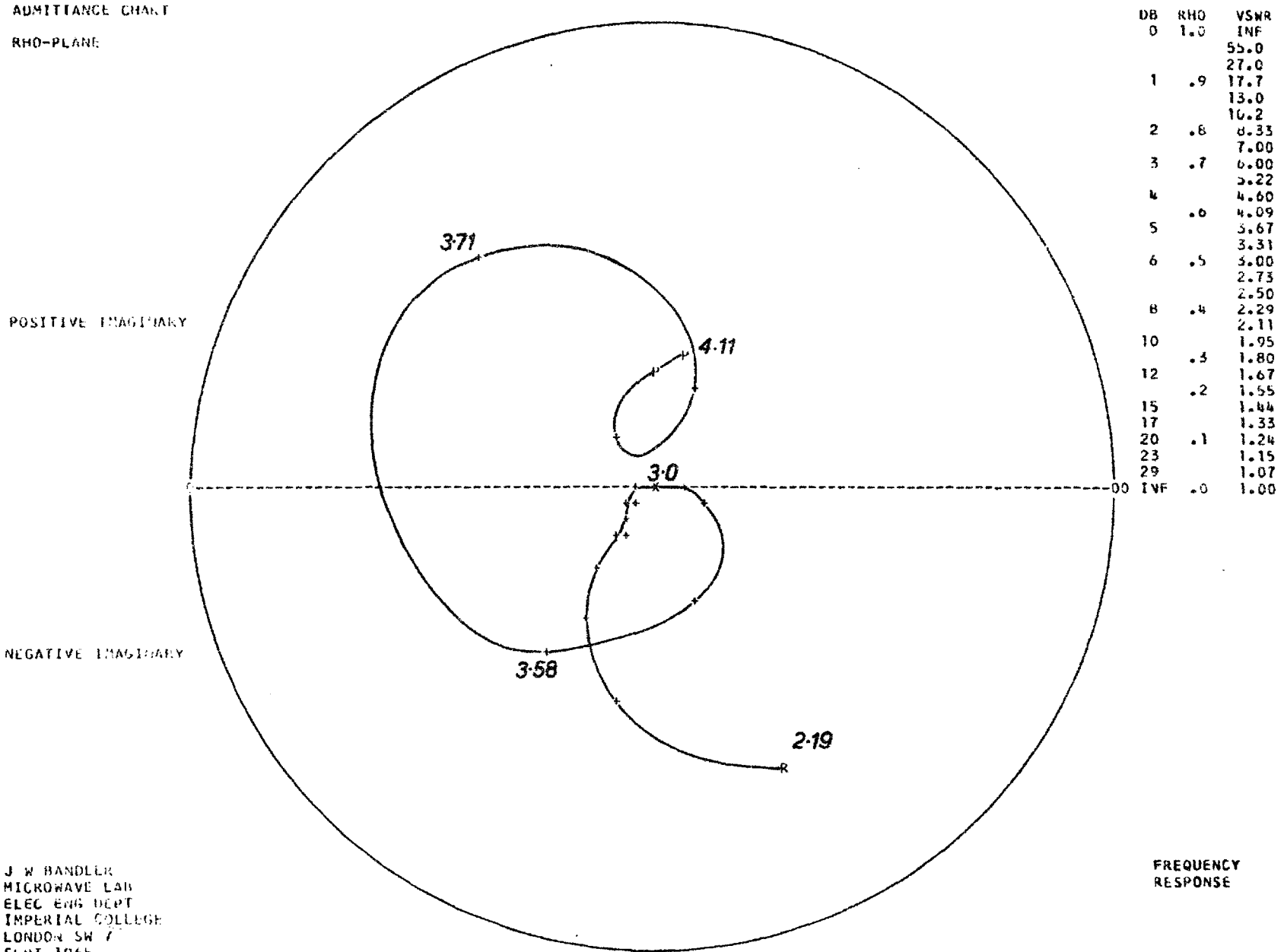

Fig. 6.1: ρ-plane plot of the admittance $y_C(j\omega)$ of port 2 of the circulator.

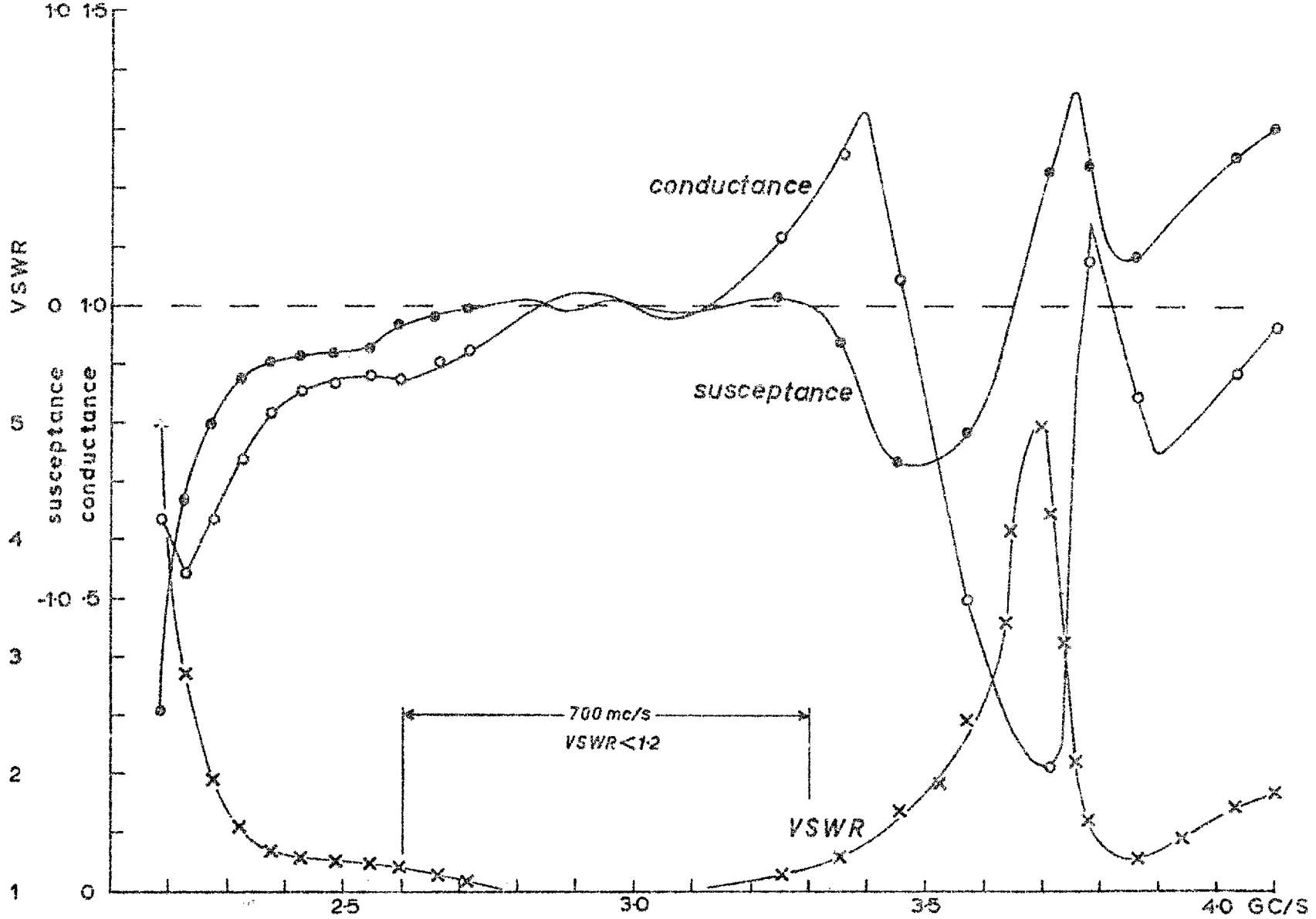

Fig. 6.2: Results of standing wave measurements on port 2 of the circulator.

6.5 THE OPTIMIZED STABILIZING NETWORK

6.5.1 Preliminary considerations

Without doubt, the stabilizing network is the most important part of the present amplifier. The following considerations have influenced its design:

(i) For the reasons given in section 6.2, it must be in series with the TD.

(ii) Because of (i), the network must exhibit zero input impedance $Z_i(j\omega)$* somewhere in the amplification region. This can be accomplished theoretically by an o.c. line shunting the input to the network. The o.c. line can then be transformed through a transmission-line section of the same electrical length by Kuroda's identity[23-27] giving a s.c. series line - it is not physically feasible in the envisaged configuration to have an o.c. shunt line very close to the TD.

(iii) The parameters of the TD were chosen to be

R_{min} = 45 Ω, C = 2 pF, r = 1 Ω, L = .12 nH, and C_1 = .3 pF.

Fig. 6.3 shows the variation of TD impedance $Z_{TD}(j\omega)$** with R. Because of the rapidly diminishing magnitude of $R_{TD}(\omega)$, the positive stabilizing resistance $R_i(\omega)$ should not be as high at the high frequency end of the amplification band as at the lower end, so as not to deteriorate the gain and noise figure. As far as stability is concerned, less positive resistance is required anyway at higher frequencies to cancel $R_{TD}(\omega)$. The magnitude of $X_i(\omega)$ must similarly be restricted; special care

---

*Z_i corresponds to Z_2 of chapter 3 (fig. 3.5 (d)).

**Z_{TD} is identically equal to $1/Y_1'$ of chapter 3.

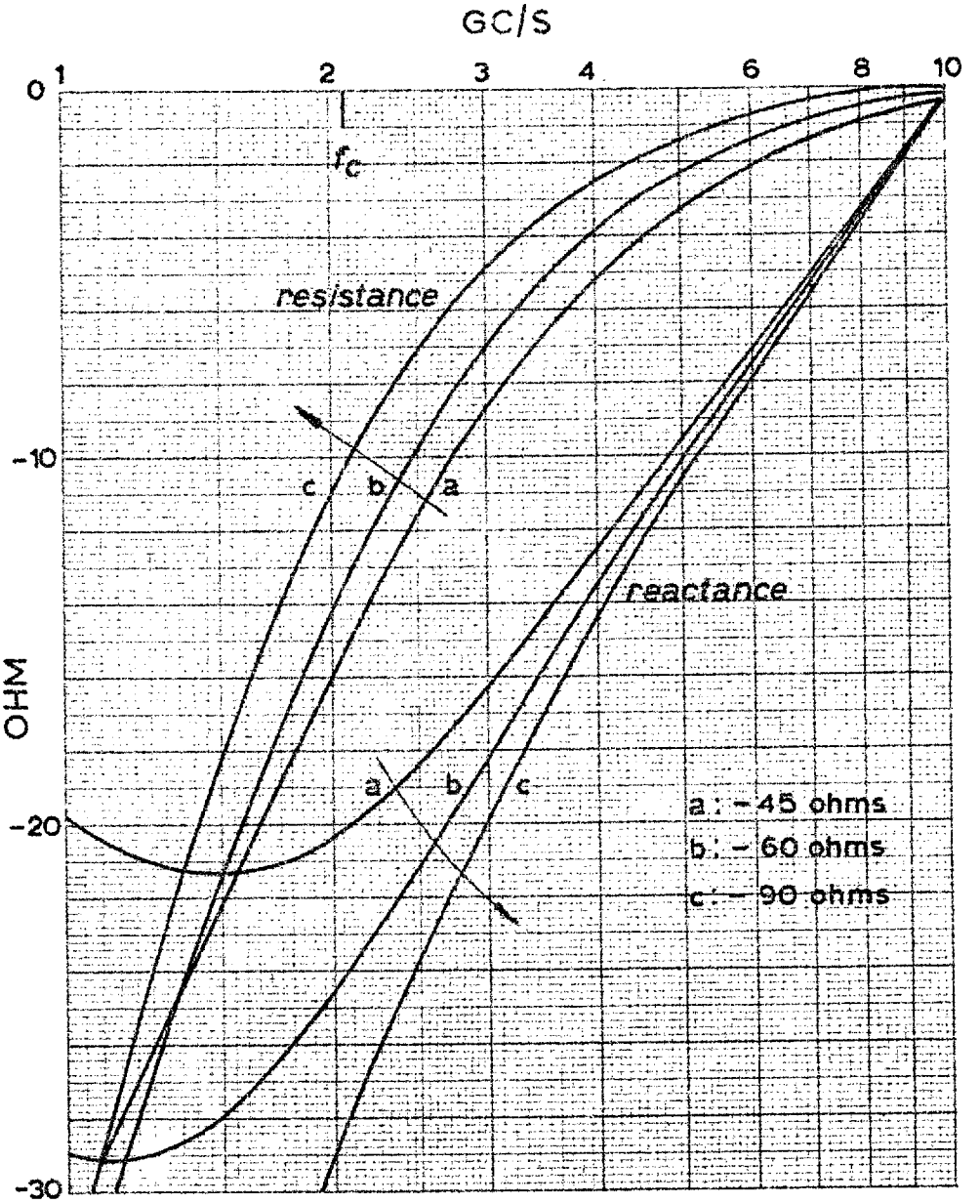

Fig. 6.3: $Z_{TD}(j\omega)$ for three values of R, when
C = 2 pF, r = 1 Ω, L = .12 nH, and C_1 = .3 pF.
a: R = 45 Ω, f_R = 11.7 Gc/s, f_X = 10.1 Gc/s
b: R = 60 Ω, f_R = 10.2 Gc/s, f_X = 10.2 Gc/s
c: R = 90 Ω, f_R = 8.3 Gc/s, f_X = 10.2 Gc/s.

N.B. Equation (3.26) is satisfied by this TD.

is necessary to ensure that it does not get out of hand at the high frequency (inductive) end before $R_i(\omega)$ cuts the TD off.

(iv) The circulator response, especially high values of VSWR, e.g. at 3.7 Gc/s in fig. 6.2.

(v) The waveguide cut-off frequency f_c, here 2.08 Gc/s. An infinitely long ideal rectangular waveguide is a straightforward case, but not so a waveguide set-up such as fig. 5.8 near f_c.

6.5.2 Its configuration

The stabilizing network configuration is shown in fig. 6.4.

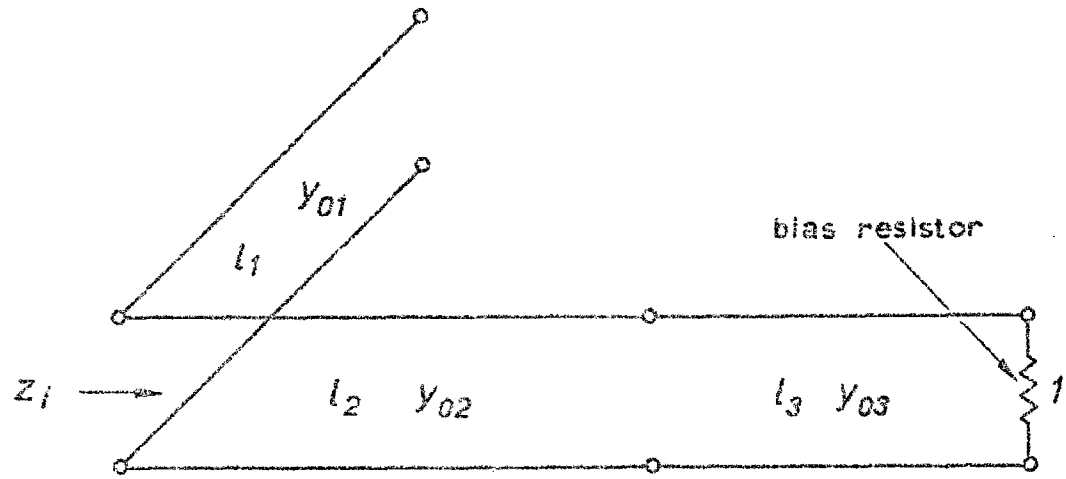

Fig. 6.4: Prototype of the stabilizing network.

It takes the form of a three section prototype of a coaxial-line band-rejection filter. Filters of this type whose sections are commensurate in length[19,24-28] have $R_i(\omega)$ and $X_i(\omega)$ symmetrical and antisymmetrical, respectively, about f_o. The necessity of some control over both $R_i(\omega)$ and $X_i(\omega)$ (rather

than insertion loss, say) has already been emphasized,* coupled with the idea of non-symmetry. Hence, it was decided to develop a computer program to optimize the response of the filter of fig. 6.4 in accordance with certain specifications.

The line lengths ℓ_1, ℓ_2, and ℓ_3 (and consequently the resonant frequencies f_{o1}, f_{o2}, and f_{o3}, respectively) and their characteristic admittances (normalized to the bias resistance) y_{01}, y_{02}, and y_{03} were allowed to vary. To use the Kuroda identity subsequently on the o.c. shunt line (see fig. 6.5)

$$\ell_2 > \text{or} = \ell_1 \tag{6.1}$$

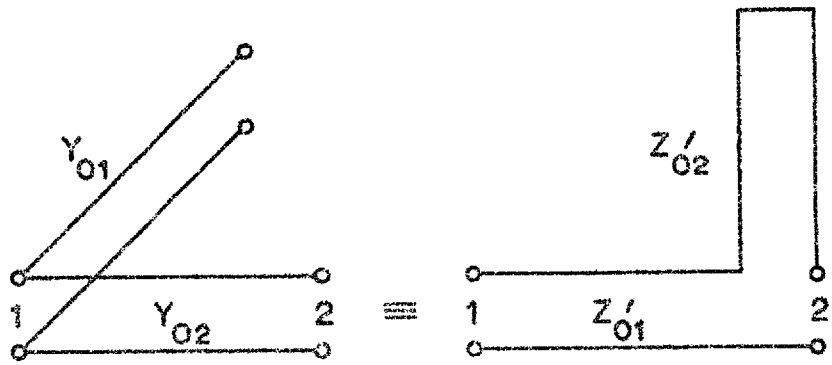

Fig. 6.5: Kuroda identity for o.c. shunt line to s.c. series line transformation. $Z_{01}' = 1/(Y_{01} + Y_{02})$. $Z_{02}' = Y_{01}Z_{01}'/Y_{02}$.

---

*Young discusses the relations between input resistance and input reactance of minimum reactance networks in a recent work.[29] The reactance of such networks is determined by the resistance.

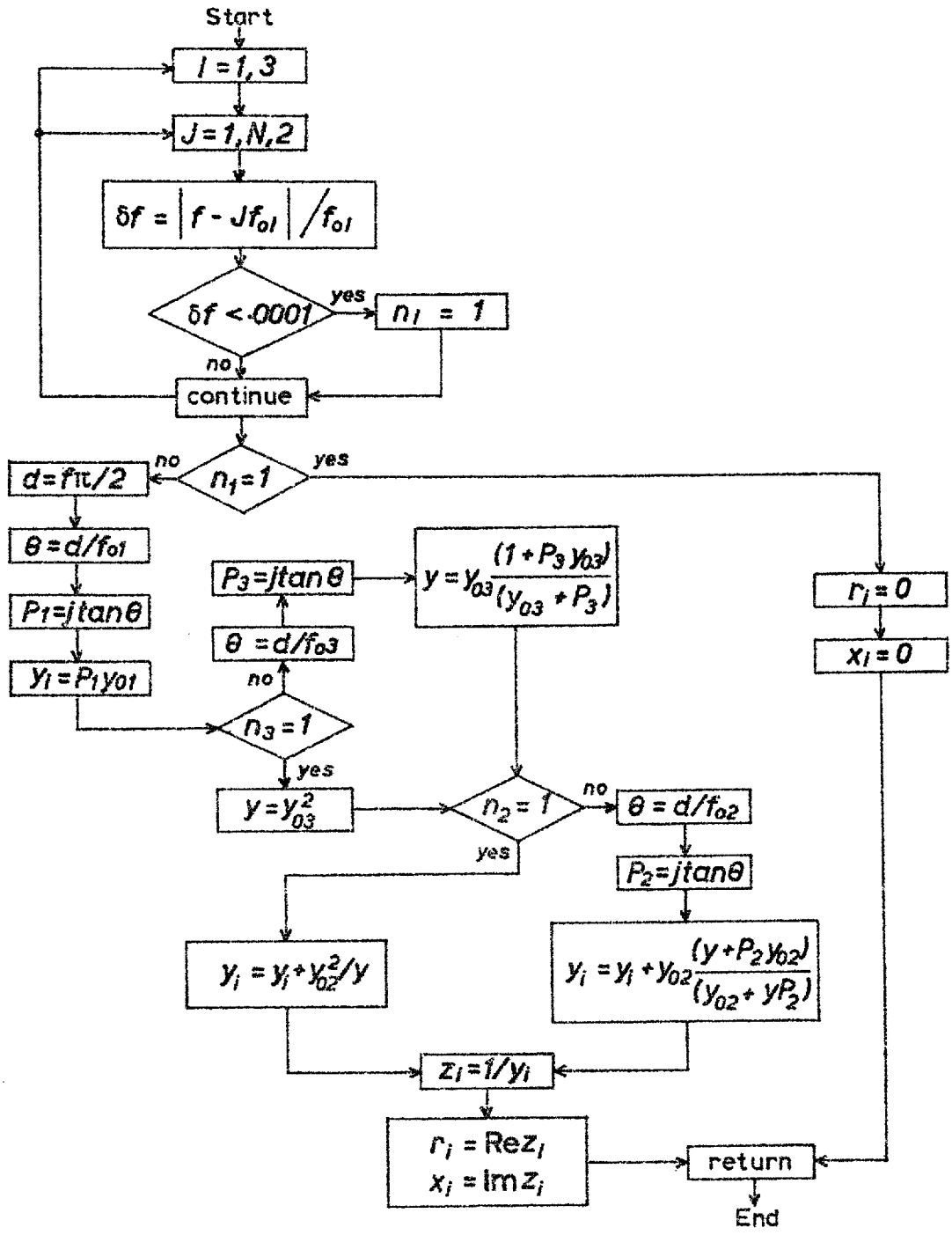

Fig. 6.6: A flow diagram for subroutine STAG written to calculate z_i ($=Z_i/R_b$) for fig. 6.4 at any specified frequency f.

6.5.3 The computer program

Fig. 6.6 serves a number of purposes. It is essentially a flow diagram for a subroutine* (called STAG) to calculate $Z_i(\omega)$; it defines the variables used in the calculation[30]; it summarizes the transmission-line transformations involved.

A definition of the "specifications" C_1 to C_9, and the frequencies f_1 to f_6 at which they operate is shown in fig. 6.7. The specifications impose limits upon R_i and X_i

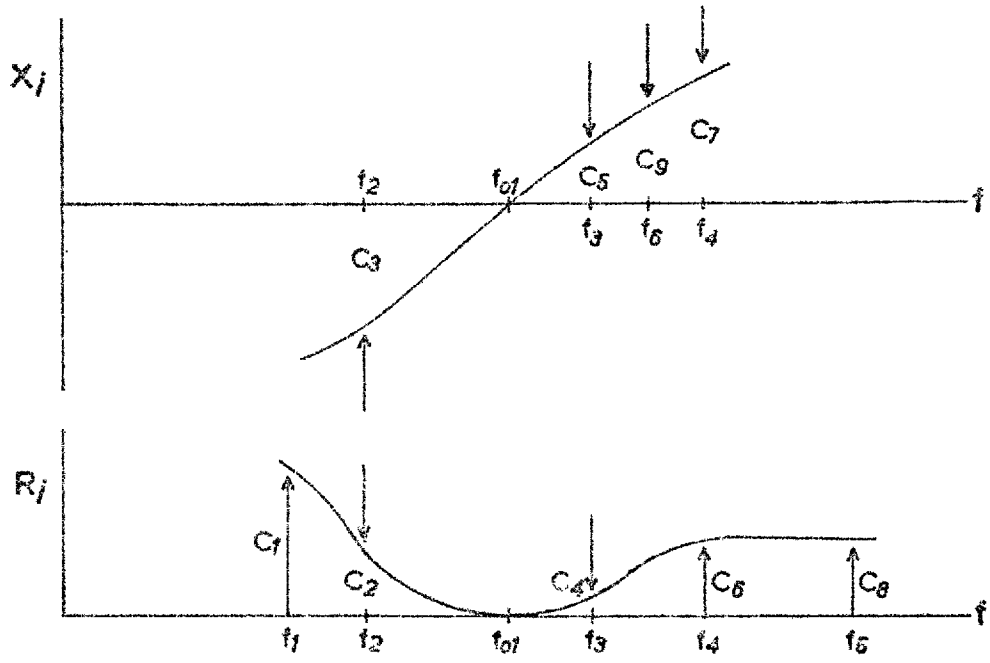

Fig. 6.7: Specifications to shape the response of the stabilizing network.

---

*The part of the diagram between "start" and "continue" was devised to determine when $f\pi/2f_{oI}$ was sufficiently close to $(2J-1)\pi/2$, where J is an integer, so that the length of the Ith line could be taken as an odd number of quarter wavelengths at f. This safeguards the computer from handling very large (or infinite) values of tan θ.

which have to be observed each time a variable is incremented. The object of the program is to minimize U, where

$$U = \sum_{j=3,5,7,9} \left[x_i^2(\omega) \Big|_{c_j} \right] * . \qquad (6.2)$$

Details of the complete program are found in appendix A3.

6.5.4 The present requirements

The test frequencies, f_1 to f_6 in Gc/s were

$f_1 = f_c = 2.078$, $f_2 = 2.6$, $f_3 = 3.3$, $f_4 = 3.7$, $f_5 = 4.2$, and $f_6 = 3.5$.

The specifications C_1 to C_9 in ohms with $R_b = 40\,\Omega$, were

$C_1 = 16$, $C_2 = 1.6$, $C_3 = 8$, $C_4 = .32$, $C_5 = 3.2$, $C_6 = 6.8$, $C_7 = 8.8$, $C_8 = 7.05$, and $C_9 = 6.8$.

A discussion of the reasons for choosing the above values follows.

With the TD inductively tuned within the 2.6 to 3.3 Gc/s region, and with $X_i(\omega)$ capacitive from d.c. to f_c, no instability problems were anticipated below f_c. Two provisos are necessary. The first is that f_R or f_X, whichever is least, must be well above S-band, i.e. the TD must exhibit an equivalent parallel susceptance $B_{TD}(\omega)$ which is capacitive and still increases with ω at S-band. The second is that the inductive tuning reactance $X_t(\omega)$ increases continuously with ω from d.c. into this band. Consider the curves from 0 to ω_X in fig. 3.6(a), and 0 to ω_R in fig. 3.6(b).

---

*This is calculated as V by the computer and set equal to U only when V < U. See appendix A3.

$B_{TD}(\omega)$ for the TD of fig. 6.3 increases steadily into X-band. Hence, with a stabilizing network of zero impedance, there should be no intersection of the tuning element and TD susceptances below S-band. This means that below f_c, at any rate, the situation roughly corresponds to that of fig. 3.12.

The foregoing discussion may give the impression that no stabilizing effect is required below the amplification band. Points (iv) and (v) of section 6.5.1 suggest, however, that unconditional stabilization around f_c itself is in order. For this reason, $C_1 + R_{TD} > 0$ at f_c. See fig. 6.3. No special precautions below f_c were considered necessary, apart from $X_i(\omega)$ being capacitive.

C_2 to C_5 were made as small as possible in accordance with point (iii) of section 6.5.1. The program was run a few times with these specifications somewhat relaxed but with the rest applying as stated: it was observed from the results that these specifications were not unreasonable. Note that the average of C_2 and C_4 is very nearly equal to r.

For unconditional stability above the amplification band, $C_6 + R_{TD} > 0$ at 3.7 Gc/s, while C_7 is as small as possible; but in any case $C_7 + X_{TD} < 0$ is a good criterion to apply. At 4.2 Gc/s, $C_8 + R_{TD} > 0$, and at 3.5 Gc/s $C_9 + X_{TD} < 0$, with reasonable safety margins.

Initially,

$$U = \frac{1}{R_b^2}\left[\sum_{j=3,5,7,9} (C_j^2)\right] \quad . \qquad (6.3)$$

6.5.5 Computer results and discussion

The program was run as described in appendix A3. No difficulties were encountered in its use. The results

obtained are

$y_{01} = 1.417001$ $\quad f_{o1} = 3.100200$ Gc/s $\quad \ell_1 = 2.417526$ cm
$y_{02} = 2.111000$ $\quad f_{o2} = 2.699709$ Gc/s $\quad \ell_2 = 2.776155$ cm
$y_{03} = 2.099800$ $\quad f_{o3} = 2.899991$ Gc/s $\quad \ell_3 = 2.584426$ cm.

Fig.6.8 is a plot of $Z_i(j\omega)$ with these values.* Note that $X_i(\omega)$ is capacitive below f_c and that $\ell_2 > \ell_1$.

It is no coincidence that y_{03}, f_{o1}, f_{o2}, and f_{o3} differ only slightly from 2.1, 3.1, 2.7, and 2.9, respectively. Two principal causes for this are proposed. Firstly, the o.c. shunt line at the input (fig. 6.4) is the predominating element in the vicinity of resonance, since

$$Z_i \approx \frac{1}{jY_{01} \tan \frac{\pi f}{2f_{o1}}} \approx 0 . \qquad (6.4)$$

Secondly, once trial and error values assigned to the variables satisfy the specifications, y_{01}, the first variable incremented (see fig. A 2), tries as far as possible to make up for the other variables before they too are incremented.

These arguments suggest that it may be possible to achieve a performance fulfilling the specifications with, say, $\ell_3 = 0$. This condition can be fed into the computer as data by setting $y_{03} = 1$, and not permitting y_{03} or f_{o3} to be incremented. The program itself is unaffected by this change. In the present case, however, y_{02} differs from y_{03} by about .5%. Thus, y_{02} can, for practical purposes, be taken as equal to y_{03}.

---

*During the second set of optimization cycles, i.e. when the initial increments of the parameters were reduced (see appendix A3), the sixth decimal place was allowed to vary. None of the cycle limits was, however, reached.

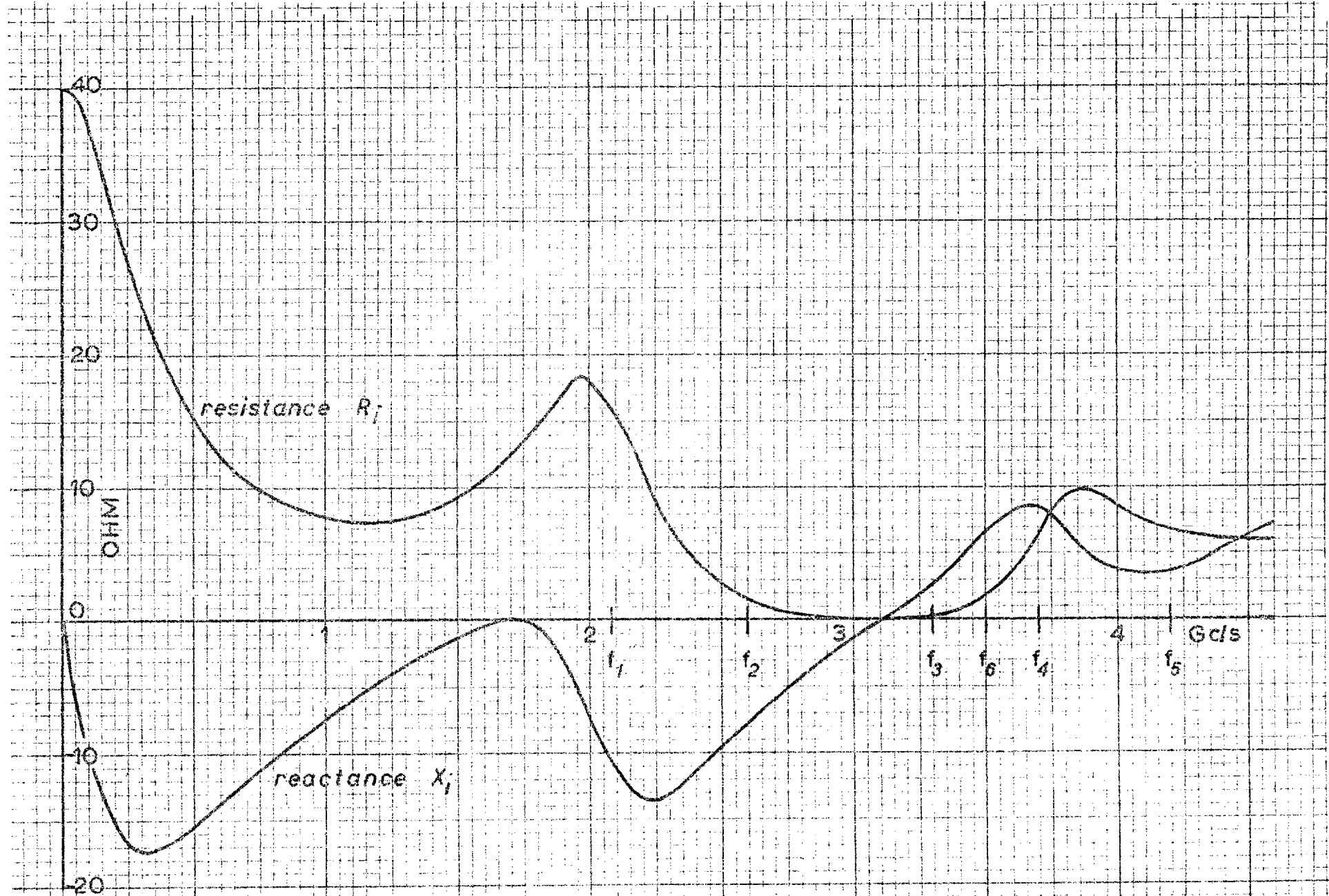

Fig. 6.8: Input impedance $Z_i(j\omega)$ to stabilizing network for parameters shown in section 6.5.5.

6.5.6 Addition of $Z_i(j\omega)$ to $Z_{TD}(j\omega)$

A print-out of $Z_i(j\omega) + Z_{TD}(j\omega)$ instructed by CHART1 is shown in fig. 6.9.* $Z_i(j\omega)$ is taken from fig. 6.8; $Z_{TD}(j\omega)$ is taken from fig. 6.3, for $R = R_{min} = 45\ \Omega$. (Fig. 6.9 was actually produced during a run of the TDA program outlined in section 6. 9.)

A number of observations should be made. The impedance has a capacitive component while its net resistance is negative. The net resistance is positive around f_c. At the upper end of the amplification band the plot leaves the negative resistance chart perpendicularly to the unit circle; but the implications of this phenomenon are not yet understood.

*The frequencies are: 0 to 175 Mc/s in steps of 25 Mc/s; 200 Mc/s to 4.6 Gc/s in steps of 100 Mc/s. Quantization inevitably caused some overwritten points - hence they are missing.

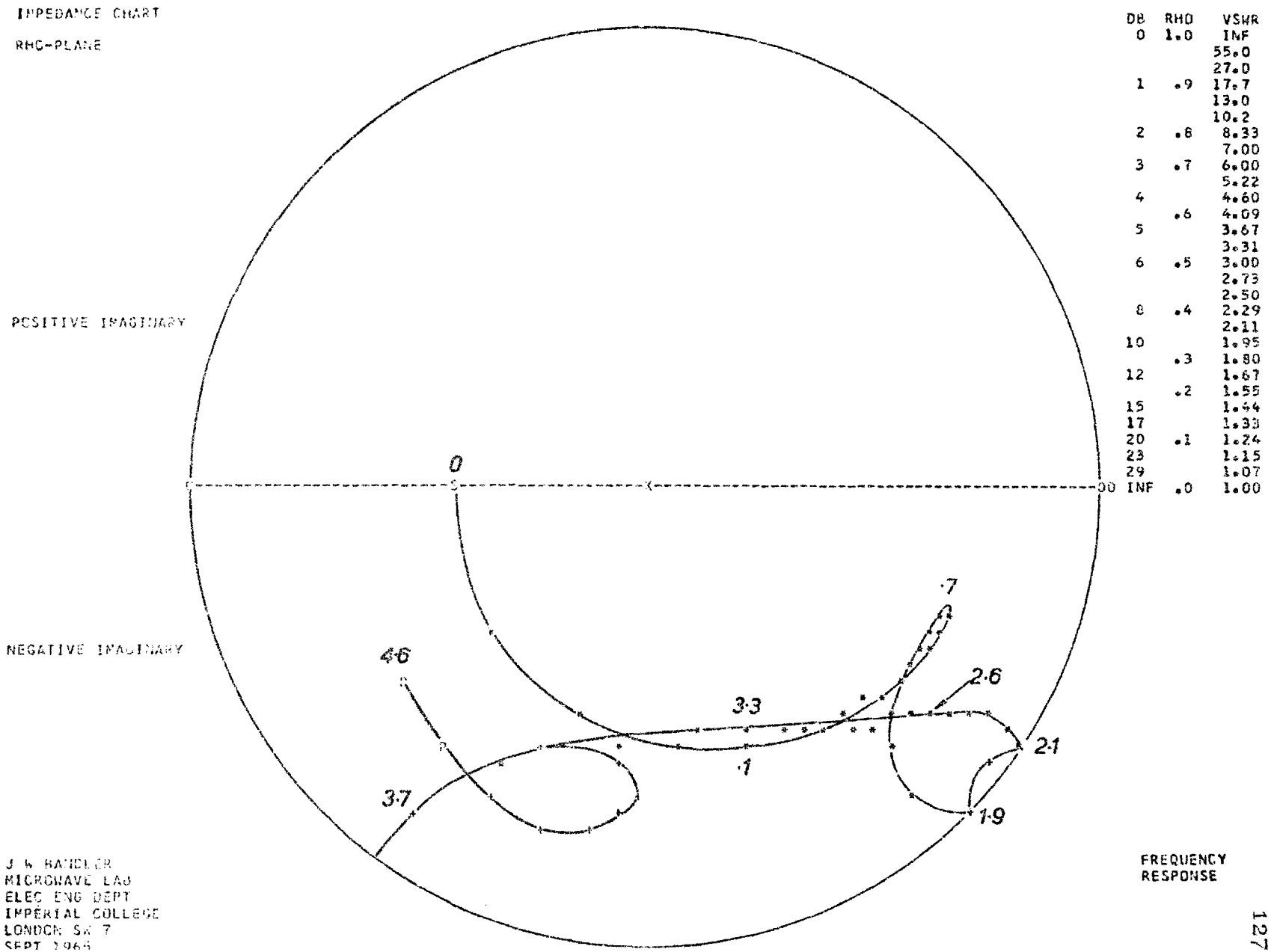

Fig. 6.9: Plot of $Z_i(j\omega)+Z_{TD}(j\omega)$ normalised to $10\,\Omega$. See section 6.5.6.

6.6 INDUCTIVE TUNING

The use of an inductive iris for tuning a TD mounted in a rectangular waveguide does not appear to have been previously investigated. The effect of the TD on the iris reactance may be likened to its effect on the waveguide Z_0. For the purpose of theoretical predictions, the normalized iris reactance x_t was taken from Marcuvitz[21] as

$$x_t = \frac{a}{\lambda_g} \tan^2 \frac{\pi d}{2a} \left\{ 1 + \frac{3}{4} \left[\frac{1}{\sqrt{1 - (\frac{2a}{3\lambda})^2}} - 1 \right] \sin^2 \frac{\pi d}{a} \right\} \qquad (6.5)$$

where a and d are defined in fig. 6.10. This formula is alleged to be correct within 5% for $a < \lambda < 2a$. The equivalent circuit is said to be valid within the range

$$\frac{2}{3}a < \lambda < 2a. \qquad (6.6)$$

It does not seem unreasonable, however, to extrapolate this range to include

$$2a < \lambda < \infty \qquad (6.7)$$

for investigating the stability of the amplifier; and also to take Z_0 as the appropriate voltage-power value (see (2.6)). X_t ($= x_t \cdot Z_0$) is continuous from $\lambda = \infty$ where $X_t = 0$ to $\lambda = 2a/3$ where $X_t = \infty$. (Experimental support for some of these assertions is furnished in chapter 7.) $\lambda = 2a/3$ when f = 6.23 Gc/s.

Equations (2.6) and (6.5) were programmed: fig. 6.10 shows $B_t(\omega)$ of the iris for b' = .075 inches (.1905 cm). As is seen in section 6.9, an aperture d = 4.2 cm tunes the amplifier (theoretically) to a peak at about 2.93 Gc/s (see section 6.8). A program for calculating the susceptance of a s.c.

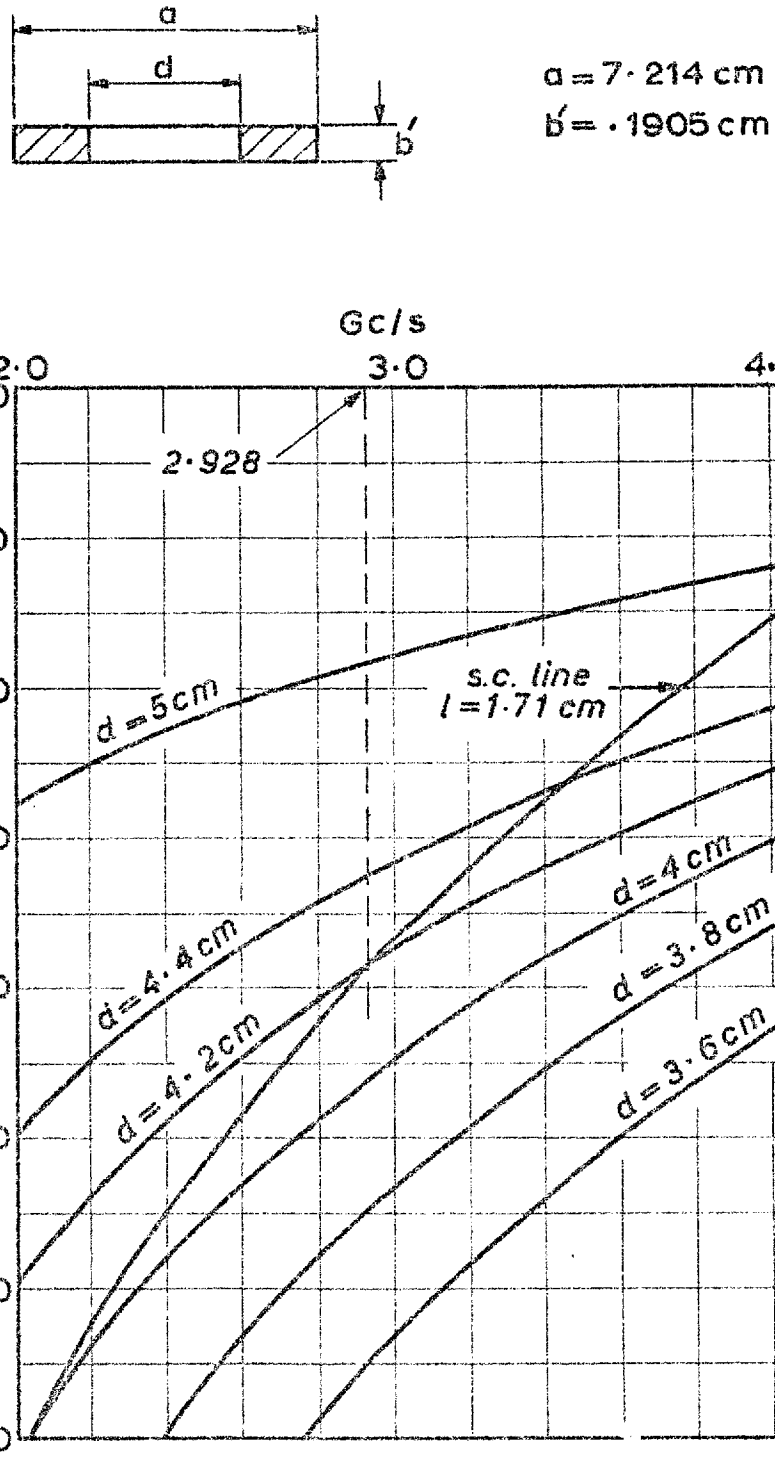

Fig. 6.10: Susceptance of the waveguide inductive iris for various values of aperture d. The susceptance of a s.c. line of the same height is shown for comparison.

line in rectangular waveguide was written. Such a line of height .1905 cm, and length 1.71 cm produces the same susceptance at 2.93 Gc/s. Fig. 6.10 compares its response with that of the iris.

6.7 POTENTIAL STABILITY OF THE TDA

At this stage, a quantitative check on the "potential" stability of the amplifier is in order. The arguments of section 6.5.4 should now be seen in the light of the addition of the stabilizing network (section 6.5.6) and the inductive iris (section 6.6) to the TD.

It is convenient to define the amplifier admittance Y_A' as

$$Y_A' = jB_t + \frac{1}{Z_i + Z_{TD}} \quad . \qquad (6.8)$$

Fig. 6.11 shows $Y_A'(j\omega)$ produced by inverting the curve of fig. 6.9 and adding $B_t(\omega)$ for d = 4.2 cm. It is clear that a positive conductance can shift the plot in the range 2.6 to 3.3 Gc/s to the right past the origin. There will then be no encirclements of the origin of the Y-plane by $Y_A'(j\omega)$, and hence no RH p-plane zeros. The resulting stable curve is similar to that shown in fig. 3.12 (b).

6.8 THE QUARTER WAVE TRANSFORMERS

It was decided to design initially a maximally flat transformer between TD and circulator. When it was certain the TDA was working successfully, an optimized transformer was to be obtained by computer to increase the bandwidth.

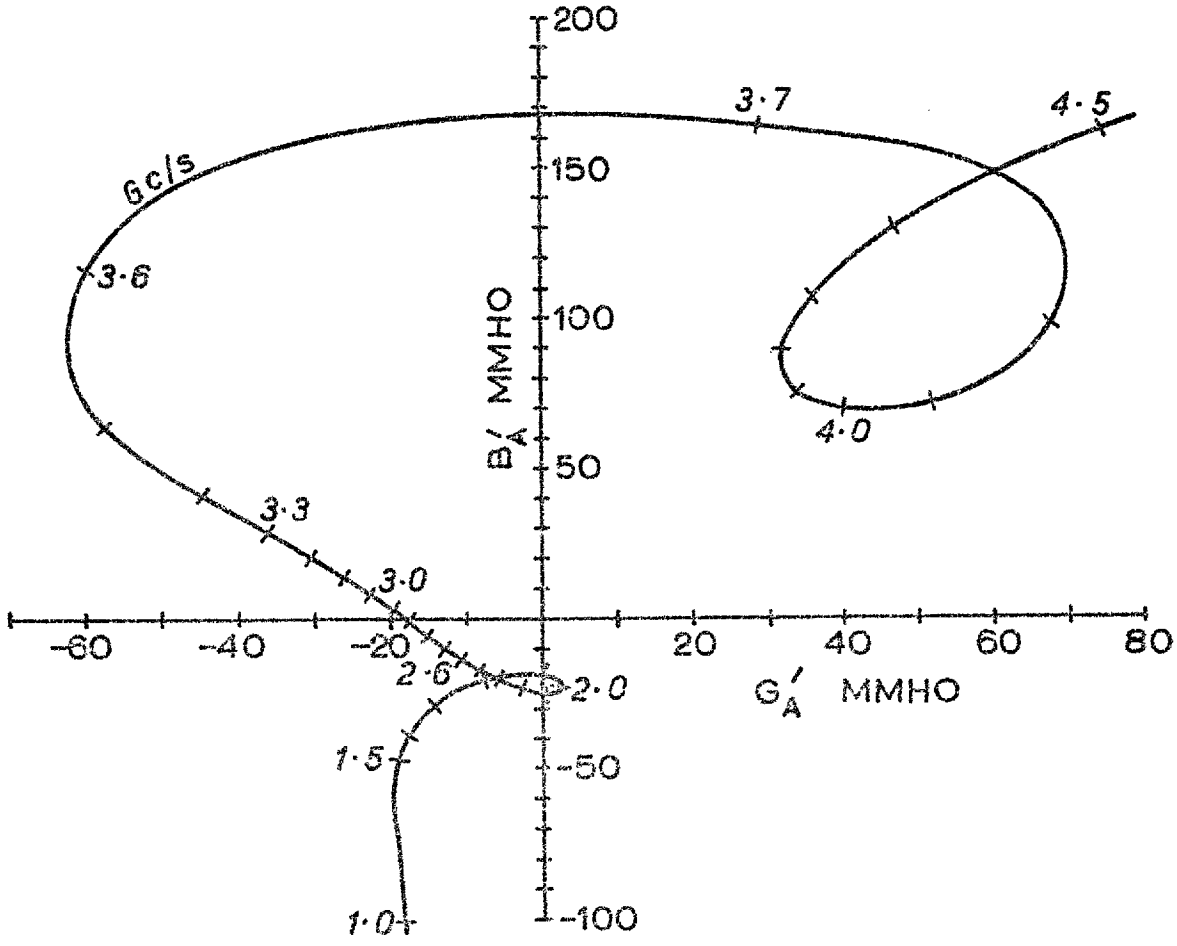

Fig. 6.11: Nyquist plot of $Y_A'(j\omega)$ (see section 6.7). The corresponding $Y_A'(p)$ has no poles in the RH p-plane: see fig. 3.11 (b) and fig. 3.12 (b).

This section deals briefly with the maximally flat transformer, and with the single section transformer at the input to the transmission amplifier.

In its simplest (tuned) form the TDA was to be represented as fig. 6.12 (a). The gain as a transmission amplifier is

$$G = |t|^2 = \frac{4 \times 1 \times 4}{(4 + 1 - 3)^2} = 4 \rightarrow 6 \text{ dB} .$$

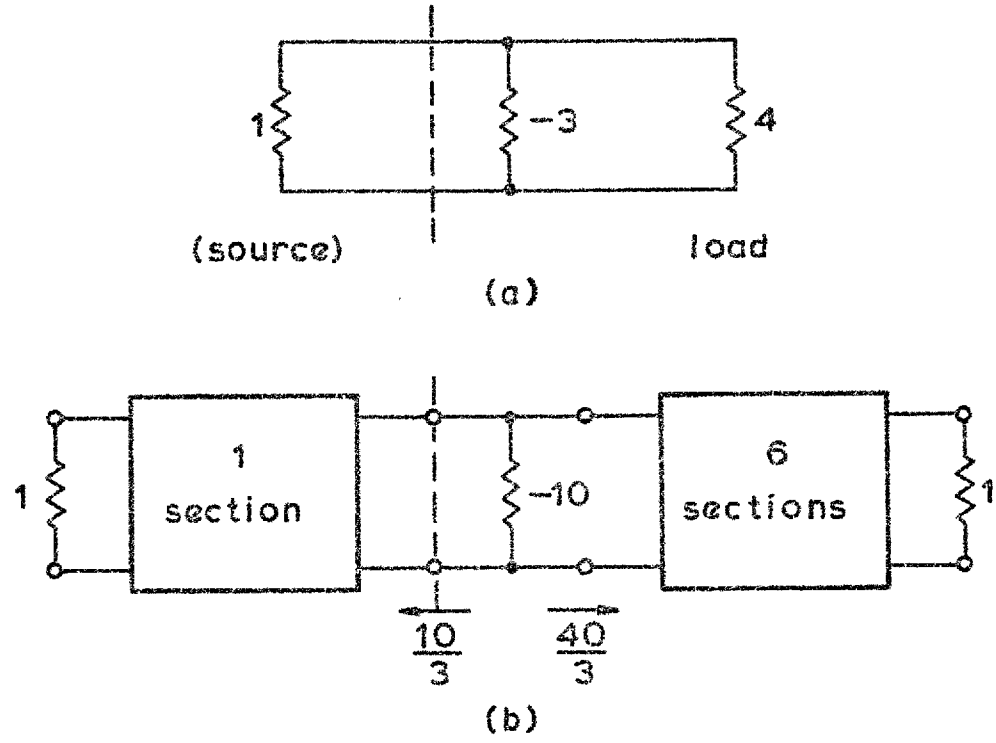

Fig. 6.12: Simplified representation of the present reflection and transmission amplifiers.

Note that the input conductance to the transmission amplifier is 1, i.e. it is matched at the input port. Its output reflection coefficient, however, gives a return gain of

$$|\rho_o|^2 = \left(\frac{4 + 2}{4 - 2}\right)^2 = 9 \rightarrow 9.5 \text{ dB.}$$

This is 3.5 dB greater than its transmission gain. The gain as a reflection amplifier (with the circuit to the left of the dashed line of fig.6.12 removed) is

$$G = |\rho|^2 = \left(\frac{4 + 3}{4 - 3}\right)^2 = 49 \rightarrow 16.9 \text{ dB.}$$

The length of each section of waveguide transformer is[16-18]

$$\ell = \frac{\lambda_{go}}{4} = \frac{\lambda_{g1} \cdot \lambda_{g2}}{2(\lambda_{g1} + \lambda_{g2})} \qquad (6.9)$$

where λ_{g1} and λ_{g2} are the guide wavelengths at the lower and upper frequencies of the transformer, respectively. For a symmetrical response between 2.6 Gc/s (λ_{g1} = 19.1813 cm) and 3.3 Gc/s (λ_{g2} = 11.6931 cm), λ_{go} = 14.5291 which gives f_o = 2.9283 Gc/s. At this frequency Z_0 for the full height waveguide is about 506 Ω. The corresponding equivalent resistance of the TD and stabilizing network is about - 50 Ω (from about -20 mmho in fig. 6.11). Fig. 6.12 (b) shows the conductances of (a) normalized approximately to the full height Y_0.

The transformation ratio of the six-section transformer is 13.333 : 1. Using tables given by Young[16] the six characteristic admittances are

$$y_{01} = 12.7499 \qquad y_{04} = 2.4514$$
$$y_{02} = 9.9382 \qquad y_{05} = 1.3413$$
$$y_{03} = 5.4377 \qquad y_{06} = 1.0455.$$

The VSWR at the band edges is 1.017.

The transformation ratio of the single section transformer is 3.333 : 1. The characteristic admittance y_{01}' of the line is 1.8248.

6.9 THEORETICAL GAIN RESPONSE OF TDA 2

Transformation of admittances to plane of TD

Let Y_{rt} represent the "load" of the TDA common to both reflection and transmission types. Let Y_{tr} be the "source" of the transmission amplifier, and B_{re} the susceptance produced through line y_{01}' of the reflection amplifier. See fig. 6.13 (a). All admittances are referred to the plane of the TD.

A computer program was written to calculate the input admittance to quarter wave transformers terminated by any specified load. See appendix A4. Some of the results obtained by computer are plotted in fig. 6.13 (b). $Y_{rt}(j\omega)$ is shown when the six-section transformer is terminated (a) by a matched load, and (b) by the circulator (fig. 6.2). Also depicted are $Y_{tr}(j\omega)$ and $B_{re}(\omega)$. These responses are necessary to compute the gain of the amplifier.

Gain equations

The gain of the reflection amplifier $|\rho_{re}(j\omega)|^2$ is obtained (see (4.31)) from

$$\rho_{re}(j\omega) = \frac{Y_{rt}^*(j\omega) - (Y_A'(j\omega) + jB_{re}(\omega))}{Y_{rt}(j\omega) + Y_A'(j\omega) + jB_{re}(\omega)} . \qquad (6.10)$$

The gain of the transmission amplifier $|t_{tr}(j\omega)|^2$ is obtained from[31]

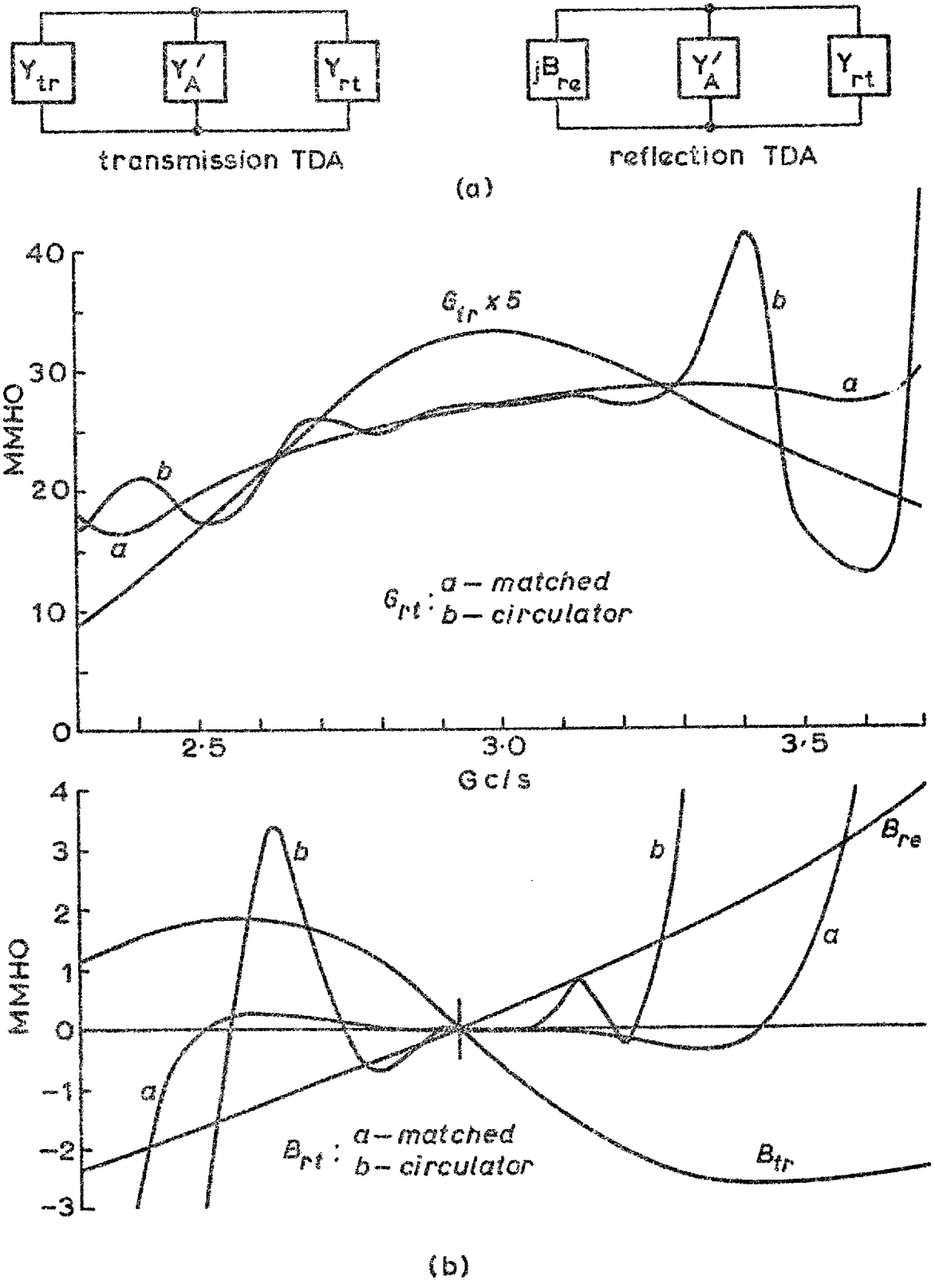

Fig. 6.13: (a) Representation of TDA 2 as transmission and reflection amplifier, (b) calculated conductances and susceptances seen from the plane of the TD. See text.

$$t_{tr}(j\omega) = \frac{\sqrt{4G_{tr}(\omega)G_{rt}(\omega)}}{D_{tr}(j\omega)} \tag{6.11}$$

where

$$D_{tr}(j\omega) = Y_{tr}(j\omega) + Y_A'(j\omega) + Y_{rt}(j\omega). \tag{6.12}$$

The input VSWR is obtained from $|\rho_{itr}(j\omega)|$ where

$$\rho_{itr}(j\omega) = \frac{Y_{tr}^*(j\omega) - (Y_A'(j\omega) + Y_{rt}(j\omega))}{D_{tr}(j\omega)} . \tag{6.13}$$

Its output reflection coefficient is

$$\rho_{otr}(j\omega) = \frac{Y_{rt}^*(j\omega) - (Y_A'(j\omega) + Y_{tr}(j\omega))}{D_{tr}(j\omega)} . \tag{6.14}$$

Stability

The stability of the amplifier can be checked by means of a Smith chart plot. As stated in section 4.5 it is simpler to consider stability in terms of H, in the present case Y. It is seen from section 6.7 that there must be no encirclements of the Y-plane origin for stability. Thus, whether we plot (6.13) or (6.14), the criterion for stability of the transmission amplifier is that there are no encirclements of the ρ'-plane origin.* One is at liberty to select either ρ_{itr} or ρ_{otr} since their denominators are identical to that of t_{tr}. The conditions for infinite gain or oscillations are therefore common to the three expressions.** In

*Compare this with the case of TDA 1 (section 5.3).

**This is hardly unexpected.

the present case it is convenient to take ρ_{otr} because it resembles ρ_{re} (see section 6.8). See fig. 6.14.

TDA program

A computer program embodying all the components of TDA 2 was written. Its purpose, apart from calculating the theoretical response of the amplifier, was to provide a rapid means of assessing the effects of component tolerances, change of TD, change of circulator, and any necessary modifications in the stabilizing network. The usefulness of such a program can not be overemphasized. A brief description follows.

(i) Any given set of TD parameters are accepted. The computer determines whether the inequality (3.26) is satisfied. f_R, f_X and $Z_{TD}(j\omega)$ are evaluated.

(ii) $Z_i(j\omega)$ is calculated for the configuration of fig. 6.4 for any given set of parameters, and is then added to $Z_{TD}(j\omega)$.

(iii) $jB_t(\omega)$ is calculated and added to $1/(Z_i(j\omega) + Z_{TD}(j\omega))$ to give . $Y_A'(j\omega)$ for any given iris dimensions.

(iv) $Y_{rt}(j\omega)$, $Y_{tr}(j\omega)$, and $B_{re}(\omega)$ are read as data.

(v) The gain and phase responses of both reflection and transmission amplifiers are calculated from (6.10) and (6.11), as well as the input VSWR, return gain at input and output of the latter.

(vi) CHART1 is called on at various stages in the calculation to provide a visual guide to the stability of the TDA. Examples of this are figs. 6.9 and 6.14.

Gain response

Fig. 6.15 shows the predicted response of the reflection amplifier as a function of R and d, for a perfect match terminating the six-section transformer.

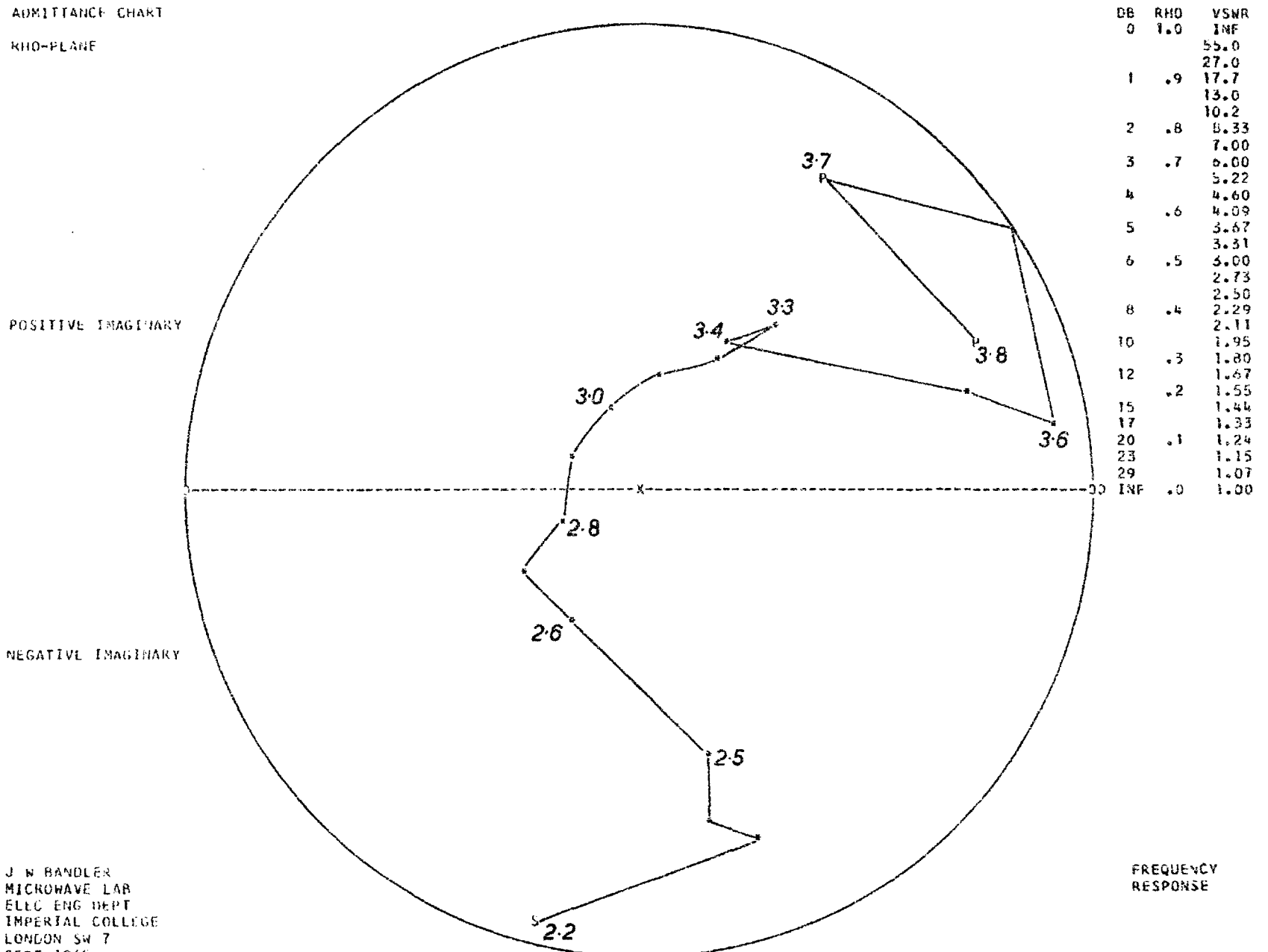

Fig. 6.14: Response of circulator loaded reflection amplifier (curve (v) of fig. 6.16) produced by CHART1.

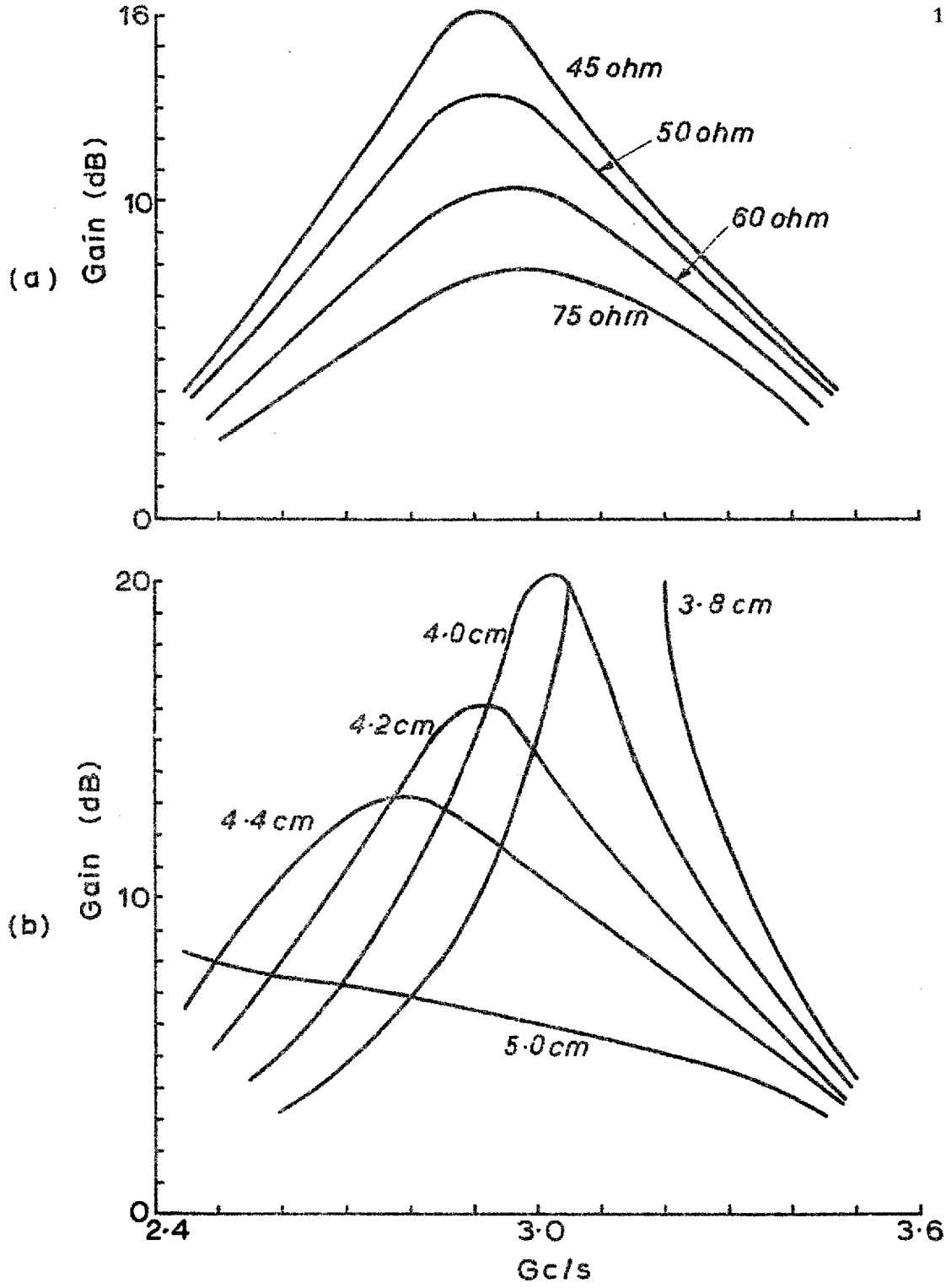

Fig. 6.15: Predicted response of the reflection amplifier, (a) as a function of R for d = 4.2 cm, (b) as a function of d for R = 45 Ω. The load is assumed to be a perfect match.

Curve (i) of fig. 6.16 is the response when r = 0, L = 0, and $Z_i(j\omega) = 0$, i.e. for an ideal stabilizing network. The 3 dB bandwidth at 21.7 dB maximum gain is 210 Mc/s. (Taking $\sqrt{G}.B = 1/\pi RC$, where C includes C_1 of the TD, this bandwidth is 252 Mc/s. The decrease is due entirely to the rectangular waveguide structure.) Note that the iris aperture needs to be 4.1 cm to "centre" the gain at about 2.93 Gc/s. Curves (ii) and (iii) are the responses when only $Z_i(j\omega) = 0$. The peak gains are, however, too high for sensible comparisons of bandwidth to be made. Curve (iv) is the 45 Ω curve of fig. 6.15 (a); curve (v) considers the effect of replacing the matched load by the present circulator (section 6.4). Note that a gain depression of almost 1 dB is caused by a circulator VSWR of only 1.05. The 3 dB bandwidth at 16 dB maximum gain (curve (iv)) is 290 Mc/s. (Taking $\sqrt{G}.B = 1/\pi RC$ as before, this bandwidth is 487 Mc/s. This value assumes r = 0 and L = 0 and is, therefore, rather optimistic.)

Fig. 6.17 shows the predicted performance of the transmission amplifier defined by its insertion gain and input VSWR. It is seen that the peak gain and minimum VSWR occur at different frequencies, and also that at no point does the VSWR ever become unity. The reasons for both phenomena are that the assumptions of fig. 6.12 are oversimplified in relation to the interaction of the responses of the components of the designed amplifier.

The results plotted in figs. 6.15 to 6.17 were produced by the TDA program.

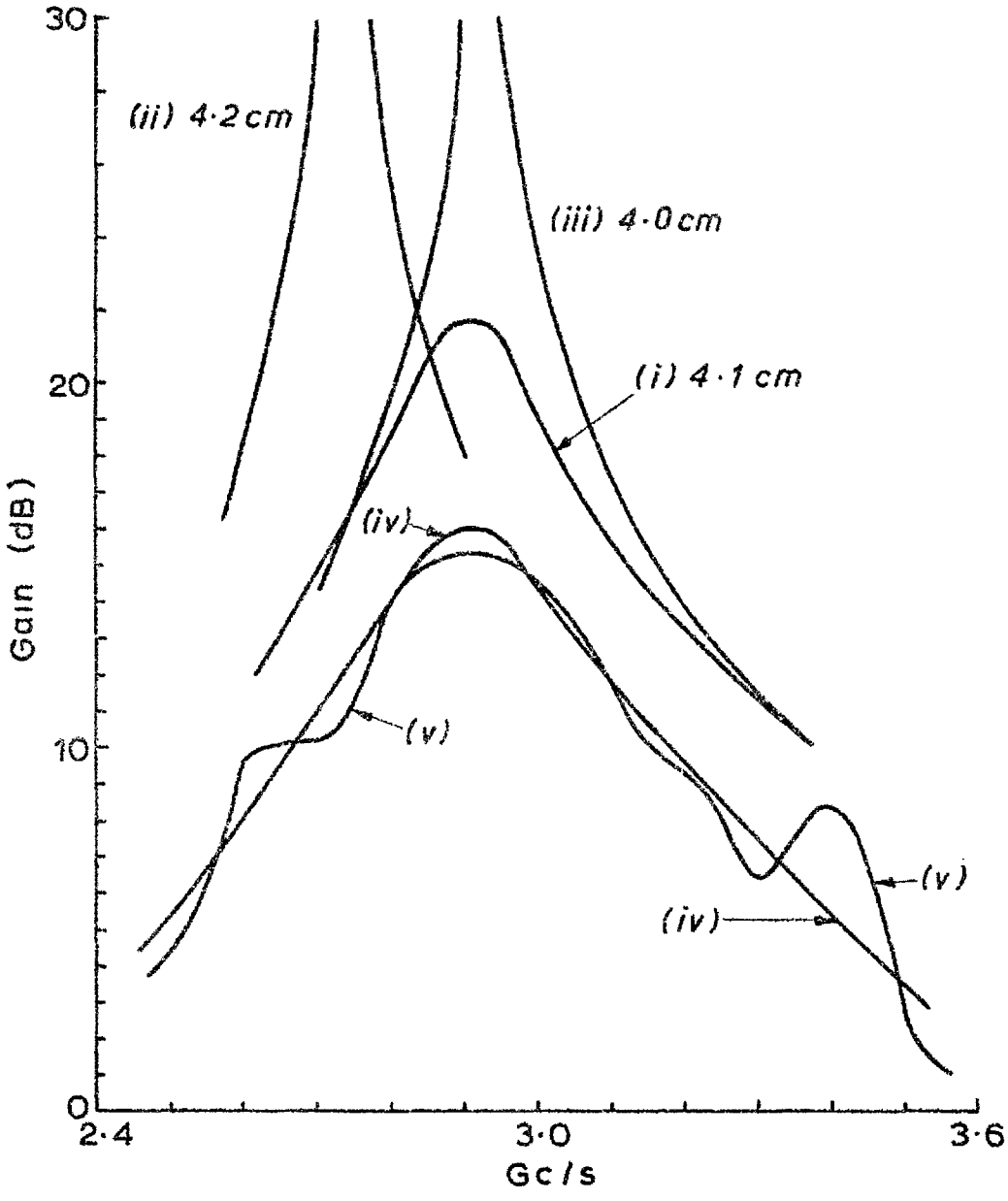

Fig. 6.16: Predicted response of the reflection amplifier. Curves (i), (ii), and (iii) assume that $Z_i(j\omega) = 0$; curve (i) that r = 0 and L = 0; curve (iv) that the amplifier is connected to a perfect match; curve (v) that the amplifier is connected to the circulator. R = 45 Ω throughout.

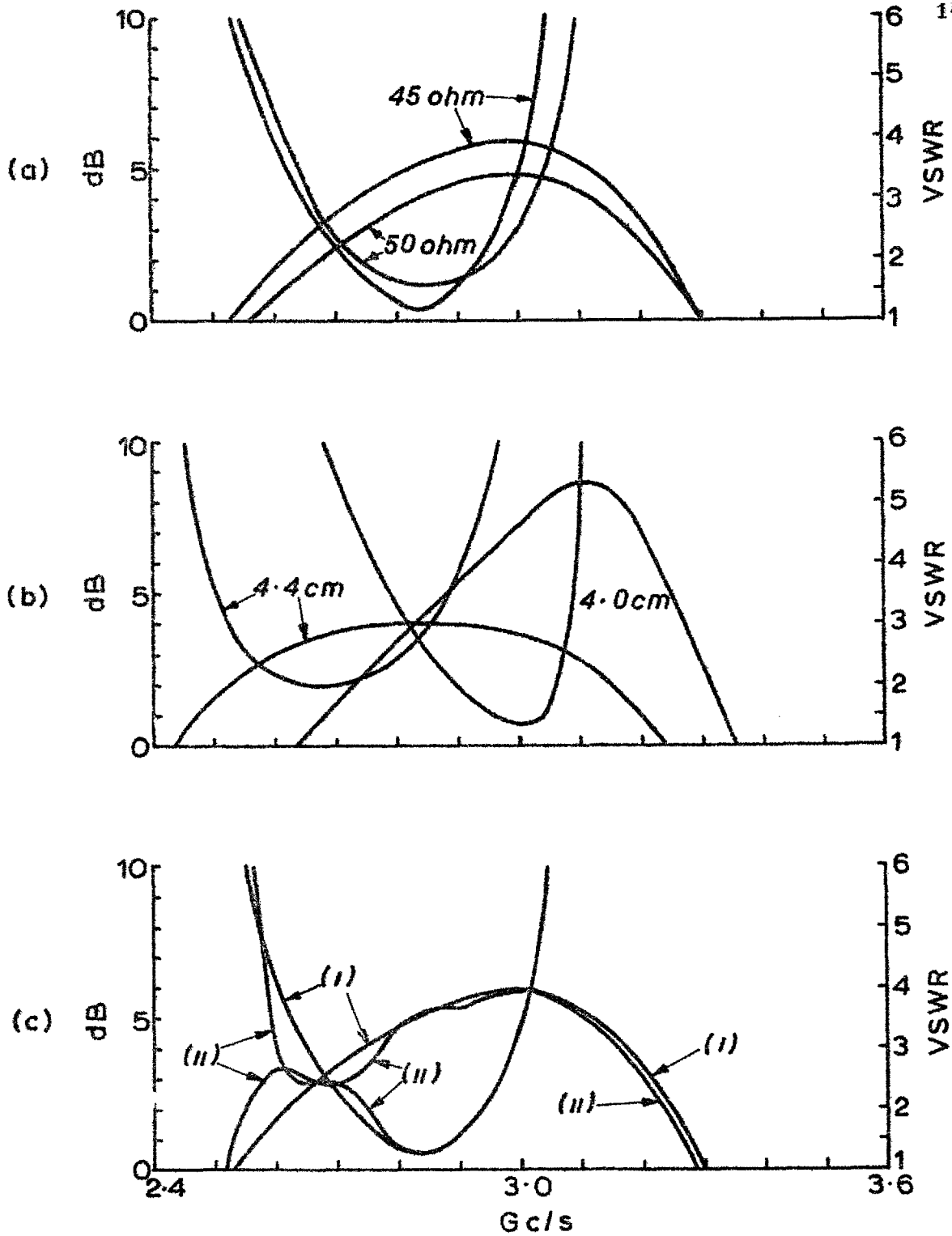

Fig. 6.17: Predicted response of the transmission amplifier, (a) for d = 4.2 cm; (b) for R = 45 Ω, (c) for d = 4.2 cm and R = 45 Ω: (i) matched load, (ii) circulator. The U-shaped curves are for input VSWR.

6.10 REALIZATION AND CONSTRUCTIONAL DETAILS

The stabilizing network

Applying Kuroda's identity (fig. 6.5) to the prototype circuit of fig. 6.4 gives

$$Z_{01}' = 11.338\ \Omega \text{ and } Z_{02}' = 7.611\ \Omega.$$

The remainder of line 2 and line 3 of fig. 6.4 give

$$Z_{02} = 18.948\ \Omega \text{ and } Z_{03} = 19.049\ \Omega.$$

The s.c. series line (2') was to be physically shortened by filling it with a suitable dielectric. A sample of Stycast Hi K having a nominal dielectric constant of 5 was chosen. The average value of dielectric constant obtained experimentally from measurements at five frequencies in X-band rectangular waveguide was found to be 5.08.

A dimensioned scale drawing of the stabilizing network is shown in fig. 6.18. The method of fixing the resistive card to the centre rod, and of locating the centre rod is the same as in section 2.4. A nut (not shown) with an internal thread clamped the card down to the outer conductor through a brass washer, whose internal diameter was the same as that of the outer conductor.

This outer conductor of the coaxial system was fabricated in two sections. The lower section was machined first; a hole was drilled in a piece of the dielectric which was then fitted over this section (see fig. 6.18). The upper section, after machining, was fitted over the dielectric - the components located each other very well without any slack in a lateral direction. The stabilizing network was fixed to the waveguide by another internally threaded nut (not shown). Discs of resistive-film cards were punched out

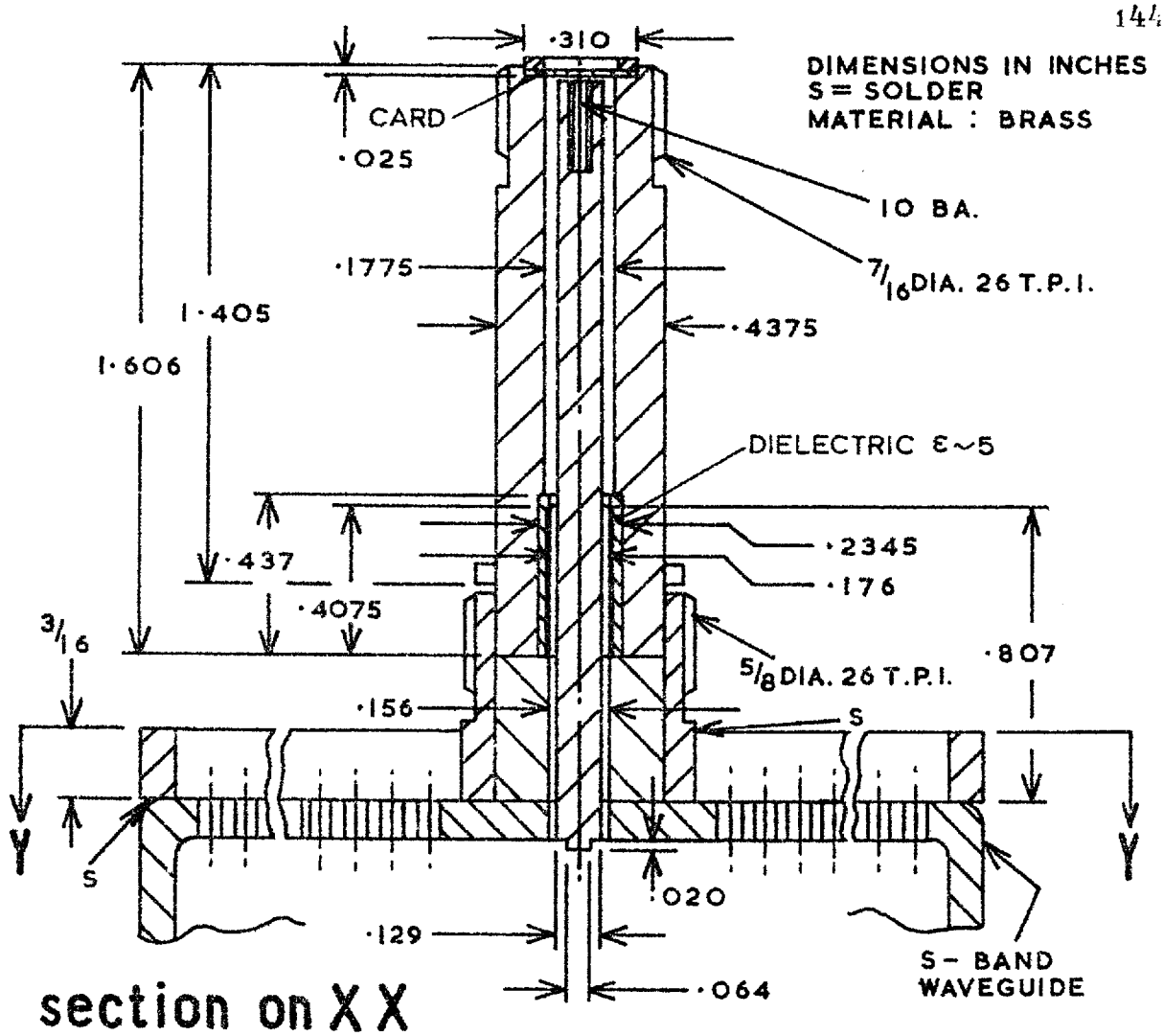

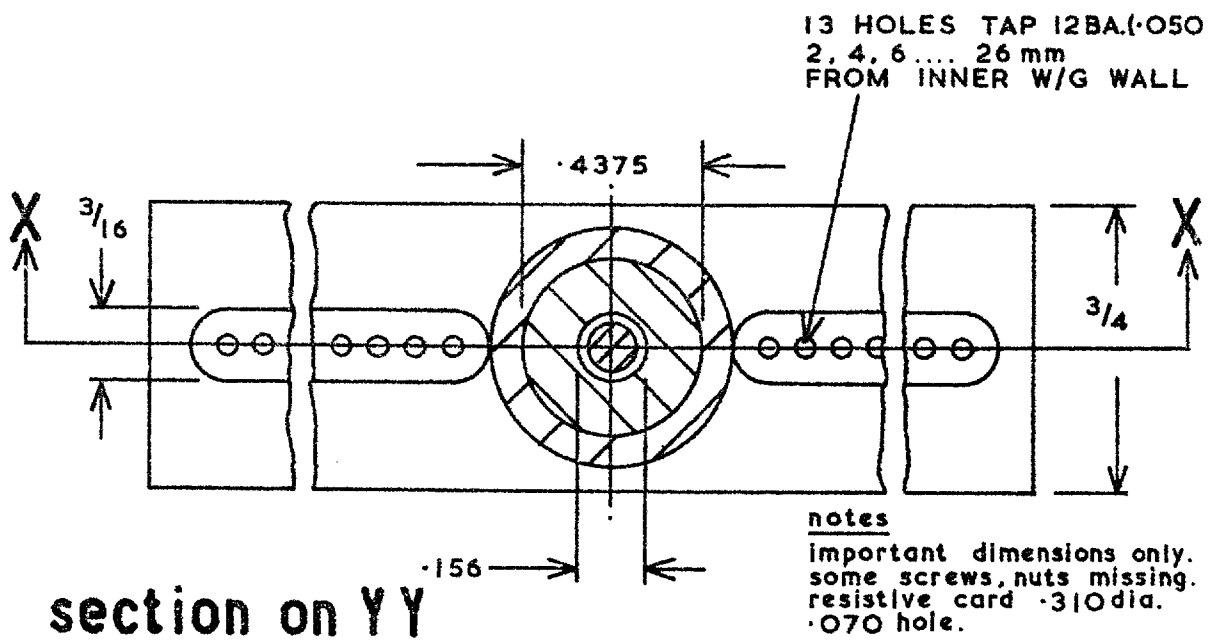

Fig.6.18: Part of TDA 2 (twice full size).

from sheets of 800 and 400 ohm per square card. Note that the line terminated by the card has a characteristic impedance of about 20 Ω: a card of resistance per square twice that of free space impedance would provide the necessary 40 Ω bias resistance.

A small spring* was fixed to the end of the centre rod to make contact with the negative terminal of the TD.

The waveguide transformers

The six section transformer and the single section transformer of section 6.8 were milled out of a block of brass. Fig. 6.19 is a scale drawing of the structure. The outline and overall length of the waveguide containing the transformers is shown in this figure. A transverse ridge of width .090 in separates the transformers, and a gap of .075 in was allowed for the TD and the inductive iris. A central hole (labelled *) in the ridge was to permit location of the TD (Mullard type AEY 16) by its pin (positive terminal).

The inductive iris

It was considered that a row of closely spaced screws would provide an adequate approximation to the inductive window. Susceptance variation could be facilitated by this means. Consequently, 26 holes 2 mm apart were drilled and tapped (see fig. 6.18) in the top broad wall of the waveguide to take 12 BA screws (.050 in diameter). The screws, which were .3 and .4 in long, were staggered so that their heads would not interfere. The 3/16 in thick slotted plate soldered to the waveguide was to protect the screws from

---

*Servometer Corp., Part No. 2146; length .082 in, diameter .066 in.

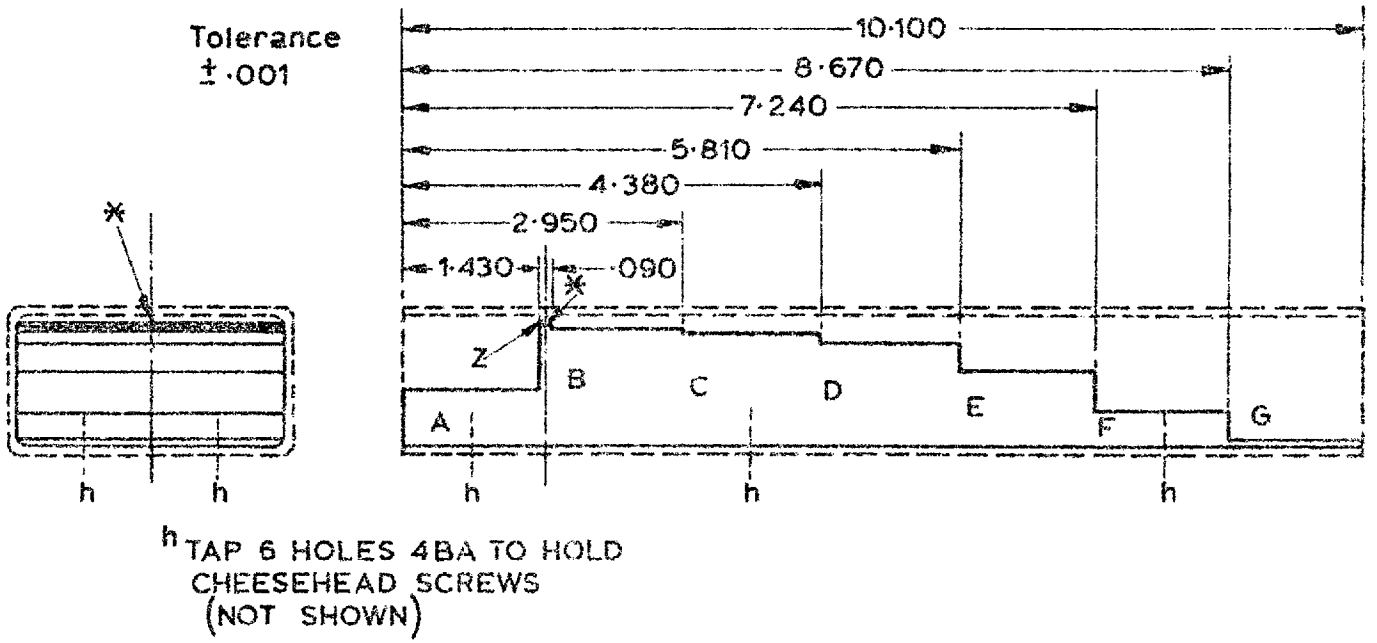

Dimension	A	B	C	D	E	F	G	Z
Gap	·734	·105	·135	·247	·547	·999	1·282	·075
Height	·606	1·235	1·205	1·093	·793	·341	·058	1·265
Tolerance	±·0005							

END AND SIDE ELEVATIONS

* Hole ·028 Dia.
·050 deep.

SCALE: HALF SIZE
MATERIAL: BRASS
DIMENSIONS IN INCHES

Fig. 6.19: Scale drawing of the waveguide transformers.

Fig. 6.20: TDA 2

accidental damage. In use the screws were either to make firm contact with the transverse ridge, or to be withdrawn from the gap in the waveguide.

Fig. 6.20 is a photograph of the assembled amplifier.

6.11 Conclusion

An account of the techniques employed in designing an S-band waveguide TDA has been given. Strong emphasis has been placed on the use of a digital computer for designing and optimizing non-commensurate systems of microwave circuits, such as the present amplifier. The design of the coaxial-line stabilizing network is, for instance, essentially a constrained optimization problem.

The potential stability of TDA 2 is investigated, and predicted curves of stable gain are given. Both the "matched" transmission amplifier and the reflection amplifier are basically single tuned. A typical 3 dB bandwidth of the latter at 16 dB maximum gain is 21%, and the corresponding 1 dB bandwidth of the former at 6 dB maximum gain is also 21%. These bandwidths are based on λ_g.

6.12 References

(1) E.S. Kuh and J.D. Patterson, ref. (20) chap.3.

(2) L.I. Smilen and D.C. Youla, ref. (21) chap. 3.

(3) B.G. King and G.E. Sharpe, "Low-gain wide-band Esaki-diode amplifiers," 1961 Int. Solid-State Circuits Conf., Digest of Technical Papers pp. 98-99.

(4) J.S. Logan, "Gain vs bandwidth limits for Easki diode amplifiers," Proc. IRE, Vol.49, p.832, April 1961.

(5) H. Rieck and R. Maurer, "Der Tunneldioden-geradeausverstärker als rauscharme Vorstufe im UHF-Gebiet (the tunnel-diode straight through amplifier as low noise first stage in the UHF region)," Archiv der Elektrischen Übertragung (Germany), Vol.15, pp. 495-507, November 1961.

(6) M.E. Pedinoff, "The negative-conductance slot amplifier," IRE Trans. Vol. MTT-9, pp.557-566, November 1961.

(7) M.C. Behnke and A.P. King, "An experimental negative-conductance slot amplifier at 6 Gc," Hughes Aircraft Co., Cal., July 1962; AD 284 691.

(8) W.F. Chow, "Principles of tunnel diode circuits," Wiley, New York, 1964; chapter 4.

(9) H.J. Carlin, "Cascaded transmission line synthesis," Polytechnic Institute of Brooklyn,27 April 1961; AD 263 832.

(10) G.I. Zysman, ref. (22) chap. 3.

(11) W. Kohler and H.J. Carlin, ref. (23) chap. 3.

(12) H. Glass and L. Cooper, "Sequential search: a method for solving constrained optimization problems, "J. of the Assn. for Computing Machinery, Vol. 12, pp. 71-82, January 1965.

(13) J.W. Bandler, "Frequency responses in the reflection coefficient plane plotted by digital computer," IEEE Trans. Vol. MTT-14, pp. 399-400, August 1966.

(14) S.B. Cohn, "Optimum design of stepped transmission-line transformers," IRE Trans. Vol. MTT-3, pp. 16-21, April 1955.

(15) H.J. Riblet, "General synthesis of quarter-wave impedance transformers," IRE Trans. Vol. MTT-5, pp. 36-43, January 1957.

(16) L. Young, "Tables for cascaded homogeneous quarter-wave transformers," IRE Trans. Vol. MTT-7, 233-237, April 1959.

(17) L. Young, "Correction to 'Tables for cascaded homogeneous quarter-wave transformers'," IRE Trans. Vol. MTT-8, pp. 243-244, March 1960.

(18) L. Young, "Stepped-impedance transformers and filter prototypes," IRE Trans. Vol. MTT-10, pp.339-359, September 1962.

(19) L. Young, "Microwave filters - 1965," IEEE Trans. Vol. MTT-13, pp. 489-508, September 1965.

(20) A.H. Hall, ref. (12) chap. 2.

(21) N. Marcuvitz, "Waveguide handbook," McGraw-Hill, New York, 1951 (first edition); pp. 221-224.

(22) E.L. Ginzton, "Microwave measurements," McGraw-Hill, New York, 1957; chapter 5.

(23) H. Ozaki and J. Ishii, "Synthesis of transmission-line networks and the design of UHF filters," IRE Trans. Vol. CT-2, pp. 325-336, December 1955.

(24) A.I. Grayzel, "A synthesis procedure for transmission line networks," IRE Trans. Vol. CT-5, pp. 172-181, September 1958.

(25) B.M. Schiffman and G.L. Matthaei, "Exact design of bandstop microwave filters," IEEE Trans. Vol. MTT-12, pp. 6-14, January 1964.

(26) R.J. Wenzel, "Exact design of TEM microwave networks using quarter-wave lines," IEEE Trans. Vol. MTT-12, pp. 94-111, January 1964.

(27) G.L. Matthaei, L. Young and E.M.T. Jones, "Microwave filters, impedance matching networks, and coupling structures," McGraw-Hill, New York, 1964.

(28) B.M. Schiffman, "A harmonic rejection filter designed by an exact method," IEEE Trans. Vol. MTT-12, pp.58-60, January 1964.

(29) L. Young, Lecture notes for lectures 12 and 13, Microwave components synthesis III and IV, IEE Microwave Summer School, Leeds University, 1966, Pt.5, pp. 88-117: "Diplexers and multiplexers".

(30) P.I. Richards, "Resistor transmission-line circuits," Proc. IRE, Vol.36, pp. 217-220, February 1948.

(31) K. Kurokawa, "Power waves and the scattering matrix," IEEE Trans. Vol. MTT-13, pp. 194-202, March 1965.

7

experimental performance of TDA 2

7.1 Introduction

The reflection/transmission amplifier as designed in chapter 6 failed to work as a stable amplifier. This chapter describes the extensive measurements made on all the passive constituents in an attempt to ascertain the cause of the failure. A rather arbitrary narrow band stabilizing filter was made to see whether stable operation was at all possible in the present configuration.

7.2 BRIDGE BIASING CIRCUIT

A number of authors[1-4] have described bridge circuits for biasing the TD and for displaying its V-I characteristic. The idea is to balance out the stabilizing resistor (here a

resistive-film card) before connecting the TD - then feed the bias voltage to the horizontal deflection and the balance detector current (proportional to the TD current) to the vertical deflection of an oscilloscope. The TD current for the circuit of fig. 7.1 is equal to $2V_{vert}/R$. The resistances marked "balance" and "scale" are provided by resistance boxes. The 56 Ω fixed resistors of the bridge were carefully selected to be very nearly equal.

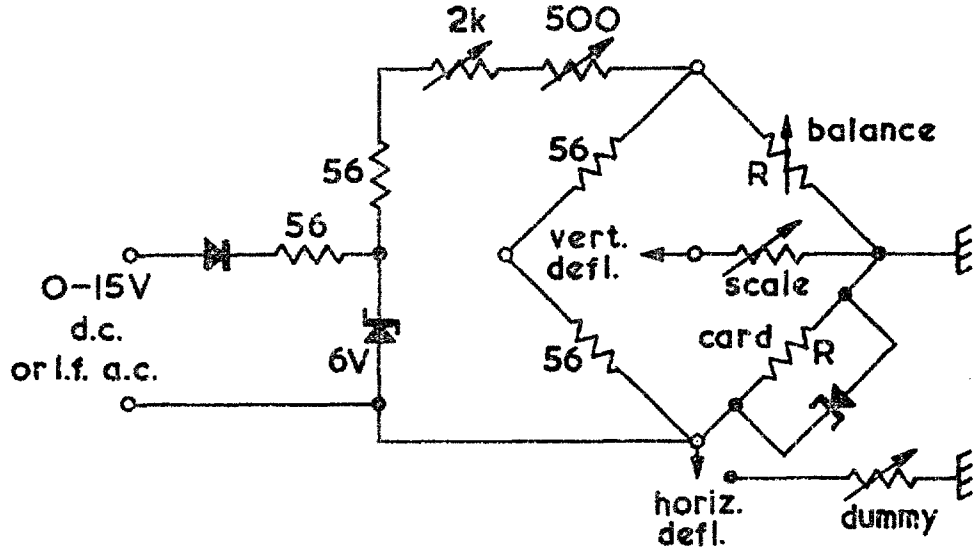

Fig. 7.1: The bridge biasing circuit at low frequencies.

The bias voltage could be swept by supplying a low frequency a.c. voltage which is rectified before being applied to the bridge. The stability of the TD in its waveguide mount could be checked at any time by this means, since a smooth continuous V-I characteristic would indicate the stable condition, whereas a discontinuity would indicate instability. The balance arm provides a direct reading of the resistance of the resistive-film card.

7.3 FAILURE OF TDA 2 TO AMPLIFY

A Mullard type AEY 16 TD was obtained, whose parameters closely matched the one of section 6.5. The parameters were, nominally,

R_{min} = 47 Ω, C = 2 pF, r = .95 Ω, L = .12 nH, and C_1 = .3 pF.

(C at the valley voltage was quoted as 2.5 pF.)

When the amplifier was ready, it was connected to an experimental set-up similar to that shown in fig. 5.8, but without the circulator. A brass plate was bolted to the "input" of the structure to test it as a reflection amplifier. The method was to observe the VSWR of the device as a function of frequency when the TD was biased in the negative resistance region (see section 4.3). Exhaustive tests and experimental adjustment of parameters, e.g. bias voltage and iris screws (section 6.10) and resistive-film card, failed to induce the TDA to amplify. The TD was replaced by others of both lower and higher f_R without success.

The V-I characteristic was swept as described in section 7.2 and displayed on an oscilloscope. It was seen that for all iris screw positions the amplifier was unstable, indicated by a moderate kink in the negative resistance portion of the curve. The amplifier could only be stabilized by wedging a .075 in brass block between the ridge and upper broad wall of the waveguide very close to the TD. No gain was, however obtained under these circumstances - only a high VSWR.

It was thought at the time that the stabilizing network was not functioning as predicted. Possibly the specifications for its design (section 6.5.4) were not severe enough causing the TD to oscillate somewhere below the

amplification band. Checks on the frequency of oscillation could be made both by an S-band wavemeter and by the SWD (fig. 5.8); this was generally below 2.6 Gc/s. No harmonics were observed in S-band.

7.4 TESTING OF COMPONENT NETWORKS

At this stage it was decided to carry out systematic measurements on the component networks of TDA 2. The results are presented in some detail as they could be of general interest.

The waveguide transformers

To facilitate the evaluation of this component, a cylindrical brass block was made to seal off the waveguide hole at the TD position (fig. 6.18). A slot 1/64 in wide was milled in the waveguide end of the block to hold a small piece of resistive-film card. The nut which fixed the stabilizing network to the waveguide served the same purpose for the block.

The reflectometer set-up of fig. 7.2 (a) was used.* The system was calibrated by placing a s.c. at the load end of the directional coupler, sweeping the required frequency band, and adjusting the X-Y recorder to plot 100% reflection, 80%, 60%, etc. With the iris screws withdrawn, the stabilizing network and TD removed, with the waveguide hole sealed off, and with a s.c. plate bolted to the "input" of the structure, the return loss of the transformers was found to be 1.5 dB. The s.c. plate was replaced by a waveguide

---

*Swept frequency measurements on the transformers were carried out at Mullard Research Laboratories, Surrey.

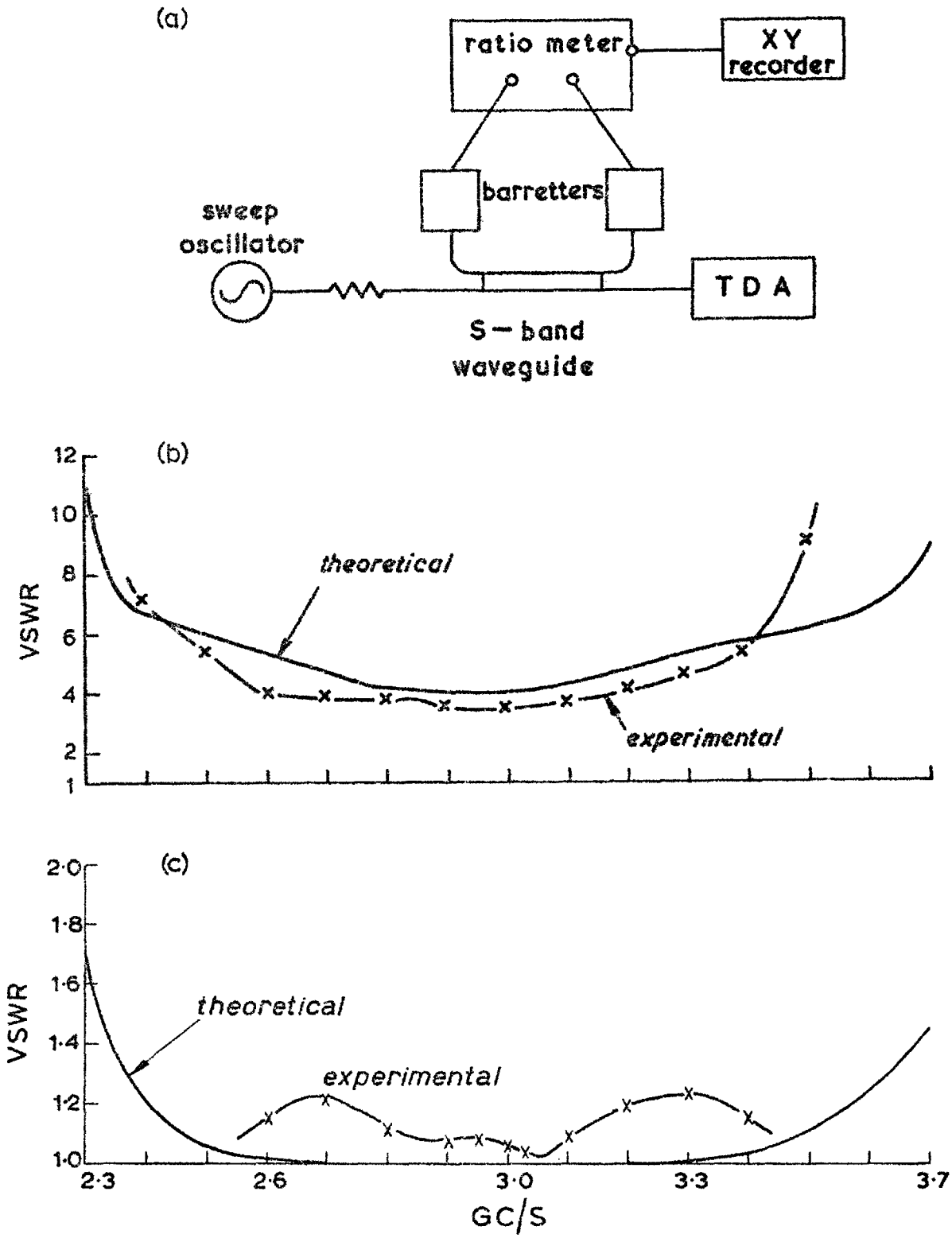

Fig. 7.2: (a) Reflectometer set-up for transformer measurements, (b) and (c) transformer responses (see text).

matched load; the experimental response thus obtained is compared with the predicted one in fig. 7.2 (b). Agreement is close. A piece of resistive-film card of 100 Ω/square (size about .15 in by .15 in) was inserted at the TD position and held in the 1/64 in slot. A very small amount of silver paint was carefully applied to the top and bottom ends of the card to ensure contact to the waveguide. The s.c. plate was then bolted back on to the waveguide. The reflectometer results obtained under these conditions are shown in fig. 7.2 (c). The card was removed and its d.c. resistance was measured. This was between 41 and 44 Ω depending on the pressure the contacts made with the card. The resistance required to match the 6 section transformer at 2.93 Gc/s is 38 Ω. Thus a VSWR between 1.08 and 1.16 was expected at this frequency. Experimental agreement is again close. The theoretical curve of fig. 7.2 (c) is for a perfect match at the card position.

Comparison of iris with s.c. line

A rectangular brass block was milled to fill the single section transformer to within .075 in of the top. See fig. 6.19. A movable s.c. plunger was made from a sheet of phosphor bronze bent round a stiff rectangular sheet of aluminium, the widths of both sheets being equal to the broad dimension of the waveguide. The bend in the phosphor bronze was the leading edge which made firm contact with the brass block and the top wall of the waveguide. The block was held in position by the s.c. plate out of which a slot had been milled to make way for the movable s.c. plunger. The position of its leading edge from the plane of the iris screws was equal to the distance of a transverse line scratched on it from the exterior surface of the s.c. plate. The arrangement is very similar to the tuning section of TDA 1 (fig. 2.10).

As previously, a piece of resistive-film card was located in the TD position. Its dimensions were approximately the same as before, but its resistance was 50 Ω/square. Two experiments were made at 2.93 Gc/s using the set-up of fig. 5.8 (without the circulator). In the first experiment, the single section transformer (empty) was terminated by the s.c. plate to produce an o.c. at the card. The VSWR was the measured for each setting of the iris screws.* In the second, the space behind the screws was filled by the block and s.c.plunger (as described earlier). All iris screws were withdrawn, and the VSWR was measured against distance of the s.c. from the card.

Fig. 7.3 shows the experimental results as iris aperture against distance of the s.c. plunger from the card necessary to produce the same VSWR. The theoretical curve is taken from fig. 6.10 using susceptance as the common variable. The VSWR ranged almost linearly from about 2.8 at screw 6 to 5.7 at screw 12. Note the very good agreement over the iris aperture range of interest.

The validity of the experiment is justified as follows. The load is essentially a parallel circuit formed by a conductance (card) and a susceptance (iris or s.c. line). For a given conductance, there is a unique negative susceptance which produces a given VSWR for this circuit, as can be seen from a Smith chart.

Determination of Z_0 at TD position

In view of the difficulty of obtaining exactly 38 Ω (the impedance the 6 section transformer is to match to) from a resistive-film card replacing the TD, it was decided

---

*The screws are numbered from 0 meaning no screw to 13 meaning all screws in position in the waveguide. Screw 9, for example, means all screws up to and including the 9th on both sides counting towards the card.

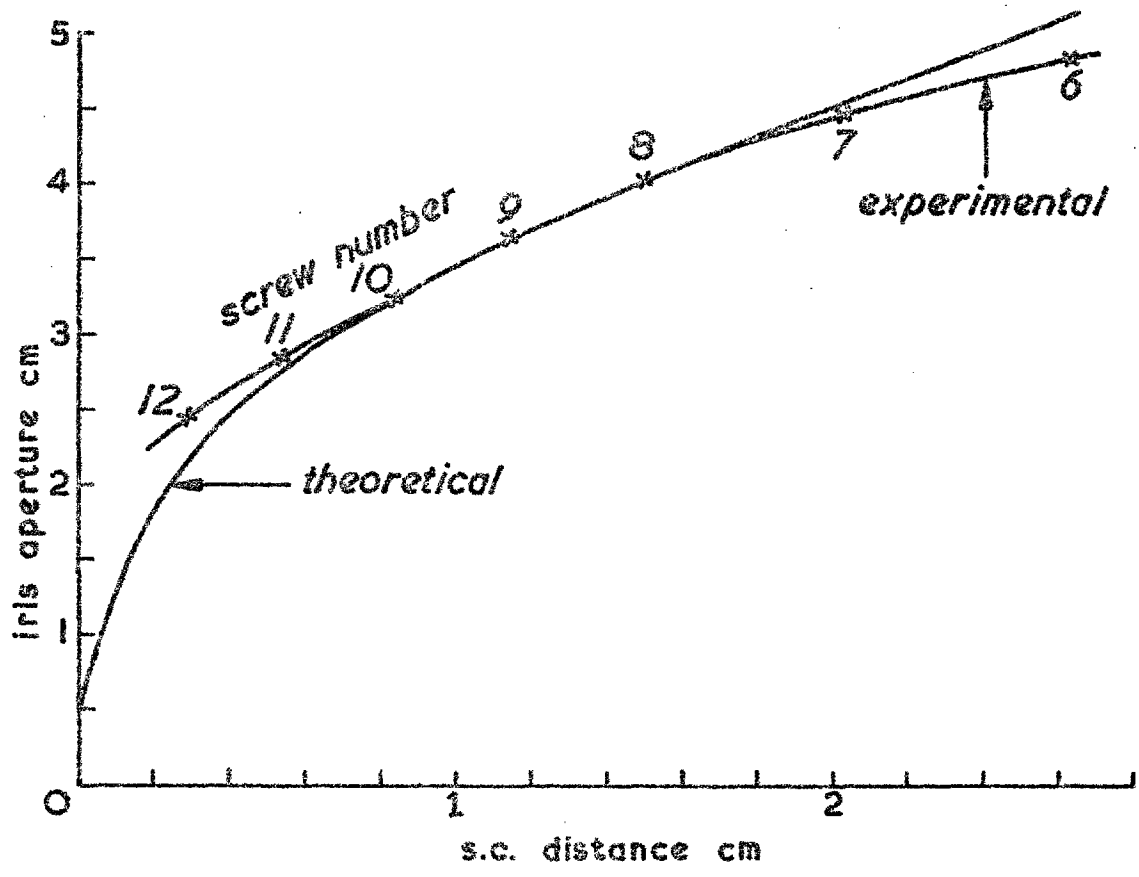

Fig. 7.3: Iris aperture against s.c. distance to produce the same VSWR in conjunction with a resistive-film card mounted in the TD position. See also fig. 6.10.

to determine the value of Z_0 from a large number of cards. The apparatus was the same as for the VSWR experiment on the iris screws, but with the screws removed. The VSWR was measured for 16 pieces of card to cover a wide range of resistance values. The results are plotted against measured d.c. resistance of the cards in fig. 7.4. Zero resistance was obtained from a brass pill replacing the card, and infinite resistance by leaving the space empty. A VSWR of 12.7 was recorded in the former case, corresponding to a return loss of 1.37 dB. The loss each way is, therefore,

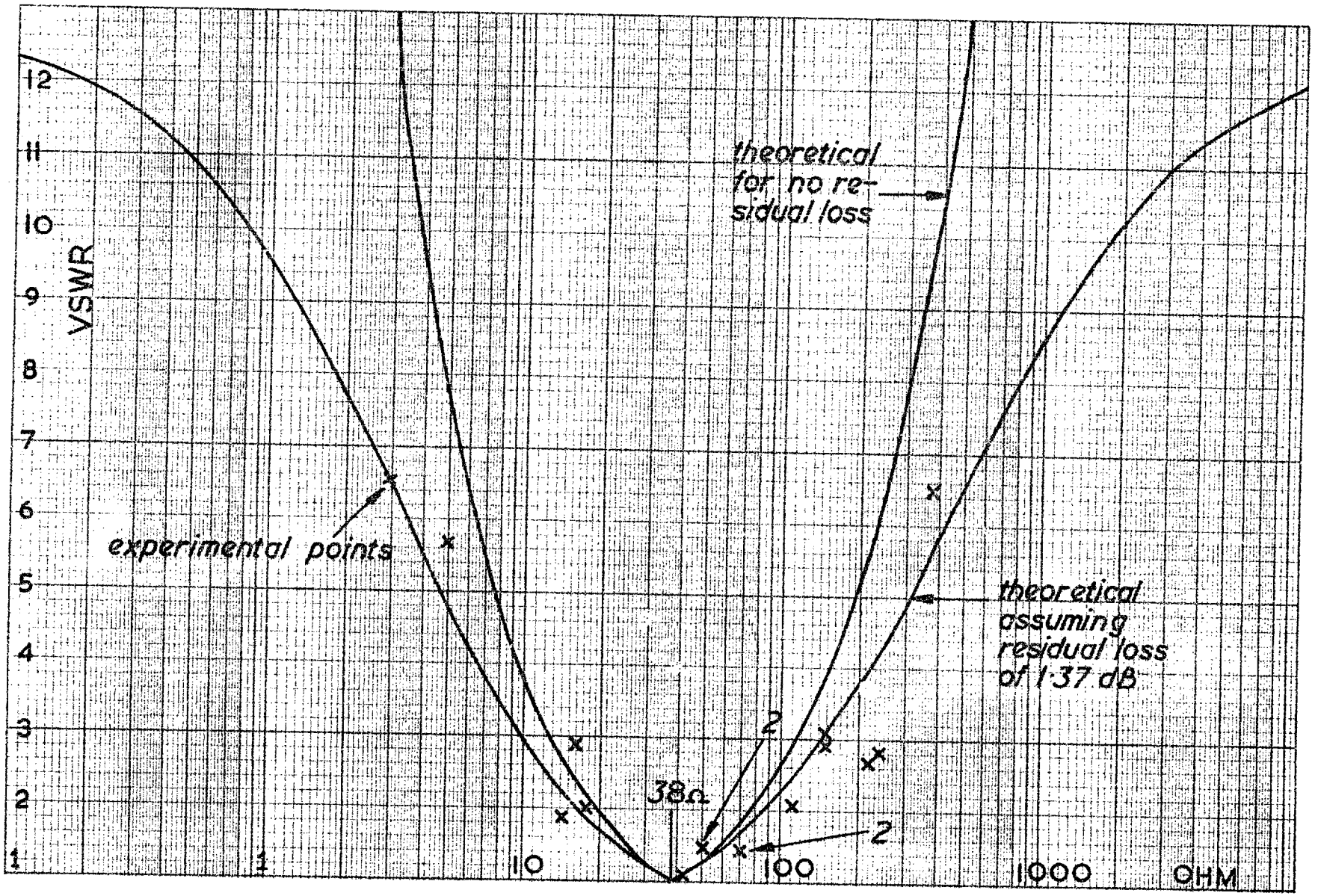

Fig. 7.4: Results of experiment to determine Z_o at the TD position.

.685 dB. The curve in fig. 7.4 marked "theoretical assuming residual loss of 1.37 dB" was obtained from the attenuation scale of the Smith chart for a range of load resistance values. This curve fits the experimental points very reasonably. The scatter can be attributed to contact problems (i) with the waveguide, and (ii) with the low frequency terminals of the d.c. resistance measurement set-up.

Test of the stabilizing network

Fig. 7.5 is a drawing of the transition that had to be made in order to connect the stabilizing network to a 50 Ω coaxial-line through an N-type connector. A female connector having a captive centre conductor (to discourage movement) was adapted to contain the transition. Note that the end to which the stabilizing network is fixed is essentially the same as that on the waveguide in fig. 6.18. .050 in is left to account for the protrusion of the centre rod into the waveguide. Contact was effected through the spring on the end of the centre rod. The dimensions of the dielectric* filled part of the transition were such as to give a 50 Ω characteristic impedance.

A reflectometer bench using coaxial-lines was available.** The swept sources (1-2 Gc/s and 2-4 Gc/s) were levelled externally through an appropriate directional coupler, and a second directional coupler sampled the reflected power. The incident power reference vs. frequency on the logarithmic scale of an oscilloscope was determined by placing a s.c. at the load terminals and recorded. The s.c. was replaced by

---

*Polythene, dielectric constant 2.26.

**Swept frequency measurements on the stabilizing network were carried out at University College, London.

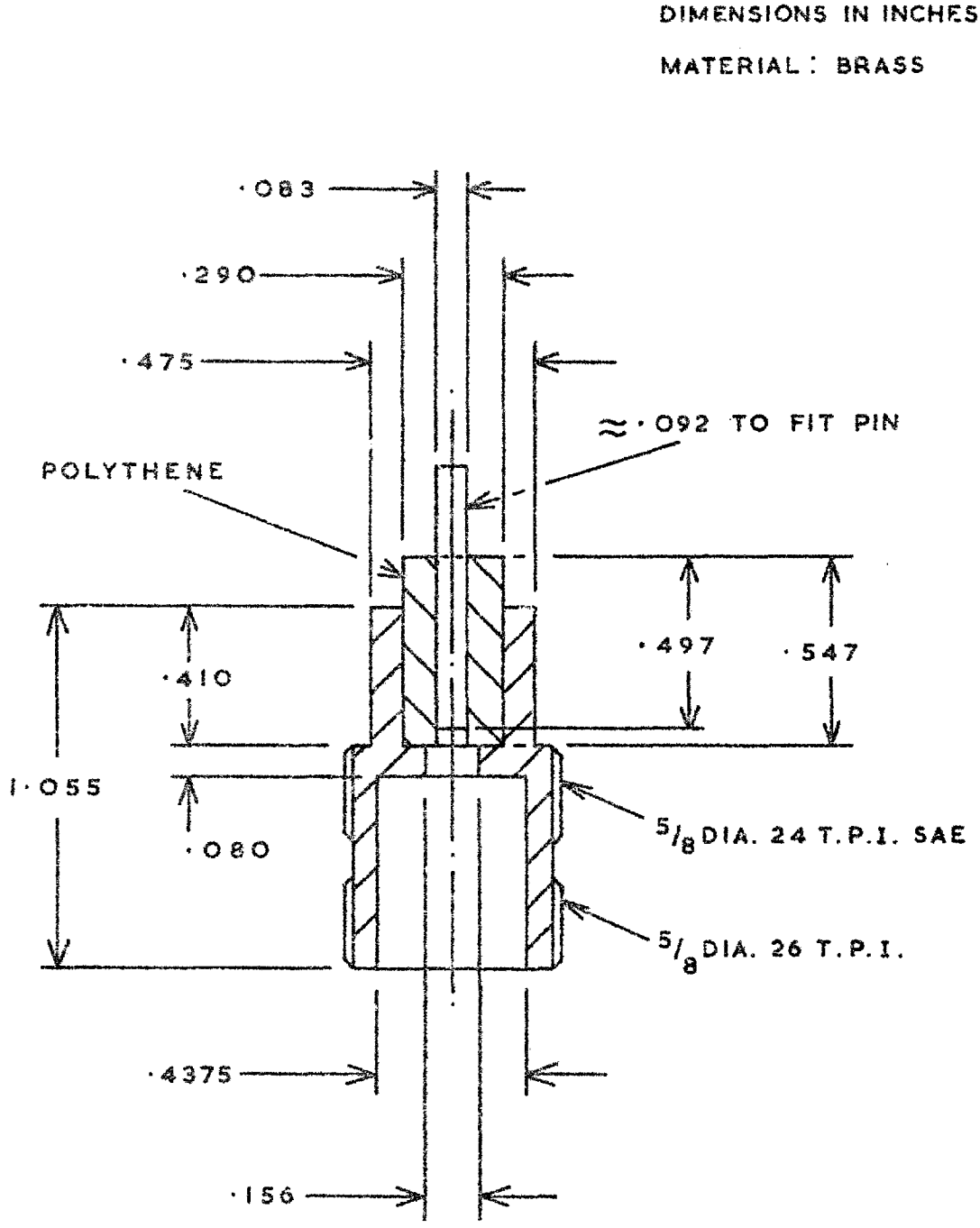

Fig. 7.5: Coaxial transition from stabilizing network to N-type connector.

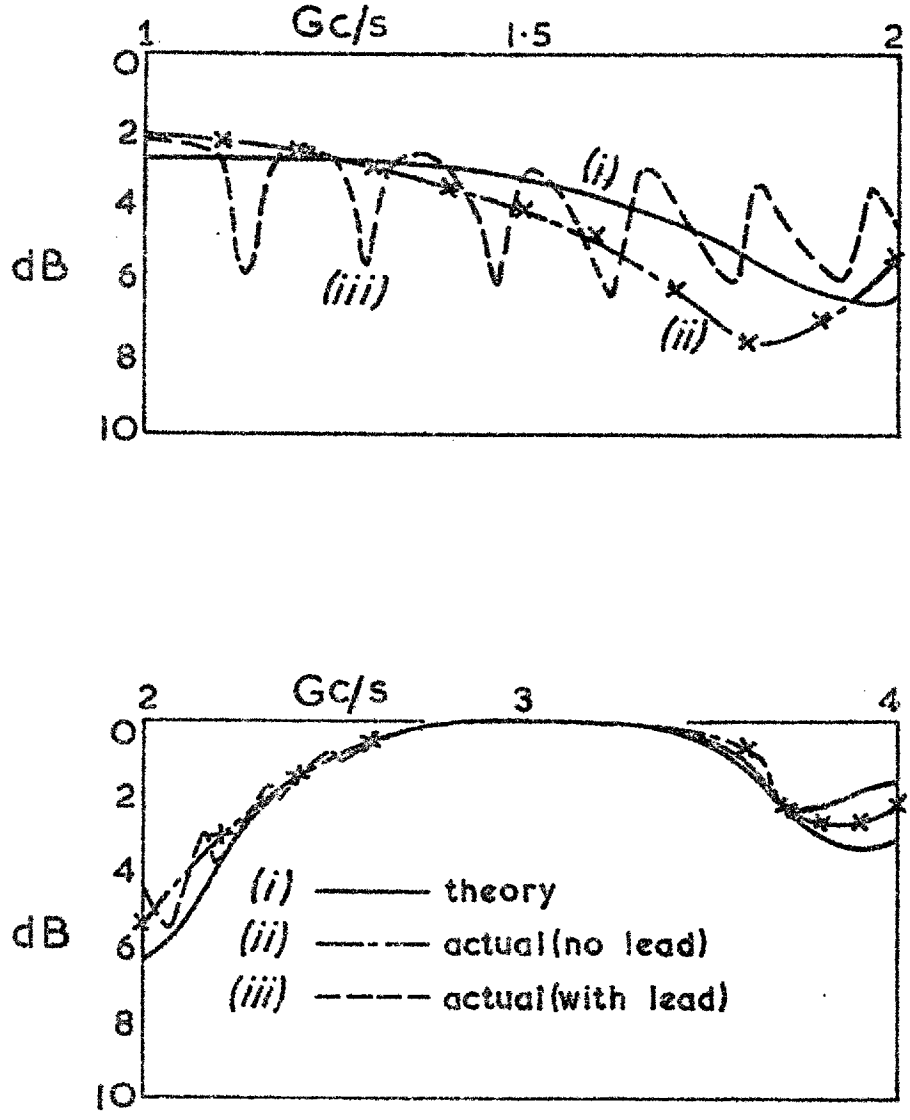

Fig. 7.6: Response of the stabilizing network.

the stabilizing network arrangement and the corresponding oscilloscope trace was also recorded.

The difference in dB between the incident and reflected power is plotted in fig. 7.6 for three cases: the theoretical curve, the experimental curve with the bias cable removed from the end of the filter, and the experimental curve with the bias cable attached. The cable was a 50 Ω miniature coaxial-line of electrical length ≈ 86.5 cm leading to the bridge biasing circuit. The ripples in the third curve are 160 Mc/s apart. λ at this frequency is 187 cm, therefore $\lambda/2$ = 93.5 cm, which is some 8% higher than the estimated electrical length. The theoretical curve was calculated using the value of the d.c. resistance of the card as actually measured. This was 45 Ω. With the small working area of the card it was not so easy to get 40 Ω exactly. Card resistances as close as 42 Ω have been obtained. The discrepancy is not significant to the response in the vicinity of the amplification band, and in any case very much less than that produced when the bias cable is attached. When comparing the curves it should be remembered that the discontinuity effects are not accounted for theoretically, e.g. between the 50 Ω line and 11.3 Ω line (Z_{01}').

Using a coaxial slotted-line, the minimum at 3.1 Gc/s for the arrangement was found to lie at the position equivalent to the inner waveguide wall. The reference s.c. plane for this experiment was provided by the cylindrical brass block used in the test of the waveguide transformers to seal off the stabilizing network, and a brass pill wedged between this and the centre rod of the transition to form a continuous 50 Ω line.

Discrepancies between predicted and experimental curves are most probably due to discontinuity effects. The oscillations observed in sections 7.3 and 7.6 could not be due to these discrepancies, however.

7.5 LUMPED EQUIVALENT CIRCUIT FOR LOSSY TRANSMISSION-LINES

The results of the experiment to determine Z_0 plotted in fig. 7.4 suggested an alternative representation of the lossy waveguide. This is shown in fig. 7.7. (a) is the conventional representation, (b) is an approximate representation for moderate loss. The conditions for equivalence are derived in appendix A5. The line attenuation is equal to half the return loss in dB when the load is perfectly reflecting. It is shown in appendix A5 that the equivalent circuit is still good up to a return loss of 1.7 dB, corresponding to a VSWR of 10.

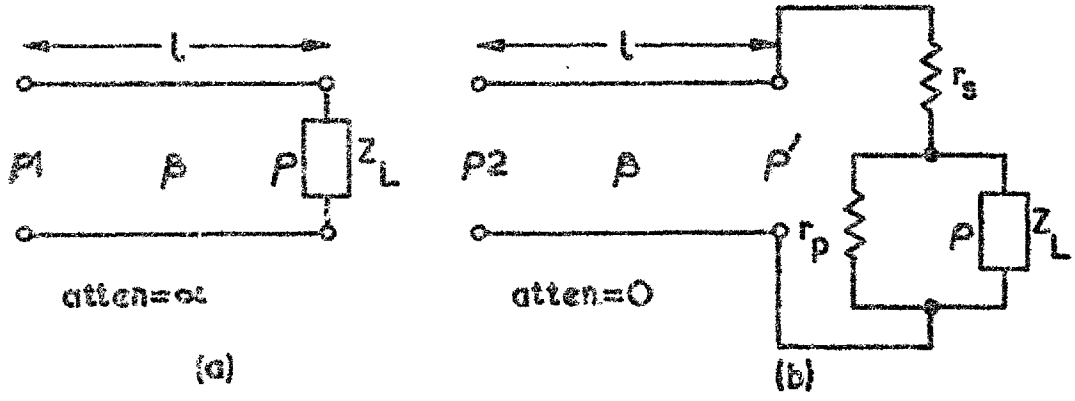

Fig.7.7: Lumped equivalent circuit for lossy transmission-lines.

The residual VSWR for fig. 7.4 is 12.7, giving a residual return loss of 1.37 dB. (This is roughly 6/7 of 1.5 dB, which was the measured return loss of all seven sections.) From (A.13), and with $Z_0 = 38\ \Omega$

$$R_P = 480\ \Omega \quad \text{and} \quad R_S = 3\ \Omega$$

where $R_P = r_P Z_0$ and $R_S = r_S Z_0$. Using the equivalent circuit in fig. 7.7 (b), with these element values, the VSWR as a function of R_{dc} produces a curve which is indistinguishable (on the same scale) from the theoretical one assuming a line attenuation of .685 dB shown in fig. 7.4.

The circuit presented in this section is useful in gaining a further understanding of the influence of transmission-line loss on its load, be it active or passive. It can be used in calculations involving the determination of the stability of active devices. It can be used in one-port microwave measurements to correct the measured load immittance for loss between it and the slotted-line.

7.6 EXPLANATION OF THE PERFORMANCE OF TDA 2

The behaviour of the amplifier could not be explained by the performance of the parts hitherto tested. It is proposed, therefore,(and after considerable deliberation), that the instability must be due to the TD and/or its mount. Recent studies by the author into techniques for measuring the parameters of TDs at microwave frequencies[4-12] revealed how sensitive they were (particularly the inductance) to a shift in the reference plane (to which the measurements are referred), especially for the present TD package (fig. 1.1 (e)) terminating a 50 Ω coaxial-line.* The concept of a "reference plane" may not be uniquely defined for every conceivable mounting configuration or for all TDs. It seems usual to replace the TD by a conducting pill of similar dimensions to establish a reference minimum and deduce the TD parameter

---

*The method in mind is SWD measurements on a TD which is biased at its valley to eliminate the junction negative resistance.

values from the shift in the minimum when the TD replaces the pill. The inductance of the pill itself, which can be quite significant is thereby removed. Recent coaxial-line measurements show that the intrinsic parameters, with the exception of r, are substantially constant from d.c. through to X-band.[12] At S-band, r is very nearly equal to its low frequency value.*

Calculation of inductance of TD mount

It will be recalled that SWD measurements on the stabilizing network showed that the minimum at the resonant frequency of the s.c. series line was at the waveguide wall .050 in above the TD position. This can be explained by the impedance change produced when a low impedance line whose input impedance is itself very small joins a much larger impedance (50 Ω) line.

The mount of the TD is responsible for most of the series inductance (see Getsinger[10]) - a good estimate of its possible magnitude is obtained by considering the reactance of a solid post having the diameter of the spring(section 6.10) joined to the upper and lower faces of a .075 in high waveguide. From Marcuvitz[13]

$$\frac{X}{Z_0} = \frac{2a}{\lambda_g} \cdot (.54) \text{ when } \frac{d}{a} = .023.$$

Hence, at 2.93 Gc/s (λ_g = 14.5 cm)

$$\frac{X}{Z_0} = .53\ \Omega.$$

Full height Z_0 is 506 Ω, therefore

$$Z_0 = \frac{b'}{b} \cdot 506 = \frac{.075}{1.34} \times 506 = 28.3\ \Omega.$$

---

*Increase in r at higher frequencies is discussed in section 5.3.

This gives the unexpectedly high value of

$$X = 15.1\ \Omega$$

from which

$$L = \frac{X}{\omega} = .82\ \text{nH}.$$

Adding the inductance quoted for the TD by the manufacturer as .12 nH gives a total of .94 nH!

Stability of TDA 2

Fig. 7.8 illustrates the effect of series inductance on the amplifier response from 1.8 to 3.3 Gc/s. The TDA program (section 6.9) was used to compute this response. The total inductance was treated as belonging to the TD equivalent circuit - an approximation which is valid as long as $\omega^2 C_1 L \ll 1$.*

To interpret the curves of fig. 7.8 in terms of stability, a prior knowledge of the number of RH p-plane poles is required. All the curves have 2 RH p-plane admittance poles such as those exhibited by fig. 3.11 (a).** 2 CCW encirclements (1 for positive frequency only) of the appropriate critical point are, therefore, required for stability. Table 7.1 summarizes the pole-zero arrangements. Note in fig. 7.8 that increasing or decreasing the aperture of the inductive iris results in a positive or negative shift of susceptance, respectively, of the curves (parallel to the imaginary axis).

---

*$\omega^2 C_1 L = .12$ when $C_1 = .3$ pF, L = 1 nH and f = 3 Gc/s.

**When L = .12 nH there are no RH p-plane poles, and no encirclements of the critical point are required for stability. See fig. 6.11.

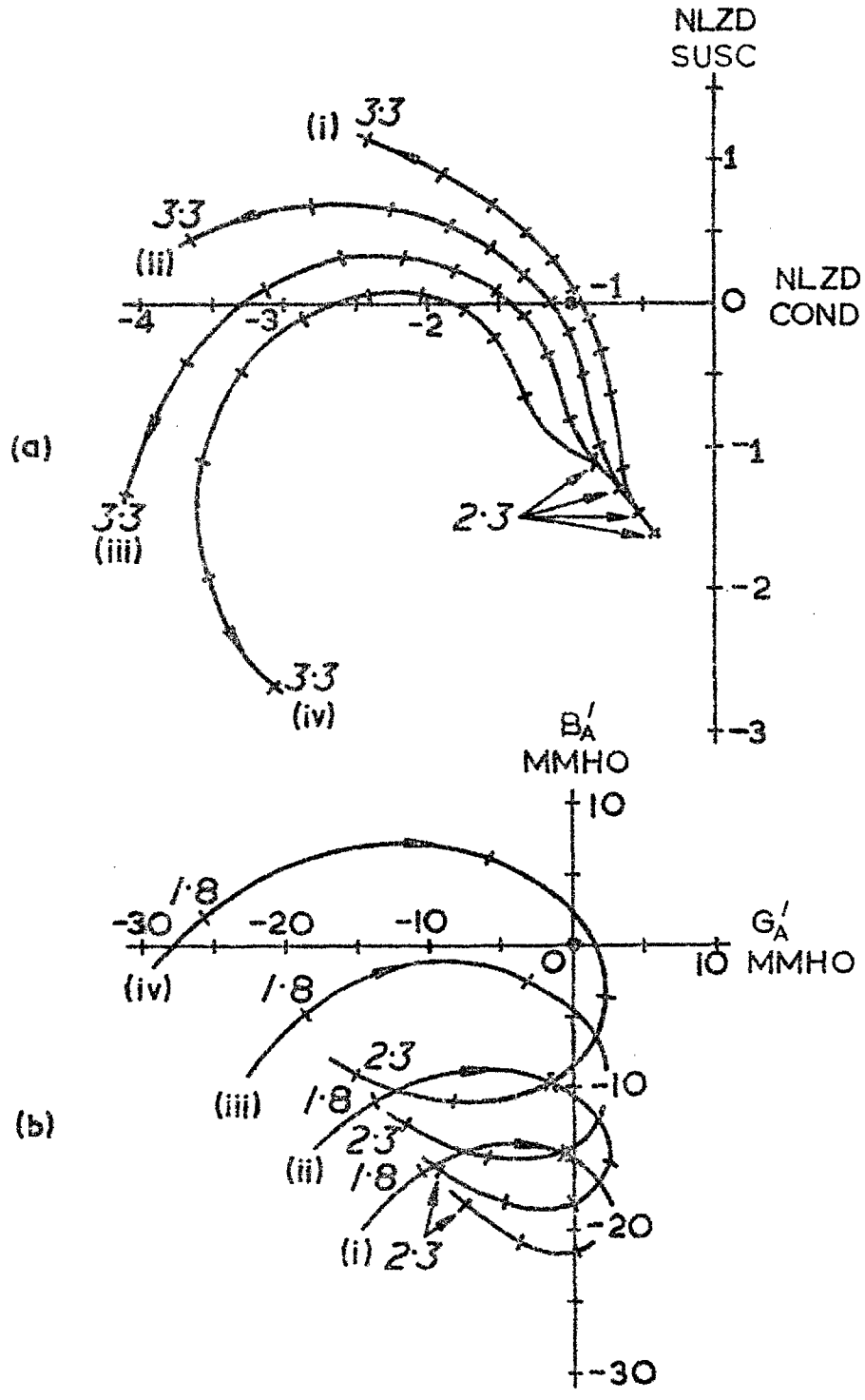

Fig. 7.8: (a) Reflection amplifier admittance normalized to waveguide characteristic admittance, (b) $Y_A'(j\omega)$ (see section 6.7). (i) L = .4 nH, (ii) L = .6 nH, (iii) L = .8 nH, (iv) L = 1 nH. Frequencies are in Gc/s.

Curve	CCW encirclements			P	Z	Stable?
	from fig. 7.8 (a)	from fig. 7.8 (b)	Total			
Fig. 6.11	-	-	0	0	0	yes
(i)	2	0	2	2	0	yes
(ii)	0	0	0	2	2	no
(iii)	0	0	0	2	2	no
(iv)	0	-2	-2	2	4	no

Table 7.1: Pole-zero arrangement in RH p-plane for TDA 2 for various values of L.

Curve (iv), corresponding to L = 1 nH, indicates the possibility of oscillations near the waveguide cut-off frequency f_c. Add to this the uncertainty of the behaviour of the experimental waveguide set-up near f_c, and it is not surprising that the oscillations were observed in this region.

Experimental observations

The TD described in section 7.3 was inadvertently destroyed. Another having the following quoted parameters was available:

R_{min} = 51 Ω, C = 1.6 pF, r = 1.2 Ω, L = .12 nH, and C_1 = .3 pF.

The TD was mounted in TDA 2 and was unstable for all iris screw positions, as seen from its swept V-I characteristic.* It was then biased at R_{min}, and a spectrum analyzer was connected to the system through a coaxial-line pad, isolator, and coaxial to S-band waveguide transformer. With all iris screws up to 13 in place oscillations at the following fre-

*Spectrum analyzer observations were made at Mullard Research Laboratories, Surrey.

quencies were detected: 2.83, 5.62, and 8.45 Gc/s. Similarly for all screws up to 11: 2.55, 5.10, and 7.61 Gc/s. (The TD then went o.c.) There can be no doubt that the lower values are fundamentals followed by their second and third harmonics. Thus, the TD oscillated in or below the desired amplification band. The frequency increased with decreasing aperture, confirming the observations made in section 7.3.

Narrow band stabilizing network

The simplest alteration to the stabilizing network that could be made was to change its centre rod (fig. 6.18). A brass rod of diameter .091 in was made and fitted into the coaxial structure with a resistive film card of 400 Ω/square. This leads to the following changes:

$$Z_{01}' = 32.4\ \Omega, \quad Z_{02} = 40\ \Omega, \quad \text{and } Z_{03} = 40\ \Omega.$$

(The value of Z_{02}' was the same as before.)

Stable narrow band gain could be obtained and recorded on an X-Y plotter for a wide range of iris screw settings, when the circulator was connected into the circuit. The theoretical response of the modified stabilizing network is shown in fig. 7.9. So long as the amplifier is stable, it is clear that the external gain will be confined to frequencies close to 3.1 Gc/s, regardless of TD, bias voltage or iris setting, since the positive stabilizing resistance eliminates the TD negative resistance elsewhere. Analysis shows that stable gain can indeed be obtained even for L = 1 nH, and that the situation at hand is substantially the same as the analysis presented in chapter 5, i.e. 2 CW encirclements by the amplifier admittance of the centre of the negative conductance Smith chart is fulfilled. Stable narrow band gain has been obtained experimentally with

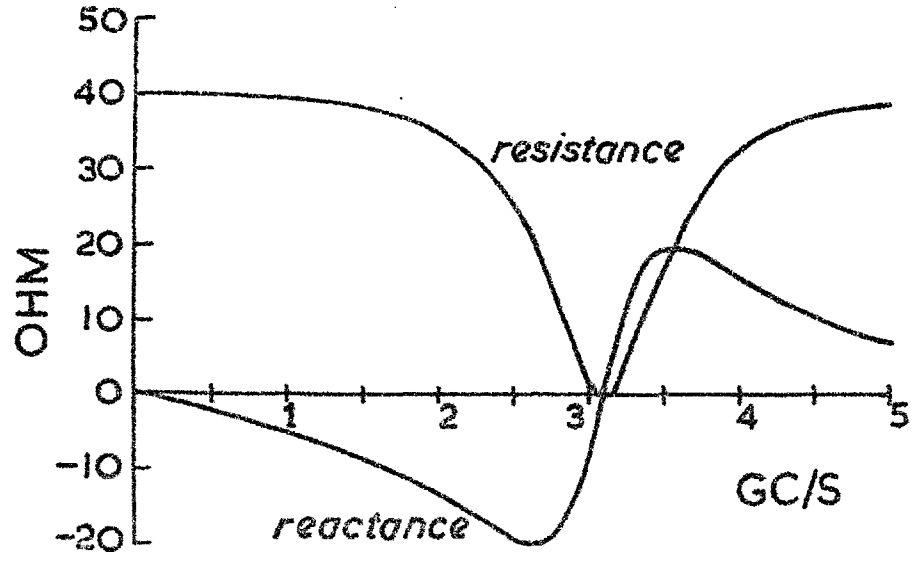

Fig. 7.9: Theoretical input impedance of narrow band stabilizing network.

several TDs in accordance with the foregoing predictions. The spectrum analyzer was always available to check for instabilities at other frequencies at the same time, but there were none.

7.7 Conclusion

It has been shown that the principal reason why TDA 2 failed to work as designed is that a large unaccounted for series inductance was present, associated with the TD mount and its waveguide environment. The possibility of such an inductance had been totally overlooked by the author when the amplifier configuration was conceived.

The corresponding (calculated) inductance for TDA 1 is approximately twice its quoted inductance, whereas in TDA 2 it may be at least seven times its quoted value. The

reasons for this are the following. The waveguide height was smaller in TDA 1, the TD was larger (fig. 1.1), its quoted L was larger, and the penetration of the centre rod of the stabilizing network into the waveguide was much smaller. A complete redesign of TDA 2 would be necessary to reduce the inductive effect and allow stable broadband operation.*

Some manufacturers when quoting an "inductance" for their TD actually imply an "excess inductance with respect to a conducting block of the same geometry" in a particular environment, e.g. coaxial-line or rectangular waveguide. Some authors of papers on the microwave measurement of TD parameters rarely distinguish between these concepts, let alone discuss any possible far-reaching implications (even qualitatively). TDA designers usually tailor the microwave environment around the TD to reduce parasitic effects as far as possible. They are, therefore, not so susceptible to divergences of inductance from the value quoted by the manufacturer. Ideally, a TD should be measured in the environment in which it is subsequently to be used, the reference terminals being the external and therefore the accessible ones, and not referred to a hypothetical reference plane.

All the component networks of the amplifier were tested and found to work substantially in accordance with theory. Finally, the performance of TDA 2 has been explained in terms of a theoretical stability analysis and the actual experimental observations. The amplifier produced stable gain only under narrow band conditions.

---

*Such a small TD package is quite unsuitable for S-band rectangular waveguide, anyway, since, for example, the advantages of the small package (reduction in L and C_1) are lost.

7.8 References

(1) A.M. Goodman, "Test set for displaying the volt-ampere characteristics of tunnel diode," Rev. Sci. Instrum., Vol. 31, p.286, March 1960.

(2) J.A. Narud and T.A. Fyfe, "Tunnel-diode curve tracer is stable in negative resistance region," Electronics, pp.74-75, 5 May 1961.

(3) W.H. Card, "Bridge measurements of tunnel diode parameters," IRE Trans., Vol. ED-8, pp. 215-219, May 1961.

(4) "IEEE Standard on tunnel diodes and backward diodes," IEEE Trans., Vol. ED-12, pp. 373-386, June 1965.

(5) W.B. Hauer, "Definition and determination of the series inductance of tunnel diodes," IRE Trans., Vol. ED- 8, pp. 470-475, November 1961.

(6) H. Fukui, ref. (2) chap. 5.

(7) T. Unotoro and H. Niizuma, "Measurement of Esaki diodes," Electronics and Communications in Japan, Vol. 47, pp. 57-74, April 1964.

(8) T. Unotoro, "Microwave measurement of Esaki diode circuit parameters," Electronics and Communications in Japan, Vol. 47, pp. 64-71, May 1964.

(9) C.S. Kim and C.W. Lee, ref. (1) chap. 5.

(10) W.J. Getsinger, ref. (10) chap. 2.

(11) P. Hawkins and M.K. McPhun, "The equivalent circuit of the tunnel diode," Proc. IEEE, Vol. 54, pp. 1451-1452, October 1966.

(12) J.O. Scanlan and V.P. Kodali, "Characterisation of tunnel diodes at microwave frequencies," Dept. of Electrical and Electronic Engineering, Leeds University, 1966.

(13) N. Marcuvitz, ref. (21) chap. 6, pp. 257-263.

8

general conclusions

Three broad fields have been brought together in this study of stable, broadband tunnel-diode amplifiers in rectangular waveguides.

The first concerns the stability of the TD in its microwave environment. Because of the numerous non-commensurate structures which can be used in conjunction with the TD, and because the TD is potentially active at all frequencies up to its effective resistive cut-off frequency, the real-frequency Nyquist approach to stability has been found the most practical one. A general method of analyzing the stability of a TD in the immittance planes (chapter 3) is presented. The method has been found straightforward, reliable, and extremely useful in gaining an understanding of the significance of real-frequency impedance or admittance loci for TD circuits of some complexity. The concepts involved have been extended to the analysis of stability in the Smith chart (ρ-plane) redefined to accommodate immittances with negative real parts. The gain and stability of TD reflection amplifiers can be simultaneously predicted on this chart. Stability has been interpreted directly in the ρ-plane

(section 4.5), but as some confusion is possible when interpreting the arbitrary closing loop in terms of ρ, it is found more convenient to formulate the stability criterion in terms of immittance.

The second field concerns the application of digital computers to the design and optimization of microwave networks. Although there is no doubt that many microwave engineers do use computers,* there is a marked absence of reports devoted to this application. It has been fashionable recently to synthesize commensurate microwave networks by exact mathematical techniques. Such techniques would have been prohibitive in the designs of TDA 1 and TDA 2, hence the recourse to the computer. In exact formulations one might not be certain of realizing components with practical values or dimensions. In a direct application of the problem to the computer, control over parameter values can always be maintained. The optimization of the coaxial-line stabilizing and biasing network of TDA 2 (chapter 6) necessitated the use of the computer not only for these reasons, but because the specifications for its response were in terms of input resistance and reactance, rather than the conventional insertion loss. Control over both quantities had to be maintained. A further use of the computer is for producing Smith chart plots (appendix A1).

The third field concerns the design and experimental performance of two TDAs. These designs serve essentially as illustrations of the interaction of the responses of the component circuits to culminate either in stable or unstable performance. The theoretical ideas of chapters 3 and 4 are drawn upon for this purpose. The means has been concentrated upon rather than the end product, since

---

*McPhun has reported a versatile microwave network analysis program.[1]

stable, broadband TDAs have been successfully manufactured for some years now. The experimental behaviour and responses of the amplifier and its components have been compared with the theoretical predictions where appropriate. The unstable behaviour of TDA 2, in particular, has been explained in terms of a rather large and unaccounted for series inductance associated with the TD mount.

The TDA has, for the reasons given in section 1.1, gradually been losing favour in microwave applications. There is a certain amount of interest, however, in lumped thin-film integrated TDAs using unencapsulated TDs, from the points of view reducing size and weight, and easing mass production. Okean[2] recently reported the design of such amplifiers.

References

(1) M.K. McPhun, "A computer programme for the analysis of branched distributed and lumped circuits," Conference on electrical nètworks, University of Newcastle-upon-Tyne, September 1966.

(2) H.C. Okean, "Integrated microwave tunnel diode device," 1966 G-MTT International symposium, Digest of technical papers, pp. 135-140.

APPENDIX

A1 SMITH CHART SUBROUTINE

Two basic methods of storing and plotting were considered. The first was to represent a square area on the page by a matrix. The points could be entered in any order, the printing instructions ensuring the correct sequence. The second was to define a row matrix containing only the relevant points. This method would necessitate sorting the points into the print-out sequence before the printing instructions could given. For a considerable number of points, the co-ordinates of which were not explicitly related or controlled, the first method would tend to use more storage space in the computer, but take less time than the second. The IBM 7090 was available to the author. As this machine is not time-sharing, it was thought that the first method would be preferable.

Since a main program is needed to read the immittance values or to calculate them, microwave engineers unfamiliar with programming should consult their programming advisers. Minor changes to suit user or machine may be found necessary. The straightforward nature of the program obviates the usual need for a flow diagram. The specific example shown in fig. A.1 is written in FORTRAN IV and is briefly described as follows.

```
      SUBROUTINE CHART1
      COMMON /RPLANE/FUNC,ITYPE,NUM
      COMPLEX FUNC(201),RHO
      DIMENSION PNT(57,95),C(10)
      DATA (C(I),I=1,10)/1H ,1H-,1HX,1HO,1H+,1HP,1HR,1H*,1HN,1HS/
      IF(NUM.GT.200) GO TO 15
      IF(ITYPE.EQ.1) GO TO 1
      IF(ITYPE.EQ.2) GO TO 2
      GO TO 16
    1 WRITE(6,20)
      GO TO 3
    2 WRITE(6,25)
    3 NUM=NUM+1
      FUNC(NUM)=FUNC(1)
      DO 4 M=1,57
      DO 4 N=1,95
    4 PNT(M,N)=C(1)
      DO 5 N=2,94
    5 PNT(29,N)=C(2)
      PNT(29,48)=C(3)
      PNT(29,1)=C(4)
      PNT(29,95)=C(4)
      J=NUM-2
      DO 9 I=2,NUM
      RHO=(FUNC(I)-1.)/(FUNC(I)+1.)
      GAIN=CABS(RHO)
      IF(GAIN.GT.1.) GO TO 8
      N=48.5+47.*REAL(RHO)
      M=29.5-28.*AIMAG(RHO)
      PNT(M,N)=C(5)
      IF(I.LT.J) GO TO 9
      IF(I.LT.NUM) PNT(M,N)=C(6)
      IF(I.EQ.NUM) PNT(M,N)=C(7)
      GO TO 9
    8 RHO=1./CONJG(RHO)
      N=48.5+47.*REAL(RHO)
      M=29.5-28.*AIMAG(RHO)
      PNT(M,N)=C(8)
      IF(I.LT.J) GO TO 9
      IF(I.LT.NUM) PNT(M,N)=C(9)
      IF(I.EQ.NUM) PNT(M,N)=C(10)
    9 CONTINUE
      WRITE(6,30) ((PNT(M,N),N=1,95),M=1,19)
      WRITE(6,35) ((PNT(M,N),N=1,95),M=20,57)
      GO TO 100
   15 WRITE(6,40)
      GO TO 100
   16 WRITE(6,45)
  100 RETURN

   20 FORMAT(17H1IMPEDANCE CHART , 97X,17H  DB   RHO    VSWR )
   25 FORMAT(17H1ADMITTANCE CHART, 97X,17H  DB   RHO    VSWR )
   30 FORMAT                    (19X,95A1,17H   0   1.0    INF  /                1
     1      19H RHO-PLANE           ,95A1,17H                55.0  /               2
     2                           19X,95A1,17H                27.0  /               3
     3                           19X,95A1,17H   1   .9       17.7  /               4
     4                           19X,95A1,17H                13.0  /               5
     5                           19X,95A1,17H                10.2  /               6
     6                           19X,95A1,17H   2   .8        8.33 /               7
     7                           19X,95A1,17H                7.00 /               8
     8                           19X,95A1,17H   3   .7        6.00 /               9
     9                           19X,95A1,17H                5.22 /              10
     1                           19X,95A1,17H   4            4.60 /              11
     2                           19X,95A1,17H       .6        4.09 /              12
     3                           19X,95A1,17H   5            3.67 /              13
     4                           19X,95A1,17H                3.31 /              14
     5                           19X,95A1,17H   6   .5        3.00 /              15
     6                           19X,95A1,17H                2.73 /              16
     7                           19X,95A1,17H                2.50 /              17
     8                           19X,95A1,17H   8   .4        2.29 /              18
     9      19H POSITIVE IMAGINARY,95A1,17H                  2.11 )              19
   35 FORMAT                    (19X,95A1,17H  10            1.95 /              20
     1                           19X,95A1,17H       .3        1.80 /              21
     2                           19X,95A1,17H  12             1.67 /              22
     3                           19X,95A1,17H       .2        1.55 /              23
     4                           19X,95A1,17H  15             1.44 /              24
     5                           19X,95A1,17H  17             1.33 /              25
     6                           19X,95A1,17H  20   .1        1.24 /              26
     7                           19X,95A1,17H  23             1.15 /              27
     8                           19X,95A1,17H  29             1.07 /              28
     9                           19X,95A1,17H0 INF  .0        1.00 .              29
     1                         9(/19X,95A1)/                                      38
     2      19H NEGATIVE IMAGINARY,95A1 ,                                       39
     3                        12(/19X,95A1)/                                     51
     4      19H J W BANDLER         ,95A1,12H   FREQUENCY/                      52
     5      19H MICROWAVE LAB       ,95A1,12H   RESPONSE /                      53
     6      19H ELEC ENG DEPT       ,95A1 /                                     54
     7      19H IMPERIAL COLLEGE    ,95A1 /                                     55
     8      19H LONDON SW 7         ,95A1 /                                     56
     9      19H SEPT 1965           ,95A1 )                                     57
   40 FORMAT(47H1THE MAXIMUM NUMBER OF POINTS HAS BEEN EXCEEDED)
   45 FORMAT(36H1THE CHART TYPE HAS NOT BEEN DEFINED)
      END
```

Fig. A.1: The complete subroutine program in FORTRAN IV.

The first card indicates the name by which the subroutine is called, i.e. CALL CHART1. The complete COMMON statement as shown, and a COMPLEX statement containing FUNC (201), must appear in the main program. FUNC stands for impedance or admittance according to whether ITYPE equals 1 or 2, and must be normalized in the main program. ITYPE also governs the page heading of the chart appropriately. NUM corresponds to the number of points entering the subroutine from the main program, in which both it and ITYPE are explicitly set before the subroutine is called. If these conditions are not satisfied the program faults. See statement numbers 40 and 45 in fig. A.1. Failure to observe the correspondence of NUM to the number of points may result in missing points or unwanted ones.

In the present example, the maximum square area which would fit the available page was used. This area is provided by a 57 by 95 matrix. The DIMENSION statement declares the size of the matrix, and also the number of characters that can be plotted, here 10. The DATA statement defines these characters and groups them in the order of importance with the least important, a blank, first. Initially all the elements of the matrix are made blanks to clear it of previous points (DO loop terminating on statement 4). Clearly, the co-ordinates can only be located in the matrix at discrete positions. To effect this use is made of the fact that a real variable entering an integer register is truncated at the decimal point. Hence, each point is located in row M, column N by

$$M = \frac{A+2.}{2.} - \frac{A-1.}{2.} \underline{\mathrm{Im}}(\rho) \qquad (A.1)$$

$$N = \frac{B+2.}{2.} + \frac{B-1.}{2.} \underline{\mathrm{Re}}(\rho) \qquad (A.2)$$

where the matrix has A rows and B columns, both of which must be odd to ensure symmetry of the chart about both real and imaginary axes.

The -sign is used for the centre line (zero reactance or susceptance), with X at the centre point (ρ-plane origin). O is printed at either extremity, with an extra O on the right to indicate infinite immittance. See fig. 6.1, for example. The +, P, and R are used for immittances with positive real parts, the *, N, and S for those with negative real parts. R or S characterize the first point (arrow tail), P or N the last two points (arrow head). The sequence of operations ensures that C(5) to C(10) can overwrite C(1) to C(4); P, R, N, or S can never be overwritten by + or *, R or S can overwrite all other characters (caused by operating on FUNC(1) last, hence the possibility of obtaining FUNC(201) due to NUM being increased by 1).

When the real part of the immittance is negative, the response is reflected back into the unit circle by the transformation (see section 4.3)

$$\rho' = \frac{1}{\rho^*} \qquad (A.3)$$

where ρ^* is the complex conjugate of ρ, accompanied by the appropriate change in the character representing the point.

After all the points have been assembled, they are plotted on a new page by an off-line printer with the scales, as shown in figs. 6.1, 6.9, and 6.14. Note that the numbers constituting the scales are taken to represent the values at the middle of the lines of the computer paper.

The program is readily modified to suit alternative scales, sizes, layouts, etc. An expanded chart could be realized by dividing RHO in the program by the maximum magnitude to be displayed, and then restricting excursive points

to the circumference, or eliminating them altogether. The adjoining scales must, for this case, be altered or removed. The program could also be rewritten to accommodate automatic scaling which would be determined internally or externally to the subroutine, and possibly generating a print-out of the scales. The chart size can similarly be altered. For some applications, a specially prepared transparency of a Smith chart may be used in conjunction with the computer plot to obtain associated parameters more accurately, e.g. the phase of ρ.

It is felt,however, that the whole ρ-plane merits a subroutine of its own, such as the one described here, as it is so frequently used.

A2 PROGRAM FOR ONE-PORT MEASUREMENTS

The reference plane (input to load) can be found by placing a s.c. at the end of the slotted-line and extrapolating the positions of the minima indicated by the SWD by an integral number of half wavelengths for at least two different frequencies until the minima coincide in position. A value (positive or negative as necessary) consistent with the scale of the slotted-line is assigned to this position.

The program used accepts any number of sets of readings, any waveguide cut-off frequency f_c including zero, and the VSWR either as a ratio or in dB. For each set of readings (when the load under test is connected to the slotted-line), 4, 6, or 8 corresponding positions about the minima can be processed to provide one "average" position of a minimum and the average value of λ_g; and 2, 3, or 4 values, respectively, of VSWR read from the SWD to provide an average value s which is used in the calculation. The normalized input impedance to the load is given by

$$z_i = \frac{1 - jst}{s - jt} \qquad (A.4)$$

where

$$t = \tan\theta = \tan\frac{2\pi d}{\lambda_g} \qquad (A.5)$$

and where d is the distance from the "average" position of the minimum to the known reference plane.

To prevent the computer from evaluating the tangents of large θ (accompanied by the inevitable loss in accuracy) the following instruction was built into the program:

$$\theta = \theta - \pi \times \text{Integral part of } \{.5+\theta/\pi\} \quad . \qquad (A.6)$$

This instruction reduces θ to its equivalent between $-\pi/2$ and $\pi/2$ for tangent calculations.

The tabulated print-out of results includes frequency obtained from

$$f = (f_c^2 + c^2/\lambda_g^2)^{\frac{1}{2}} \quad , \qquad (A.7)$$

λ_g, VSWR, reflection coefficient, return and transmission losses in dB, r_i, x_i, g_i, and b_i. CHART1 is incorporated as a subroutine: this provides a plot of either z_i or y_i, as desired.

A3 STABILIZING NETWORK PROGRAM

Summary

The program consists of five parts:

(i) OPT, the main program. This reads all the data, instructs execution of the trial and error loops and the optimization process.

(ii) STAG, a subroutine which calculates the input impedance of the stabilizing network shown in fig. 6.4 at any specified frequency. See fig. 6.6 for the flow diagram.

(iii) TEST, a subroutine which compares input resistance or input reactance of the network at frequencies f_1 to f_6 determined by the operator with specified test values C_1 to C_9 (see fig. 6.7). Control is returned to the main program if any specification is violated. V (see fig. A.2) is calculated by this subroutine. See equation (6.2).

(iv) FREQ, a subroutine which arranges the calculated frequency response into a form convenient for printing out (with the current values of y_{o1} to y_{o3} and f_{o1} to f_{o3}) and for feeding into

(v) XYPLOT,* a subroutine which instructs a graphical print-out of the resistance and reactance as a function of frequency.

The program was written in FORTRAN IV and used on the IBM 7090.

---

*Devised by P. Newbold, Electrical Engineering Dept., Imperial College, London, March 1965.

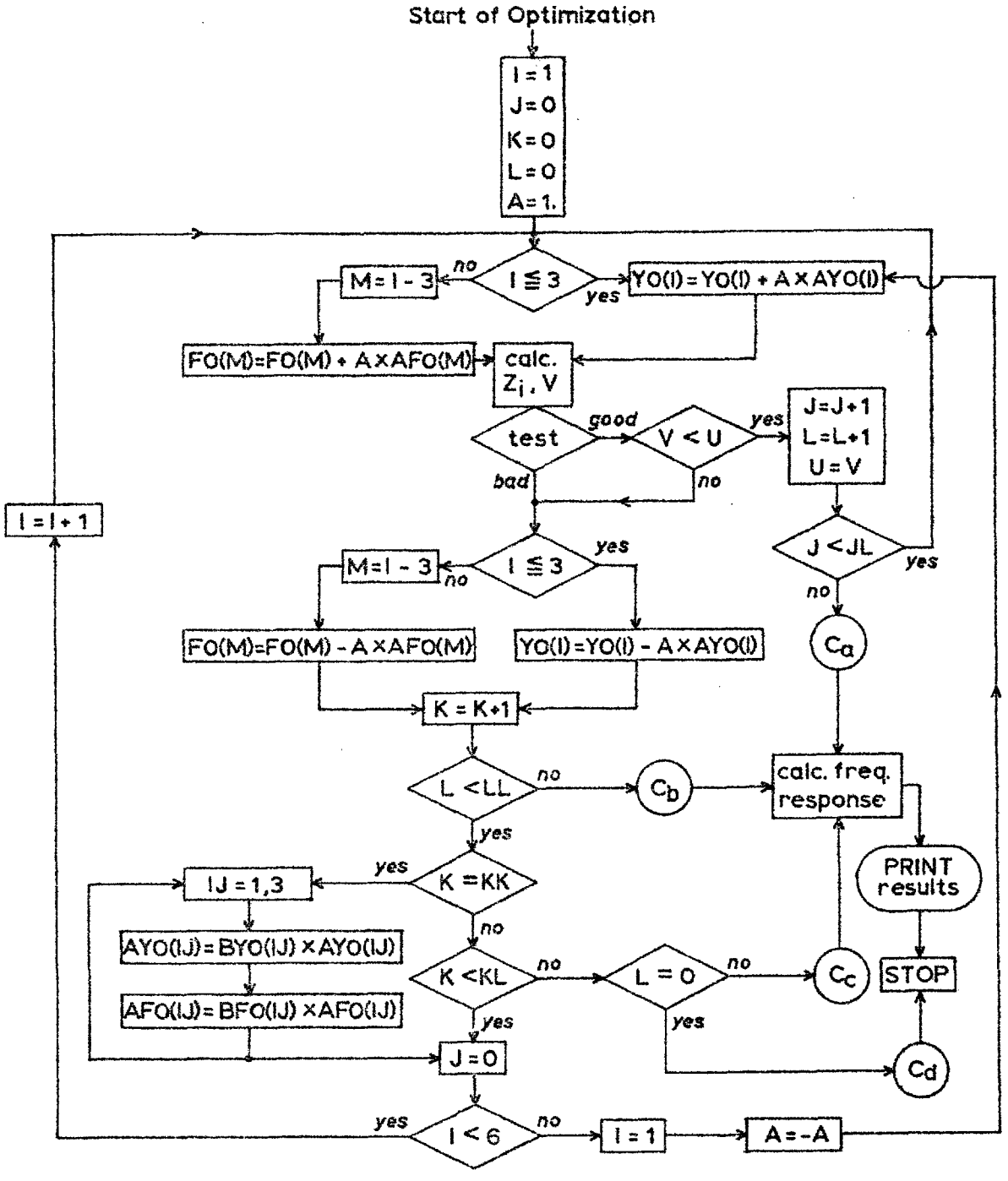

Fig. A.2: A flow diagram of the optimization loops of the stabilizing network program. YO and FO correspond to y_0 and f_o, respectively. Z_i is calculated by STAG; calculation of V and "test" is effected by TEST; FREQ is called to instruct the calculation of the frequency response of Z_i by STAG, and the printing out of the results in tabular form, and graphically through XYPLOT. See text.

Description of OPT

The essentials of this program are presented partly as an algorithm and partly by a flow diagram (fig. A.2).

1) Read 21 integers and 7 associated scale factors to determine the trial and error cycles for the y_0 and f_o parameters and the frequencies for the desired frequency response.
Read 6 test frequencies f_1 to f_6.
Read 4 integers JL, LL, KK, and KL which limit the number of iterations around the optimization loops (see fig. A.2).
Read 3 values each for subscripted variables AYO, BYO, AFO, and BFO for adjusting the step width.
Read the bias resistance value R_b (for normalization) and 9 test numbers C_1 to C_9 (in ohms).

2) Normalize the Cs to R_b.

3) Calculate $U = C_3^2 + C_5^2 + C_7^2 + C_9^2$.

4) Store this first value of U in W.

5) Set values for y_{01}, y_{02}, y_{03}, f_{o1}, f_{o2}, f_{o3}.

6) Call "TEST". (TEST calls STAG).

7) If any specification is violated go to (11).

8) If V > or = to U go to (11).

9) Set U = V.

10) Store the present values of y_{01}, y_{02}, y_{03}, f_{o1}, f_{o2}, f_{o3}; at the same time overwrite any previously stored values.

11) Continue with next iteration from (5) until loops are completed.

12) If U < W go to (15).

13) Write "THE SPECIFICATIONS CANNOT BE MET".

14) Stop.

15) Put y_{01}, y_{02}, y_{03}, f_{o1}, f_{o2}, f_{o3} equal to the respective stored values.

16) Call "FREQ". (FREQ calls STAG and XYPLOT).

17) Start of optimization. See fig. A.2.

Appropriate comments for fig. A.2 are:

C_a THE LIMIT OF THE CYCLE HAS BEEN REACHED

C_b THE TOTAL LIMIT OF THE CYCLE HAS BEEN REACHED

C_c THE OPTIMUM SOLUTION IS GIVEN ON THE NEXT PAGE

C_d THE TRIAL AND ERROR VALUES ARE BEST, RECOMMEND FINER STEPS

I(maximum value 6) determines which of the y_0 or f_o is incremented, e.g. I = 2 refers to y_{02}; I = 6 refers to f_{o3}. J is the consecutive number of times a successful change in one parameter value is made. If the limit JL is reached comment C_a is printed out. K is the number of times I has changed, limited to KL times. When K = KK (for instance 12) the AYO and AFO values are multiplied by the fractions BYO and BFO to reduce the step width. L is the total number of successful changes in the parameters. When L reaches the limit LL comment C_b is printed out. When K reaches KL and L $\neq$ 0 comment C_c is printed out; if L = 0 comment C_d is printed out instead. The current values of I, J, K, and L are all printed out following any of the comments. Subroutine FREQ is called, except after C_d (because no change

has taken place in parameter values). The choice of step widths and limits for the loops depends on the past experience of the operator with regard to the behaviour of the program and on the refinements required, e.g. the number of decimal places for the y_0 or f_o parameters.

A4 IMMITTANCE TRANSFORMATION THROUGH TRANSMISSION-LINES

An iterative form of the well-known transformation for cascaded transmission-line sections is

$$H_{in} = H_{On} \left\{ \frac{H_{i(n+1)} + P_n H_{On}}{H_{On} + P_n H_{i(n+1)}} \right\} \qquad (A.8)$$

where n signifies the nth line in the cascade, i signifies input, and where $P = j \tan \beta \ell$. The termination of the cascade is represented as the input immittance to an additional transmission-line (which it often is). The special cases of lines terminated by a s.c. and an o.c. are obtained for $H_{i(n+1)} = 0$, giving

$$H_{in} = P_n H_{On}. \qquad (A.9)$$

H = Z applies to the s.c. and H = Y applies to the o.c.

A5 REPRESENTATION OF TRANSMISSION-LINE LOAD WHEN THE LINE HAS A SMALL BUT FINITE LOSS

The conditions for fig. 7.7 (b) to approximate fig. 7.7 (a) are derived here. The notation used is defined in these figures.

It can be shown that

$$\rho_1 = \rho e^{-2\alpha \ell_e - 2j\beta\ell} \tag{A.10}$$

where

$$\rho = \frac{z_L - 1}{z_L + 1} \quad . \tag{A.11}$$

The impedance z of the circuit of fig. 7.7 (b) is

$$z = r_S + \frac{r_P z_L}{r_P + z_L} \quad . \tag{A.12}$$

When $z_L = 0$, $z = r_S$; when $z_L = \infty$, $z = r_S + r_P$. $|\rho_2| = |\rho_1|$ for these cases if

$$\frac{1}{r_S} = \frac{r_S + r_P}{1} = s \tag{A.13}$$

where s is the corresponding VSWR. Now

$$\rho' = \frac{r_S + \dfrac{r_P z_L}{r_P + z_L} - 1}{r_S + \dfrac{r_P z_L}{r_P + z_L} + 1}$$

$$= \frac{r_S r_P + r_S z_L + r_P z_L - r_P - z_L}{r_S r_P + r_S z_L + r_P z_L + r_P + z_L} \quad . \tag{A.14}$$

Let s be fairly large, say greater than 10. Then

$$\frac{r_S + r_P}{r_S} = s^2 > 100 .$$

Therefore

$$r_P >> r_S , \tag{A.15}$$

and

$$r_S r_P \approx 1 . \tag{A.16}$$

This reduces (A.14) to

$$\rho' \approx \frac{1 + r_P z_L - r_P - z_L}{1 + r_P z_L + r_P + z_L}$$

$$= \frac{(z_L - 1)(r_P - 1)}{(z_L + 1)(r_P + 1)}$$

$$= \rho \frac{(r_P - 1)}{(r_P + 1)}$$

$$\approx \rho(\frac{s-1}{s+1}) . \tag{A.17}$$

Therefore

$$\rho_2 = \rho' e^{-2j\beta\ell} \approx \rho(\frac{s-1}{s+1}) e^{-2j\beta\ell} \tag{A.18}$$

and

$$e^{-2\alpha\ell} \approx \frac{s-1}{s+1} \approx 1 - \frac{2}{s}$$

giving

$$\alpha\ell \approx \frac{1}{s} \text{ nepers.} \tag{A.19}$$

Note that (A.19) does not depend on the "equivalent circuit" because s is independently defined.

Suppose $z_L = 1$. Then the VSWR produced by the circuit of fig. 7.7 (b) is given (without approximation) by

$$VSWR = \frac{1 - \frac{1}{s^2} + s}{1 - \frac{1}{s} + s} \quad . \tag{A.20}$$

When s = 10, VSWR = 1.008; when s = 20, VSWR = 1.002. This is an indication of the error involved under fairly large attentuations. The return losses for these values of VSWR are about 1.7 dB and .9 dB, respectively.

AUTHOR INDEX

Principal authors only are given. The chapter in which a reference is mentioned comes first, followed by the reference number.

Bandler	3	1
	4	1
	4	6
	6	13
Behnke	6	7
Blaeser	3	9
Bode	3	5
Bolinder	2	11
Brown	2	6
Card	7	3
Carlin et al.	4	28
Carlin	6	9
Chang	1	2
	3	26
Chow	1	3
	3	28
	4	12
	6	8
Clorefeine	3	18
Cohn	6	14
Cristal	3	14
Davidsohn et al.	3	6
DeLoach Jr	2	1
DeLoach	2	7
Easter	1	8
	5	5
Esaki	1	1
Fukui	5	2
	7	6
Gallagher	4	22
Getsinger	1	7
	2	10
	3	30
	7	10
Ginzton	5	4
	6	22
Glass et al.	6	12
Goodman	7	1
Grayzel	6	24
Gunston	2	2
Hall, A.H.	2	12
	6	20
Hall, R.D.	4	20
Hamasaki	3	15
Harrington	2	4
Hauer	7	5
Havens	4	24
Hawkins et al.	7	11
Henoch et al.	3	2
	3	3
	4	3
	4	4

Hines	3	29
Hoover	4	19
Kaplan et al.	4	11
	4	14
Kim et al.	3	13
	5	1
	7	9
King et al.	6	3
Kitsuregawa et al.	4	21
Kohler et al.	3	23
	6	11
Kuh et al.	3	20
	6	1
Kurokawa	6	31
Kvaerna	3	4
Kyhl	4	13
Lane	2	8
Lane et al.	2	9
Lee	1	10
	5	6
Lenzing et al.	4	8
Lepoff	3	11
	3	12
Logan	6	4
Lowry et al.	3	25
McPhun	4	5
	4	7
	4	25
	5	3
	8	1
Marcuvitz	6	21
	7	13
Matthaei et al.	6	27
Meinke	3	10
Millican et al.	3	7
Narud et al.	7	2
Okean	3	16
	8	2
Ozaki et al.	6	23
Pedinoff	6	6
Plutchok	3	17
Ramo et al.	2	3
	4	27
Riblet	6	15
Richards	6	30
Rieck et al.	6	5
Rosen	4	17
Rothe	4	9
Scanlan	1	4
	3	27
Scanlan et al.	3	19
	3	24
	4	26
	7	12
Schiffman	6	28
Shiffman et al.	6	25
Smilen et al.	3	21
	6	2
Smith	4	2
Sovetov	4	10
Stelzried	4	18
Stock et al.	4	15
Suchkin	4	16
Unotoro et al.	7	7
Unotoro	7	8
Wenzel	6	26
Wexler	2	5
Whitzon	3	8
Youla et al.	1	9
Young	6	16
	6	17
	6	18
	6	19
	6	29

Yunoki *et al.*	4	23	Zysman	3	22
				6	10